LUND UNIVERSITY

Measurement of the azimuthal anisotropy for charged particle production in root s(NN)=2.76 TeV lead-lead collisions with the ATLAS detector

Aad, G.; Abbott, B.; Abdallah, J.; Khalek, S. Abdel; Abdelalim, A. A.; Abdesselam, A.; Abdinov, O.; Abi, B.; Abolins, M.; AbouZeid, O. S.; Abramowicz, H.; Abreu, H.; Acerbi, E.; Acharya, B. S.; Adamczyk, L.; Adams, D. L.; Addy, T. N.; Adelman, J.; Aderholz, M.; Adomeit, S.; Adragna, P.; Adye, T.; Aefsky, S.; Aguilar-Saavedra, J. A.; Aharrouche, M.; Ahlen, S. P.; Ahles, F.; Ahmad, A.; Ahsan, M.; Aielli, G.; Akdogan, T.; Åkesson, Torsten; Akimoto, G.; Akimov, A. V.; Akiyama, A.; Alam, M. S.; Alam, M. A.; Albert, J.; Albrand, S.; Aleksa, M.; Aleksandrov, I. N.; Alessandria, F.; Alexa, C.; Alexander, G.; Alexandre, G.; Alexopoulos, T.; Alhroob, M.; Aliev, M.; Alimonti, G.; Alison, J.

Published in:
Physical Review C (Nuclear Physics)

DOI:
10.1103/PhysRevC.86.014907

2012

Link to publication

Citation for published version (APA):
Aad, G., Abbott, B., Abdallah, J., Khalek, S. A., Abdelalim, A. A., Abdesselam, A., Abdinov, O., Abi, B., Abolins, M., AbouZeid, O. S., Abramowicz, H., Abreu, H., Acerbi, E., Acharya, B. S., Adamczyk, L., Adams, D. L., Addy, T. N., Adelman, J., Aderholz, M., ... Zwalinski, L. (2012). Measurement of the azimuthal anisotropy for charged particle production in root s(NN)=2.76 TeV lead-lead collisions with the ATLAS detector. *Physical Review C (Nuclear Physics)*, *86*(1), Article 014907. https://doi.org/10.1103/PhysRevC.86.014907

Total number of authors:
3056

General rights
Unless other specific re-use rights are stated the following general rights apply:
Copyright and moral rights for the publications made accessible in the public portal are retained by the authors and/or other copyright owners and it is a condition of accessing publications that users recognise and abide by the legal requirements associated with these rights.
• Users may download and print one copy of any publication from the public portal for the purpose of private study or research.
• You may not further distribute the material or use it for any profit-making activity or commercial gain
• You may freely distribute the URL identifying the publication in the public portal

Read more about Creative commons licenses: https://creativecommons.org/licenses/

Take down policy
If you believe that this document breaches copyright please contact us providing details, and we will remove access to the work immediately and investigate your claim.

Download date: 10. Dec. 2025

LUND UNIVERSITY

PO Box 117
221 00 Lund
+46 46-222 00 00

PHYSICAL REVIEW C **86**, 014907 (2012)

Measurement of the azimuthal anisotropy for charged particle production in $\sqrt{s_{NN}} = 2.76$ TeV lead-lead collisions with the ATLAS detector

G. Aad *et al.*[*]
(ATLAS Collaboration)

(Received 14 March 2012; published 24 July 2012)

Differential measurements of charged particle azimuthal anisotropy are presented for lead-lead collisions at $\sqrt{s_{NN}} = 2.76$ TeV with the ATLAS detector at the LHC, based on an integrated luminosity of approximately 8 μb^{-1}. This anisotropy is characterized via a Fourier expansion of the distribution of charged particles in azimuthal angle relative to the reaction plane, with the coefficients v_n denoting the magnitude of the anisotropy. Significant v_2–v_6 values are obtained as a function of transverse momentum ($0.5 < p_\text{T} < 20$ GeV), pseudorapidity ($|\eta| < 2.5$), and centrality using an event plane method. The v_n values for $n \geqslant 3$ are found to vary weakly with both η and centrality, and their p_T dependencies are found to follow an approximate scaling relation, $v_n^{1/n}(p_\text{T}) \propto v_2^{1/2}(p_\text{T})$, except in the top 5% most central collisions. A Fourier analysis of the charged particle pair distribution in relative azimuthal angle ($\Delta\phi = \phi_\text{a} - \phi_\text{b}$) is performed to extract the coefficients $v_{n,n} = \langle \cos n\Delta\phi \rangle$. For pairs of charged particles with a large pseudorapidity gap ($|\Delta\eta = \eta_\text{a} - \eta_\text{b}| > 2$) and one particle with $p_\text{T} < 3$ GeV, the $v_{2,2}$–$v_{6,6}$ values are found to factorize as $v_{n,n}(p_\text{T}^\text{a}, p_\text{T}^\text{b}) \approx v_n(p_\text{T}^\text{a})v_n(p_\text{T}^\text{b})$ in central and midcentral events. Such factorization suggests that these values of $v_{2,2}$–$v_{6,6}$ are primarily attributable to the response of the created matter to the fluctuations in the geometry of the initial state. A detailed study shows that the $v_{1,1}(p_\text{T}^\text{a}, p_\text{T}^\text{b})$ data are consistent with the combined contributions from a rapidity-even v_1 and global momentum conservation. A two-component fit is used to extract the v_1 contribution. The extracted v_1 is observed to cross zero at $p_\text{T} \approx 1.0$ GeV, reaches a maximum at 4–5 GeV with a value comparable to that for v_3, and decreases at higher p_T.

DOI: 10.1103/PhysRevC.86.014907 PACS number(s): 25.75.Dw, 25.75.Ld

I. INTRODUCTION

The primary goal of high-energy heavy-ion physics is to understand the properties of the hot and dense matter created in nuclear collisions at facilities such as the Relativistic Heavy Ion Collider (RHIC) and the Large Hadron Collider (LHC). An important observable toward this goal is the azimuthal anisotropy of particle emission. At low p_T ($\lesssim$3–4 GeV), this anisotropy results from a pressure-driven anisotropic expansion of the created matter, with more particles emitted in the direction of the largest pressure gradients [1]. At higher p_T, this anisotropy is understood to result from the path-length-dependent energy loss of jets as they traverse the matter, with more particles emitted in the direction of smallest path-length [2]. These directions of maximum emission are strongly correlated, and the observed azimuthal anisotropy is customarily expressed as a Fourier series in azimuthal angle ϕ [3,4]:

$$E\frac{d^3N}{dp^3} = \frac{d^2N}{2\pi p_\text{T} dp_\text{T} d\eta}\left(1 + 2\sum_{n=1}^{\infty} v_n(p_\text{T}, \eta)\cos n(\phi - \Phi_n)\right), \quad (1)$$

where p_T is the transverse momentum, η is the pseudorapidity, and v_n and Φ_n represent the magnitude and direction of the nth-order harmonic, respectively (see Sec. IV A). The nth-order harmonic has n-fold periodicity in azimuth, and the coefficients at low p_T are often given descriptive names, such as "directed flow" (v_1), "elliptic flow" (v_2), or "triangular flow" (v_3).

In typical noncentral heavy-ion collisions where the nuclear overlap region has an "elliptic" shape (or quadrupole asymmetry) on average, the azimuthal anisotropy is expected to be dominated by the v_2 component [5–7]. However, it was recently pointed out that the positions of the nucleons in the overlap region can fluctuate to create matter distributions with additional shape components, such as dipole ($n = 1$) and sextupole ($n = 3$) asymmetries [8–11]. Owing to strong final-state interactions, manifested as either pressure or jet energy loss, these spatial asymmetries can be converted into final-state momentum anisotropies, leading to nonzero first-order and higher-order harmonic coefficients [11,12].

The observation of large v_2 for $p_\text{T} \lesssim$ 3–4 GeV at the RHIC [13,14] and LHC [15,16] has led to the conclusion that the hot and dense medium behaves like a "perfect fluid" [14,17,18]. This is because the large v_2 values require hydrodynamic models [19–21] with a shear viscosity to entropy density ratio that is close to the conjectured lower bound of $1/4\pi$ [22,23]. Precise determination of this ratio using only v_2 data is limited by many model uncertainties [24]. Because the shear viscosity tends to dampen the harmonics, with more damping for larger n [11,25,26], measurements of harmonic coefficients beyond v_2 can provide stronger constraints for the shear viscosity of the medium. Extending these measurements to higher p_T is also valuable for discriminating between

[*]Full author list given at the end of the article.

Published by the American Physical Society under the terms of the Creative Commons Attribution 3.0 License. Further distribution of this work must maintain attribution to the author(s) and the published article's title, journal citation, and DOI.

 ©2012 CERN, for the ATLAS Collaboration

jet-quenching models, as high-p_T v_n is sensitive to the path-length dependence of the jet energy loss [27–29]. These coefficients can also help to distinguish between different models of the initial geometry [30–33] and provide insights into the granularity of the initial state fluctuations [26,34–36].

Another related observable for studying the properties of the medium is the correlation function between two particles in relative azimuthal angle $\Delta\phi = \phi_a - \phi_b$ and pseudorapidity $\Delta\eta = \eta_a - \eta_b$ [37]. The distribution of pairs in $\Delta\phi$ can be expanded into a Fourier series:

$$\frac{dN_{\text{pairs}}}{d\Delta\phi} \propto 1 + 2\sum_{n=1}^{\infty} v_{n,n}\left(p_T^a, p_T^b\right)\cos n\Delta\phi, \tag{2}$$

where the coefficients $v_{n,n}$ are symmetric functions with respect to p_T^a and p_T^b. The harmonics defined in Eq. (1) also contribute to this distribution:

$$\frac{dN_{\text{pairs}}}{d\Delta\phi} \propto 1 + 2\sum_{n=1}^{\infty} v_n\left(p_T^a\right)v_n\left(p_T^b\right)\cos n\Delta\phi, \tag{3}$$

where the global direction Φ_n drops out in the convolution, and v_n is assumed to be independent of η (which is approximately true within $|\eta| < 2.5$ at the LHC; see Sec. V A). Thus, if the anisotropy is driven by collective expansion, $v_{n,n}$ should factorize into the product of two single-particle harmonic coefficients [37]:

$$v_{n,n}\left(p_T^a, p_T^b\right) = v_n\left(p_T^a\right)v_n\left(p_T^b\right). \tag{4}$$

Such factorization may also be valid if the anisotropies of the two particles are independently driven by collective expansion and path-length-dependent jet energy loss (both are associated with the same initial spatial asymmetries). This factorization relation has been used to calculate the single-particle v_n [38–40]. However, autocorrelations induced by resonance decays or fragmentation of back-to-back jets, are expected to break the factorization. Therefore, Eq. (4) can be used to identify the regions of p_T^a and p_T^b where correlations are dominated by effects controlled by the initial spatial asymmetries.

The study of the structures of two-particle correlation in $\Delta\eta$ and $\Delta\phi$ has been the focus of major experimental and theoretical efforts in the last decade. In typical proton-proton collisions, where a medium is presumably not formed, the pair distributions are dominated by strong correlation peaks at $(\Delta\phi, \Delta\eta) \sim (0, 0)$ and $\Delta\phi \sim \pi$. These peaks reflect mainly autocorrelations among particles from fragmentation of back-to-back jets. In heavy-ion collisions, additional structures have been observed for $p_T < 3$–4 GeV and large $\Delta\eta$ at $\Delta\phi \sim 0$ (known as the "ridge") [41,42] and $|\Delta\phi - \pi| \sim 1.1$ (known as the "double-hump") [37,43]. These unexpected structures have been interpreted as the response of the medium to the energy deposited by quenched jets [44,45]. However, similar structures can also be generated by the flow harmonics, as they all contribute constructively at $\Delta\phi \sim 0$ but tend to cancel on the away side according to Eq. (3) [8]. Therefore, a detailed comparison between the measured pair distribution [Eq. (2)] and that expected from anisotropic flow [Eq. (3)] can determine whether the structures in two-particle correlations are a consequence of the so-called "jet-induced medium response," or whether they are a consequence of a sum of the flow harmonics.

The v_2 coefficient has been extensively studied at the RHIC [13,28,46–49] and LHC [15,16]. Results for higher-order v_n for $n \geqslant 3$ also became available recently [30,31,40]. In contrast, no experimental measurement of v_1 including systematic uncertainties exists at the LHC, although an estimate has recently been performed by a theoretical group [50] based on published ALICE data [39]. A primary complication for v_1 measurements is global momentum conservation, which induces a significant dipole component [51,52]. A "sideward" deflection of colliding ions can also lead to a small rapidity-odd (i.e., changes sign crossing $\eta = 0$) dipole component [53,54]. Therefore, the extraction of v_1 values associated with the initial dipole asymmetry requires careful separation of these contributions, which generally break the factorization relation given by Eq. (4).

This paper presents comprehensive results for v_1–v_6 over broad ranges of centrality, pseudorapidity, and p_T for charged particles in lead-lead (Pb-Pb) collisions at $\sqrt{s_{NN}} = 2.76$ TeV with the ATLAS detector at the LHC. The v_n values are measured directly using an "event plane" (EP) method for $n =$ 2–6, and are also derived from the $v_{n,n}$ measured using a two-particle correlation (2PC) method for $n =$ 1–6. These detailed measurements provide new insights into the hydrodynamic picture at low p_T, the jet energy loss picture at high p_T, and the nature of the fluctuations in the initial geometry. They also allow a detailed study of the factorization relation [Eq. (4)] over broad ranges of centrality, $\Delta\eta$, p_T^a, and p_T^b. Together, these measurements should shed light on the physics underlying the structures observed in two-particle correlation functions.

The paper is organized as follows. Sections II and III give a brief overview of the ATLAS detector, trigger, and selection criteria for events and tracks. Section IV discusses the details of the EP method and the 2PC method used to measure the v_n. Section V A presents results for v_2–v_6 from the EP method as a function of p_T, η, and centrality. Section V B presents a detailed Fourier analysis of the two-particle correlation functions to measure $v_{n,n}$ as a function of p_T^a, p_T^b, $\Delta\eta$, and centrality, which are then used to calculate v_2–v_6 via the factorization relation [Eq. (4)]. These v_n values are compared with those obtained from the EP method in Sec. V C, with a focus on understanding the structures of the 2PC in terms of single-particle v_n. Section V D presents results for v_1 based on a two-component fit of the $v_{1,1}$ data with a modified functional form of Eq. (4) that includes the contribution of global momentum conservation. Section VI gives a summary of the results and main observations.

II. ATLAS DETECTOR AND TRIGGER

The ATLAS detector [55] provides nearly full solid angle coverage of the collision point with tracking detectors, calorimeters, and muon chambers, well suited for measurements of azimuthal anisotropies over a large pseudorapidity

range.[1] This analysis primarily uses three subsystems for v_n measurement: the inner detector (ID), the barrel and endcap electromagnetic calorimeters (ECals), and the forward calorimeter (FCal). The ID is contained within the 2-T field of a superconducting solenoid magnet and measures the trajectories of charged particles in the pseudorapidity range $|\eta| < 2.5$ and over the full azimuth. A charged particle passing through the ID typically traverses three modules of the silicon pixel detector (pixel), four double-sided silicon strip modules of the semiconductor tracker (SCT) and, for $|\eta| < 2$, a transition radiation tracker composed of straw tubes. The electromagnetic energy measurement of the ECal is based on a liquid-argon sampling technology. The ECal covers the pseudorapidity range $|\eta| < 3.2$ and is used as a reference detector in the event plane measurements. The FCal consists of three longitudinal sampling layers and extends the calorimeter coverage to $|\eta| < 4.9$. It uses tungsten and copper absorbers with liquid argon as the active medium, and has a total thickness of about ten interaction lengths. The centrality measurement uses towers in all three layers of the FCal, while the event plane measurements use towers in the first two layers of the FCal excluding those at the edge of the FCal η acceptance. These selection criteria are found to minimize the effect of fluctuations in the reaction plane measurement.

The minimum-bias level-1 trigger used for this analysis requires signals in two zero-degree calorimeters (ZDCs), each positioned at 140 m from the collision point, detecting neutrons and photons with $|\eta| > 8.3$, or either one of the two minimum-bias trigger scintillator (MBTS) counters, covering $2.1 < |\eta| < 3.9$ on each side of the nominal IP. The ZDC level-1 trigger thresholds on each side are set below the peak corresponding to a single neutron, for example, as produced from Coulomb dissociation of the lead ion [56]. A level-2 timing requirement based on signals from each side of the MBTS is imposed to remove beam backgrounds.

III. EVENT AND TRACK SELECTIONS

This paper is based on approximately 8 μb^{-1} of Pb-Pb data collected in 2010 at the LHC with a nucleon-nucleon center-of-mass energy $\sqrt{s_{NN}} = 2.76$ TeV. An offline event selection requires a reconstructed vertex and a time difference $|\Delta t| < 3$ ns between the MBTS trigger counters on either side of the IP to suppress noncollision backgrounds. A coincidence between the ZDCs at forward and backward pseudorapidity is required to reject a variety of background processes, while maintaining high efficiency for non-Coulomb processes.

Events satisfying these conditions are then required to have a reconstructed primary vertex within $|z_{\rm vtx}| < 150$ mm of the nominal center of the ATLAS detector for the EP analysis. A more stringent vertex cut of 100 mm is required for the 2PC analysis, such that enough events can be found in the same $z_{\rm vtx}$ bin for the event mixing procedure (see discussion in Sec. IV B). About 48×10^6 and 43×10^6 events pass the requirements for the EP and 2PC analysis, respectively. Pileup probability is estimated to be at the 10^{-4} level and is therefore negligible.

The Pb-Pb event centrality is characterized using the total transverse energy ($\sum E_{\rm T}$) deposited in the FCal over the pseudorapidity range $3.2 < |\eta| < 4.9$ at the electromagnetic energy scale. An analysis of this distribution after all trigger and event selections gives an estimate of the fraction of the sampled non-Coulomb inelastic cross-section to be 98% ± 2% [57]. This estimate is obtained from a shape analysis of the measured FCal $\sum E_{\rm T}$ distributions compared with a convolution of proton-proton data with a Monte Carlo Glauber calculation [58]. The FCal $\sum E_{\rm T}$ distribution is then divided into a set of 5% or 10% percentile bins, together with a bin defined for the 1% most central events. The uncertainty associated with the centrality definition is evaluated by varying the effect of trigger and event selection inefficiencies as well as background rejection requirements in the most peripheral FCal $\sum E_{\rm T}$ interval [57].

Tracks are reconstructed within the full acceptance of the ID, requiring $p_{\rm T} > 0.5$ GeV and $|\eta| < 2.5$. To improve the reliability of track reconstruction in the high-multiplicity environment of heavy-ion collisions, more stringent requirements on track quality, compared to those defined for proton-proton collisions [59], are used. At least nine hits in the silicon detectors (out of a typical value of 11) are required for each track, with no missing pixel hits and not more than one missing SCT hit, in both cases where such hits are expected. In addition, the point of closest approach is required to be within 1 mm of the primary vertex in both the transverse and the longitudinal directions [16]. This selection is varied in the analysis to check the influence of both the acceptance and fake tracks. The tracking efficiency for charged particles is studied by comparing data to Monte Carlo calculations based on the HIJING event generator [60] and a full GEANT4 [61] simulation of the detector. This efficiency is estimated to be about 72% near midrapidity in central events. However, this analysis is found to be insensitive to variations in the tracking efficiency, as found previously [16]. Fake tracks from random combinations of hits are generally negligible, reaching only 0.1% for $|\eta| < 1$ for the highest multiplicity events. This rate increases slightly at large η.

IV. DATA ANALYSIS

Equation (1) implies that each harmonic component of the final-state momentum distribution is represented by its magnitude v_n and azimuthal direction Φ_n. In general, any distribution can be expanded into a set of Fourier components. However, the distinguishing feature of correlation owing to initial geometry, as opposed to other sources of correlations, is that it is a "global" correlation. That is, Φ_n specifies a common

[1] ATLAS uses a right-handed coordinate system with its origin at the nominal interaction point (IP) in the center of the detector and the z axis along the beam pipe. The x axis points from the IP to the center of the LHC ring, and the y axis points upward. Cylindrical coordinates (r, ϕ) are used in the transverse plane, ϕ being the azimuthal angle around the beam pipe. The pseudorapidity is defined in terms of the polar angle θ as $\eta = -\ln\tan(\theta/2)$.

direction, independent of the particle species, p_T and η, and it drops out in the two-particle correlations [Eq. (3)]. This feature is quite different from the correlations expected from jet fragmentation or resonance decays, which typically involve a subset of particles correlated over a finite range in $\Delta\eta$ with no preferred global direction. Thus, v_n can be measured either by correlating tracks with the Φ_n estimated in the forward direction, or it can be measured from two-particle correlations with a large $\Delta\eta$ gap. In the following, the details of these two methods are discussed.

A. Event plane method

The azimuthal angle Φ_n and the beam direction define the nth-order reaction plane.[2] However, owing to incomplete detector acceptance and finite event multiplicity, the true reaction plane angle Φ_n cannot be determined. Instead, it is approximated by the event plane angle Ψ_n, which is defined as the direction of the "flow vector" $\vec{Q}_n$, calculated in this analysis from the E_T deposited in the FCal towers in each event:

$$\begin{aligned}\vec{Q}_n &= (Q_{x,n}, Q_{y,n}) \\ &= \left(\sum E_T \cos n\phi - \left\langle \sum E_T \cos n\phi \right\rangle, \right. \\ &\quad \left. \sum E_T \sin n\phi - \left\langle \sum E_T \sin n\phi \right\rangle \right), \\ \tan n\Psi_n &= \frac{Q_{y,n}}{Q_{x,n}},\end{aligned} \tag{5}$$

where the sum ranges over towers in the first two layers of the FCal (see Sec. II). Subtraction of the event-averaged centroid removes biases owing to detector effects [62]. A standard flattening technique is then used to remove the residual nonuniformities in the event plane angular distribution [63]. These calibration procedures are similar to those used by the RHIC experiments [62,64].

The coefficient v_n is measured by correlating tracks with Ψ_n to obtain the raw values $v_n^{\text{obs}} = \langle \cos n(\phi - \Psi_n)\rangle$. The value of v_n^{obs} is then corrected by a resolution factor that accounts for the dispersion of Ψ_n about Φ_n [4]:

$$v_n = \frac{v_n^{\text{obs}}}{\text{Res}\{n\Psi_n\}} = \frac{\langle \cos n(\phi - \Psi_n)\rangle}{\langle \cos n(\Psi_n - \Phi_n)\rangle}, \tag{6}$$

where the average is performed over all events for the denominator and all tracks and all events for the numerator. The EP resolution of the FCal, $\text{Res}\{n\Psi_n\}$, is [4]

$$\begin{aligned}\text{Res}\{n\Psi_n\} &= \langle \cos n(\Psi_n - \Phi_n)\rangle \\ &= \frac{\chi_n\sqrt{\pi}}{2} e^{-\frac{\chi_n^2}{2}} \left[I_0\left(\frac{\chi_n^2}{2}\right) + I_1\left(\frac{\chi_n^2}{2}\right)\right],\end{aligned} \tag{7}$$

where I_α are the modified Bessel functions of the first kind, and χ_n (known as the "resolution parameter") is the fundamental variable that quantifies the precision of a detector for determining the event plane. The value of χ_n is proportional to the E_T-weighted harmonic coefficient v_n^{FCal} and the square root of the total multiplicity M in the FCal acceptance [4]:

$$\chi_n \propto v_n^{\text{FCal}}\sqrt{M}. \tag{8}$$

The values of χ_n and $\text{Res}\{n\Psi_n\}$ are obtained from a two-subevents (2SE) method and a three-subevents (3SE) method [4]. In the 2SE method, the signal of a detector used to measure the event plane is divided into two "subevents" covering equal pseudorapidity ranges in opposite hemispheres, such that the two subevents nominally have the same resolution. The FCal detectors located at positive and negative η, FCal_P and FCal_N, provide such a division. The resolution of each FCal subevent is calculated directly from the correlation between the two subevents:

$$\text{Res}\left\{n\Psi_n^{\text{P(N)}}\right\} = \left\langle \cos n\left(\Psi_n^{\text{P(N)}} - \Phi_n\right)\right\rangle = \sqrt{\left\langle \cos n\left(\Psi_n^{\text{P}} - \Psi_n^{\text{N}}\right)\right\rangle}. \tag{9}$$

The resolution parameter of the FCal subevent $\chi_{n,\text{sub}}$ is determined by inverting Eq. (7). The resolution parameter for the full FCal is $\chi_n = \sqrt{2}\chi_{n,\text{sub}}$, with $\sqrt{2}$ accounting for a factor of two increase in the total multiplicity [Eq. (8)]. Finally, χ_n is incorporated into Eq. (7) to obtain the resolution for the full FCal.

In the 3SE method, the $\text{Res}\{n\Psi_n\}$ value for a given subevent A is determined from its correlations with two subevents B and C covering different regions in η:

$$\text{Res}\left\{n\Psi_n^{\text{A}}\right\} = \sqrt{\frac{\left\langle \cos n\left(\Psi_n^{\text{A}} - \Psi_n^{\text{B}}\right)\right\rangle\left\langle \cos n\left(\Psi_n^{\text{A}} - \Psi_n^{\text{C}}\right)\right\rangle}{\left\langle \cos n\left(\Psi_n^{\text{B}} - \Psi_n^{\text{C}}\right)\right\rangle}}. \tag{10}$$

The large η coverage of the ID and ECal, with their fine segmentation, allows for many choices for subevents B and C. The ID and ECal are divided into a set of 22 reference subevents, each covering 0.5 units in η. The subevents B and C are chosen to ensure a minimum separation in η of 1 unit between all three subevents. This separation in η is required to suppress short-range correlations [62]. Various 3SE combinations are studied to check the sensitivity to the size of the chosen pseudorapidity gaps, as well as potential systematic effects owing to the explicit use of the correlation between FCal_P and FCal_N in the 2SE method.

Figure 1 shows the values of χ_n and $\text{Res}\{n\Psi_n\}$ measured as a function of centrality for $n = 2$–6 using the full FCal. The data points and associated statistical uncertainties are calculated using the 2SE method. However, 5% upward and 15% downward centrality-independent corrections are applied to $n = 5$ and $n = 6$, respectively, to adjust to the average of the 2SE and the 3SE estimates for the $\text{Res}\{n\Psi_n\}$. The differences between the two estimates are quoted as systematic uncertainties for $\text{Res}\{n\Psi_n\}$, and they are propagated via Eq. (7) to obtain a systematic uncertainty for χ_n. In this analysis, the centrality range for each harmonic n is chosen such that the relative statistical uncertainty for $\text{Res}\{n\Psi_n\}$ is less than 30% of its mean value, and the 2SE and 3SE estimations show good agreement. They are 0%–80% for v_2, 0%–70% for v_3 and v_4, and 0%–50% for v_5 and v_6, as indicated in Fig. 1.

[2]If the shape of Pb nuclei is approximated by the smooth Woods-Saxon function without fluctuations, Φ_n coincides with the azimuthal angle of the reaction plane defined by the beam axis and the impact parameter (the vector separating the barycenters of the two nuclei).

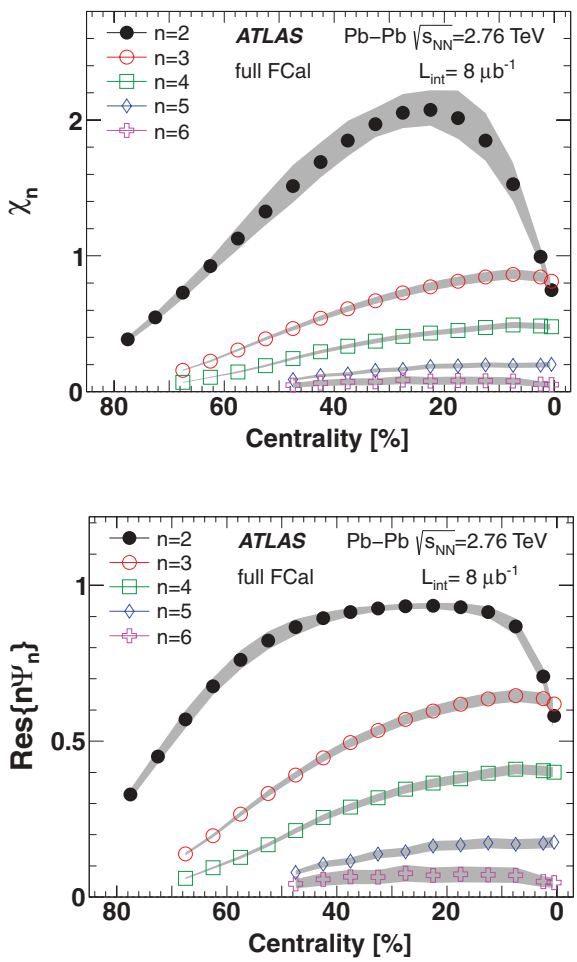

FIG. 1. (Color online) The χ_n (top) and EP resolution factor (bottom) vs centrality (smaller value refers to more central events) for $n = 2$–6, together with the systematic uncertainty as shaded bands. The EP is measured by both sides of the FCal detector (denote by "full FCal"). Note that the $\mathrm{Res}\{n\Psi_n\}$ value cannot be greater than 1 [see Eq. (7)]; thus, its systematic uncertainty shrinks as it approaches 1.

In the event plane analysis, two complementary methods are employed to measure v_n. The first ("full FCal") method calculates v_n^{obs} by correlating tracks in the ID with the EP from the full FCal detector; the resolution correction for the full FCal is then applied to obtain the final v_n [Eq. (6)]. In the second ("FCal subevent" or simply $\mathrm{FCal_{P(N)}}$) method [16], tracks with $\eta \geqslant 0$ ($\eta < 0$) are correlated with the EP in the opposite hemisphere given by the $\mathrm{FCal_N}$ ($\mathrm{FCal_P}$). The resolution correction for the $\mathrm{FCal_{P(N)}}$ is then applied to obtain the final v_n. Note that the relative statistical and systematic uncertainties for $\mathrm{Res}\{n\Psi_n\}$ are almost identical for the two methods because they both rely on similar subevent correlations [Eqs. (9) and (10)]. However, the values of v_n^{obs} from the FCal subevent method are smaller than those from the full FCal method owing to its poorer EP resolution. Therefore, these v_n^{obs} values have a larger fractional statistical uncertainty. The primary advantage of the FCal subevent method is that it increases the minimum (maximum) pseudorapidity separation between the track and the EP from about 0.8 (4.8) units for the full FCal method to about 3.3 (7.3) units. Thus, the subevent approach is less affected by short-range autocorrelations, stemming primarily from jet fragmentation and resonance decays. In this analysis, the $\mathrm{FCal_{P(N)}}$ method is used for the η dependence of v_n to minimize short-range correlations, while the full FCal method is used for the p_{T} and centrality dependence of v_n to optimize the EP resolution (see Sec. V A). However, the potential influence of short-range correlations on the full FCal method is cross-checked with the $\mathrm{FCal_{P(N)}}$ method. Good agreements are always observed for η-integrated v_n, within the systematic uncertainties for the two methods.

The systematic uncertainty in v_n^{obs} is determined by varying the track quality cuts, comparing data for different running periods, varying the full centrality range by $\pm 2\%$ according to the uncertainty in the trigger and event selections, as well as by determining the value of $\langle \sin n(\phi - \Psi_n)\rangle$. The study of track quality cuts accounts for influences of background contaminations and tracking inefficiency. Finite sine terms can arise from detector biases that introduce a correlation between the ID and the FCal. Their magnitudes relative to the cosine terms are included in the uncertainty for v_n^{obs}. All these uncertainties are generally small, except for $n = 6$. They are also quite similar for the full FCal and FCal subevent methods, so the larger of the two is quoted as the main uncertainty. As a cross-check, v_2–v_6 values are also extracted using the EP measured either for the three layers of FCal individually or for two η regions of FCal ($3.3 < |\eta| < 4.0$ and $4.0 < |\eta| < 4.8$). Although these five FCal subevents have up to a factor of four difference in their resolution corrections, the measured v_2–v_6 all agree to within 2%–10%.

Tables I–V summarize the systematic uncertainties for v_2–v_6 in various centrality intervals. The total uncertainties are calculated as the quadrature sum of all sources in these

TABLE I. Summary of relative systematic uncertainties in percentage for v_2 for both full FCal and $\mathrm{FCal_{P(N)}}$. See text for explanation of the arrangement of the uncertainties.

Centrality	0%–20%	20%–50%	50%–70%	70%–80%
Resolution (%)	5.0–2.0	1.0–2.0	3.0–4.0	4.0–6.0
Track selection (%)	2.0	0.5	0.5	1.0
Residual sine term (%)	0.8	0.6	0.5	0.2
Running periods (%)	0.2	0.2	0.5	1.0
Trigger and event selection (%)	1.0	1.0–0.5	1.0	1.5
Total (%)	5.6–3.2	1.4–2.3	3.4–4.2	4.6–6.4

TABLE II. Summary of relative systematic uncertainties in percentage for v_3 for both full FCal and $\mathrm{FCal_{P(N)}}$.

Centrality (%)	0%–20%	20%–50%	50%–70%
Resolution (%)	3.0	3.0	3.0–5.6
Track selection (%)	2.0	0.5	0.5–2.0
Residual sine term (%)	1.0	1.0	1.5
Running periods (%)	0.5	0.5–1.5	2.0
Trigger and event selection (%)	0.4	0.5–1.0	1.5–3.5
Total (%)	3.8	3.5–3.9	4.6–7.4

tables. In most cases, they are specified for multiple 5% wide centrality intervals. For example, 0%–20% in Tables I–V refers to four bins: 0%–5%, 5%–10%, 10%–15%, and 15%–20%; a "5.0–2.0" notation indicates the values of relative systematic uncertainty in percentage at the beginning and at the end of the 0%–20% centrality interval. Tables IV and V also quote the uncertainty for the 0%–1% centrality interval, which generally has the same systematic uncertainty as that for the 0%–5% centrality interval, but with a larger statistical uncertainty. The systematic uncertainties include only those associated with the measurements themselves, and no attempt is made to disentangle potential contributions from various sources of autocorrelations, as their exact origin and quantitative effects on v_n are not fully understood [5]. Nevertheless, these autocorrelations should be largely suppressed by the large average η gap between the ID and the detector used for determining the EP.

B. Two-particle correlation method

The two-particle correlation function is generally defined as the ratio of the same-event pair (foreground) distribution to the combinatorial pair (background) distribution in two-particle phase space $(\phi_\mathrm{a}, \phi_\mathrm{b}, \eta_\mathrm{a}, \eta_\mathrm{b})$:

$$C(\phi_\mathrm{a}, \phi_\mathrm{b}, \eta_\mathrm{a}, \eta_\mathrm{b}) = \frac{\frac{d^4N}{d\phi_\mathrm{a}d\eta_\mathrm{a}d\phi_\mathrm{b}d\eta_\mathrm{b}}}{\frac{d^2N}{d\phi_\mathrm{a}d\eta_\mathrm{a}} \times \frac{d^2N}{d\phi_\mathrm{b}d\eta_\mathrm{b}}}. \tag{11}$$

In practice, the correlation function is usually studied as a function of relative azimuthal angle $(\Delta\phi)$ and relative pseudorapidity $(\Delta\eta)$, by averaging pair distributions over the detector acceptance:

$$C(\Delta\phi, \Delta\eta) = \frac{S(\Delta\phi, \Delta\eta)}{B(\Delta\phi, \Delta\eta)}, \tag{12}$$

TABLE III. Summary of relative systematic uncertainties in percentage for v_4 for both full FCal and $\mathrm{FCal_{P(N)}}$.

Centrality	0%–20%	20%–50%	50%–70%
Resolution (%)	4.0	4.0	4.4–16.0
Track selection (%)	1.0	1.0–2.0	4.0
Residual sine term (%)	2.0	2.0	3.0–5.0
Running periods (%)	1.0	1.5–2.0	4.0
Trigger and event selection (%)	0.6	0.7	1.0–2.0
Total (%)	4.9	4.9–5.4	7.9–17.5

TABLE IV. Summary of relative systematic uncertainties in percentage for v_5 for both full FCal and $\mathrm{FCal_{P(N)}}$.

Centrality	0%–1%	0%–20%	20%–40%	40%–50%
Resolution (%)	10.8	10.2	10.2–10.4	11.2–22.4
Track selection (%)	1.0	1.0	1.0	2.0
Residual sine term (%)			5.0	
Running periods (%)	2.0	2.0	2.0	4.0
Trigger and event selection (%)			1.0	
Total (%)	12.1	11.6	11.6–12.1	13.0–23.0

where

$$S(\Delta\phi, \Delta\eta) = \int d\phi_\mathrm{a}d\eta_\mathrm{a}d\phi_\mathrm{b}d\eta_\mathrm{b}\delta_\mathrm{ab}\frac{d^4N}{d\phi_\mathrm{a}d\eta_\mathrm{a}d\phi_\mathrm{b}d\eta_\mathrm{b}}, \tag{13}$$

$$B(\Delta\phi, \Delta\eta) = \int d\phi_\mathrm{a}d\eta_\mathrm{a}d\phi_\mathrm{b}d\eta_\mathrm{b}\delta_\mathrm{ab}\frac{d^2N}{d\phi_\mathrm{a}d\eta_\mathrm{a}}\frac{d^2N}{d\phi_\mathrm{b}d\eta_\mathrm{b}}. \tag{14}$$

The δ_ab is a shorthand notation for $\delta(\phi_\mathrm{a} - \phi_\mathrm{b} - \Delta\phi)\delta(\eta_\mathrm{a} - \eta_\mathrm{b} - \Delta\eta)$.

For an ideal detector, the combinatorial pair distribution is uniform in $\Delta\phi$ and has a nearly triangular shape in $\Delta\eta$ owing to the weak dependence of the single-particle distribution on η [57]. In reality, both same-event and combinatorial pair distributions are modulated by detector inefficiencies and nonuniformity. These detector effects influence the two distributions in the same way so they cancel in the ratio. Therefore, $B(\Delta\phi, \Delta\eta)$ is often referred to as the pair acceptance function [37]. In this analysis, $B(\Delta\phi, \Delta\eta)$ is estimated from track pairs from two events with similar centrality (matched within 5%) and z_vtx (matched within 1 mm). The two particles in the pair are typically selected with different conditions, such as different p_T ranges, pseudorapidities, and charge signs. In this analysis, charged particles measured by the ID with a pair acceptance extending up to $|\Delta\eta| = 5$ are used.

Figure 2(a) shows the two-dimensional (2D) correlation function for pairs from a representative p_T range of 2–3 GeV and 0%–5% centrality interval. It reveals the characteristic long-range near-side ridge and away-side double-hump structures that were observed previously in heavy-ion collisions at the RHIC for a similar p_T range [41–43]. A narrow short-range correlation peak is also seen at $(\Delta\phi, \Delta\eta) \sim (0, 0)$, presumably owing to autocorrelations from jet fragmentation and resonance decays. From the 2D correlation function, a one-

TABLE V. Summary of relative systematic uncertainties in percentage for v_6 for both full FCal and $\mathrm{FCal_{P(N)}}$.

Centrality	0%–1%	0%–20%	20%–40%	40%–50%
Resolution (%)	58	34–31	31	32–38
Track selection (%)			10	
Residual sine term (%)			10	
Running periods (%)			10	
Trigger and event selection (%)			1	
Total (%)	61	38–35	36	37–42

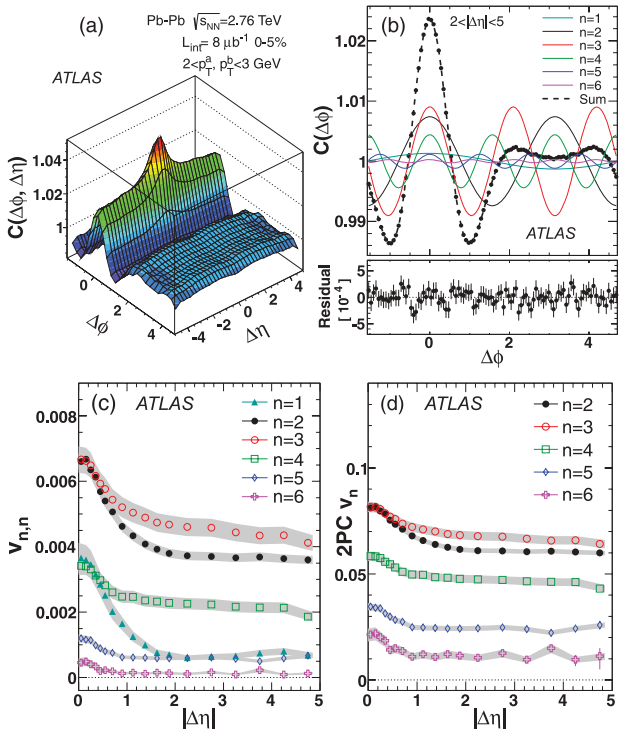

FIG. 2. (Color online) The steps involved in the extraction of v_n values for 2–3 GeV fixed-p_T correlations in the 0%–5% centrality interval: (a) 2D correlation function; (b) the 1D $\Delta\phi$ correlation function for $2 < |\Delta\eta| < 5$ (rebinned into 100 bins), overlaid with contributions from the individual $v_{n,n}$ components and their sum, as well as the residual difference between the data and the sum; (c) Fourier coefficient $v_{n,n}$ vs $|\Delta\eta|$ for $n = 1$–6; and (d) v_n vs $|\Delta\eta|$ for $n = 2$–6. The shaded bands in (c) and (d) indicate the systematic uncertainties, as described in the text.

dimensional (1D) $\Delta\phi$ correlation function can be constructed for a given $\Delta\eta$ interval:

$$C(\Delta\phi) = A \times \frac{\int S(\Delta\phi, \Delta\eta) d\Delta\eta}{\int B(\Delta\phi, \Delta\eta) d\Delta\eta}. \quad (15)$$

The normalization constant A is determined by scaling the number of pairs in $2 < |\Delta\eta| < 5$ to be the same between the foreground (S) and background (B). This normalization is then applied to other $\Delta\eta$ intervals. Each 1D correlation function is expanded into a Fourier series according to Eq. (2), with coefficients $v_{n,n}$ calculated directly via a discrete Fourier transformation (DFT):

$$v_{n,n} = \langle \cos n\Delta\phi \rangle = \frac{\sum_{m=1}^{N} \cos(n\Delta\phi_m) C(\Delta\phi_m)}{\sum_{m=1}^{N} C(\Delta\phi_m)}, \quad (16)$$

where $n = 1$–15, and $N = 200$ is the number of $\Delta\phi$ bins. A small upward relative correction is applied ($\sim$0.15% for $n = 6$ and increasing to 1% for $n = 15$) to account for the finite $\Delta\phi$ bin width. Figure 2(b) shows one such 1D correlation function for $2 < |\Delta\eta| < 5$, overlaid with the corresponding contributions from individual $v_{n,n}$ components. The shape of the correlation function is well described by the sum of the first six $v_{n,n}$ components.

According to Eq. (4), if the correlations are dominated by those arising from asymmetry of the initial geometry such as flow, $v_{n,n}$ should factorize into the product of two single-particle harmonic coefficients. This is found to be the case for $n \geqslant 2$ at low p_T for pairs with a large $\Delta\eta$ gap, but is not true for $n = 1$ (see Secs. V B and V C), similar to what was also found in other measurements [39,40]. Thus, if the two particles are selected from the same p_T interval ("fixed-p_T" correlations) as in Fig. 2, the single-particle v_n for $n \geqslant 2$ can be calculated as $v_n = \sqrt{v_{n,n}}$. When $v_{n,n} < 0$, v_n is defined as $v_n = -\sqrt{|v_{n,n}|}$ (or $v_n = v_{n,n}/\sqrt{|v_{n,n}|}$ in general). This calculation is repeated for all 1D correlation functions in each $|\Delta\eta|$ slice. The resulting full $|\Delta\eta|$ dependencies of $v_{n,n}$ and v_n are shown in Figs. 2(c) and 2(d), respectively.

The $v_{n,n}$ and v_n values are found to vary rapidly for $|\Delta\eta| \lesssim 1$, presumably reflecting the influence of the short-range correlation at $(\Delta\phi, \Delta\eta) \sim (0, 0)$ [Fig. 2(a)], but they decrease much more slowly for larger $|\Delta\eta|$. This slow decrease is expected because the single-particle v_n also decreases very slowly with η (see Fig. 3), and the factorization relation Eq. (4) is valid for the present p_T range (see Sec. V B). These behaviors suggest that the autocorrelations from near-side jet fragmentation and resonance decays can be largely eliminated by requiring a large $\Delta\eta$ gap (e.g., $|\Delta\eta| > 2$).

Each "fixed-p_T" correlation function provides a reference v_n for a chosen p_T range (denoted by superscript "a"). Tracks from this p_T range are then correlated with those from a target p_T range (denoted by superscript "b"), and this "mixed-p_T" correlation is used to calculate $v_{n,n}$ and to obtain the v_n in the target p_T via Eq. (4). Because factorization is expected to be valid for the anisotropies driven by the initial geometry, but is broken by the presence of autocorrelations among the jet fragmentation products, the level of consistency between v_n obtained from different reference p_T ranges reveals whether the 2PC is dominated by anisotropies driven by the initial geometry. A detailed study of the factorization properties of v_1–v_6 is presented in Sec. V B.

The correlation function relies on the pair acceptance function to reproduce and cancel the detector acceptance effects in the foreground distribution. Mathematically, the pair acceptance function in $\Delta\phi$ is simply a convolution of two single-particle azimuthal distributions and should be uniform in $\Delta\phi$ without detector imperfections. A natural way of quantifying the influence of detector effects on $v_{n,n}$ and v_n is to transform the single-particle and pair acceptance functions into the Fourier space. The resulting coefficients for pair acceptance $v_{n,n}^{\rm det}$ are the product of those for the two single-particle acceptances $v_n^{\rm det,a}$ and $v_n^{\rm det,b}$. In general, the pair acceptance function is quite flat: The maximum variation from its average is observed to be less than 0.001 for pairs integrated over $2 < |\Delta\eta| < 5$, and the corresponding $|v_{n,n}^{\rm det}|$ values are found to be less than 1.5×10^{-4}. These $v_{n,n}^{\rm det}$ values are expected to mostly cancel in the correlation function, and only a small fraction contributes to the uncertainties of the pair acceptance function. Three possible residual effects for $v_{n,n}^{\rm det}$ are studied: (1) the time dependence of the pair acceptance, (2) the effect of imperfect centrality matching, and (3) the effect of imperfect $z_{\rm vtx}$ matching. In each case, the residual $v_{n,n}^{\rm det}$ values

are evaluated by a Fourier expansion of the ratio of the pair acceptances before and after the variation. Overall, significant deviations are observed only for the effect of imperfect $z_{\rm vtx}$ matching, and they are generally larger for narrower $|\Delta\eta|$ ranges and higher $p_{\rm T}$.

The systematic uncertainty of the pair acceptance is the quadrature sum of these three estimates, which is $\delta v_{n,n} = (2.5–8) \times 10^{-6}$ depending on n, $p_{\rm T}$, and the width of $|\Delta\eta|$ interval. This absolute uncertainty is propagated to the uncertainty in v_n, and it is the dominant uncertainty when v_n is small, for example, for v_6. Moreover, results for inclusive charged particles are compared to those obtained independently using same-charge and opposite-charge pairs. These two types of correlations have somewhat different pair acceptances owing to different relative bending directions between the two tracks. They are found to give consistent results for $n \leqslant 6$, where the $v_{n,n}$ values are dominated by physics effects. However, small systematic deviations are observed for $n \geqslant 8$, where the $v_{n,n}$ values are expected to be dominated by acceptance effects. Therefore, the systematic uncertainty also includes the RMS difference of the $v_{n,n}$ values averaged for $8 \leqslant n \leqslant 15$ between the two types of correlations. This uncertainty is usually much smaller than those associated with $v_{n,n}^{\rm det}$, except for large $p_{\rm T}$.

The second type of systematic uncertainty includes the sensitivity of the analysis to track quality cuts, variation between different running periods, trigger and event selection, as well as the ability to reproduce the input v_n in fully simulated, digitized, and reconstructed HIJING events with azimuthal anisotropy imposed on the generated particles. Most systematic uncertainties cancel for the correlation function when dividing the foreground and background distributions. The estimated residual effects are summarized in Table VI.

The total systematic uncertainties are the quadrature sum of the uncertainties calculated from pair acceptance, the rms difference of the $v_{n,n}$ averaged for $8 \leqslant n \leqslant 15$ between the same-charge and opposite-charge correlations, and those listed in Table VI. They are then propagated to uncertainties for v_n. These uncertainties are plotted as shaded bands around the data points in Figs. 2(c) and 2(d). Most of these uncertainties are correlated between different $p_{\rm T}$ ranges. However, a fraction of them are found to be uncorrelated with $p_{\rm T}$, coming mainly from the track selection, running period variation, and MC comparison in Table VI and the pair acceptance. This fraction (point to point in $p_{\rm T}$) is estimated to be about 30% of the final systematic uncertainty, and the remaining uncertainty is treated as a $p_{\rm T}$-correlated systematic uncertainty. They are used in the discussion of the $v_{1,1}$ results in Sec. V D.

TABLE VI. Relative systematic uncertainties for v_n in percentage from tracking cuts, variation between different running periods, centrality variation, consistency between truth and reconstructed v_n in HIJING simulation, and the quadrature sum of individual terms.

	v_1	v_2	v_3	v_4	v_5	$v_{n\|n\geqslant 6}$
Track selection (%)	3.0	0.3	0.3	1.0	2.0	4
Running periods (%)	5.0	0.3–1.0	0.7–2.1	1.2–3.1	2.3	7–11
Trigger and event selection (%)	1.0	0.5–1.0	0.5–1.5	0.5–1	1.0	5
MC consistency (%)	2.0	1.0	1.5	2.0	3.5	5
Sum of above (%)	6.3	1.2–1.8	1.8–3.0	2.6–3.9	4.8	11–14

V. RESULTS

A. v_2–v_6 from the event plane method

Figure 3 shows the η dependence of v_n for several centrality intervals in the 2- to 3-GeV $p_{\rm T}$ range from the $\rm FCal_{P(N)}$ EP method. Similar behaviors are observed in other $p_{\rm T}$ ranges (see also [16] for v_2). The v_2 values decrease by less than 5% toward large $|\eta|$ for central and midcentral events, and the decrease is more pronounced both for $n \geqslant 3$ and for peripheral events.

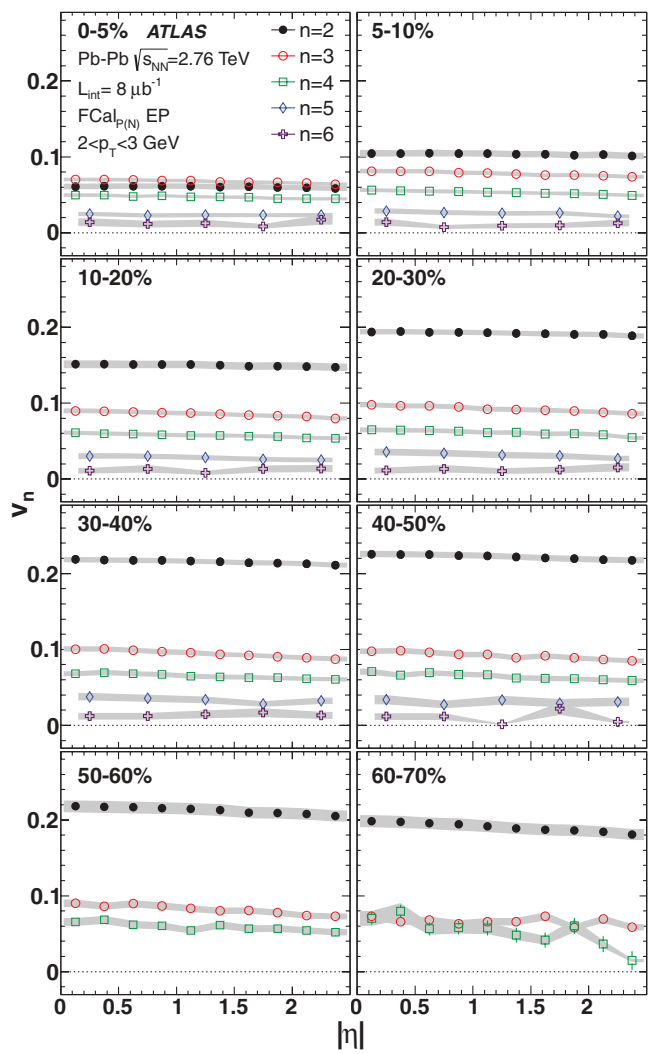

FIG. 3. (Color online) v_n vs η for $2 < p_{\rm T} < 3$ GeV from the $\rm FCal_{P(N)}$ method (i.e., the EP is measured by either $\rm FCal_N$ or $\rm FCal_P$) with each panel representing one centrality interval. The shaded bands indicate systematic uncertainties from Tables I–V.

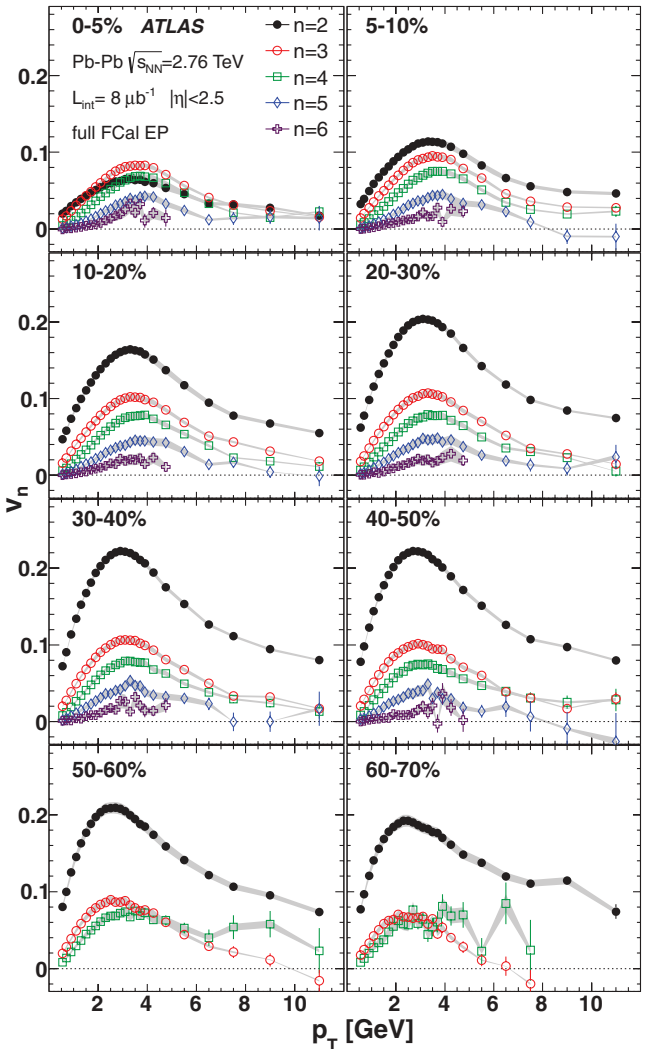

FIG. 4. (Color online) v_n vs p_T for several centrality intervals. The shaded bands indicate the systematic uncertainties from Tables I–V.

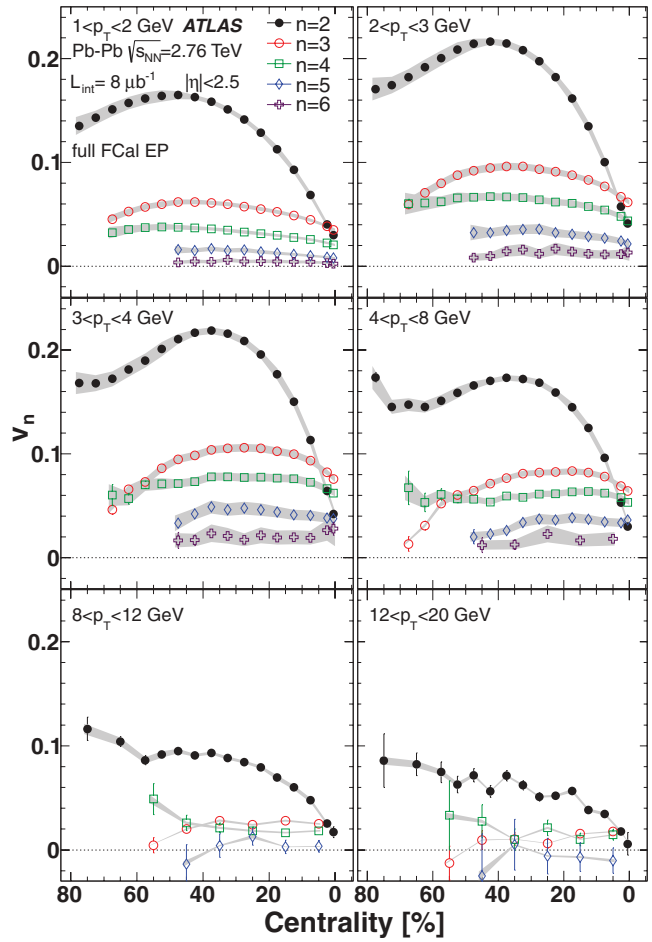

FIG. 5. (Color online) v_n vs centrality for six p_T ranges from the full FCal event plane method. The shaded bands indicate systematic uncertainties from Tables I–V.

Figure 4 shows the p_T dependence of v_2–v_6 for several centrality intervals. All v_n increase with p_T in the range up to 3–4 GeV and then decrease. However, they remain positive even at the highest measured p_T, where occasional fluctuations to negative values do not exceed the statistical precision. This turnover behavior in p_T was also observed at RHIC for v_2 [28,65], and it is associated with the transition from anisotropy driven by the collective expansion to anisotropy driven by a path-length-dependent jet energy loss [2,29]. The overall magnitude of v_n also decreases with increasing n, except in the most central events where v_3 is the largest.

Figure 5 shows the centrality dependence of v_n for several p_T ranges. The centrality intervals are presented in 5% or 10% increments, with an additional interval for the 1% most central events. Going from central to peripheral events (from right to left along the x axis), v_2 first increases, reaching a maximum in the 30%–50% centrality range, and then decreases. The higher-order coefficients v_3–v_6 show a similar, but much weaker, centrality dependence, and this behavior is consistent with an anisotropy related to the fluctuations in the initial geometry [32]. For most of the measured centrality range, v_2 is much larger than the other harmonic coefficients. In central events, however, v_3 and/or v_4 becomes larger than v_2 for some p_T ranges. At high p_T (>4 GeV), v_2 increases toward more peripheral events, presumably reflecting the dominance of autocorrelations from dijets.

In an ideal hydrodynamics scenario, v_n at low p_T is a power-law function of the radial expansion velocity of the fluid, leading to the qualitative expectation that $v_n(p_T)$ is a power-law function of p_T [9,66]. Previous RHIC results have shown that v_4/v_2^2 (or equivalently $v_4^{1/4}/v_2^{1/2}$) is almost independent of p_T [48,49].[3] Figure 6 shows $v_n^{1/n}/v_2^{1/2}$ vs p_T for various centrality intervals. These ratios vary weakly with p_T except in the 5% most central events, suggesting that such a scaling relation largely accounts for the p_T dependence.

[3]This v_4 was measured relative to the Φ_2 instead of the Φ_4 reaction plane and is known as mixed harmonics [4]. It can be regarded as a projection of v_4 measured in the Φ_4 onto the Φ_2.

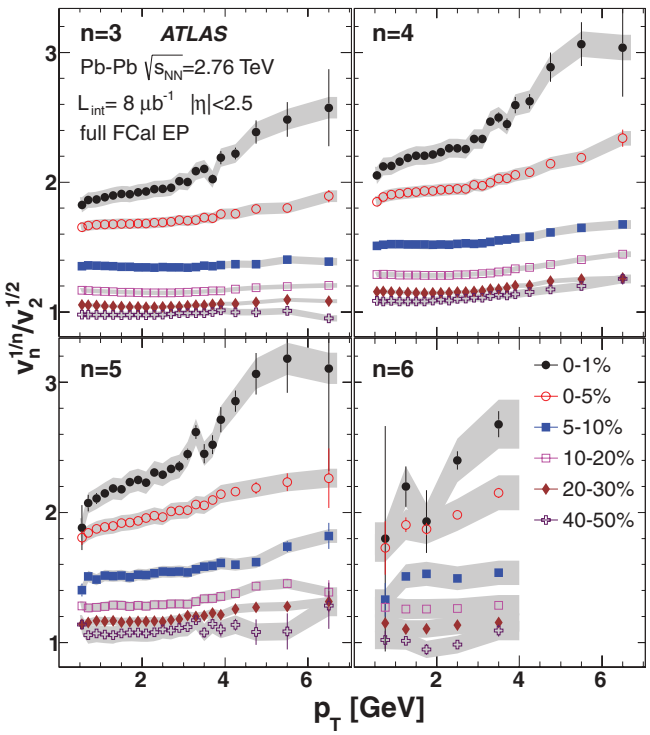

FIG. 6. (Color online) $v_n^{1/n}/v_2^{1/2}$ vs p_{T} for several centrality intervals. The shaded bands indicate the total systematic uncertainties.

However, the overall magnitudes of the ratios seem to vary with centrality and also vary slightly with n.

Figure 7 shows the centrality dependence of $v_n^{1/n}/v_2^{1/2}$ for $2 < p_{\mathrm{T}} < 3$ GeV. Given that the ratios vary weakly with p_{T}, the results for other p_{T} ranges are similar. The ratios are almost independent of centrality in midcentral and peripheral events, but then increase sharply toward more central events, with a total change of almost a factor of two over the 0%–20% centrality range. In addition, the ratios for $n = 4$–6 are similar to each other, while they are systematically higher than those for $n = 3$. A similar centrality dependence was observed for the v_4/v_2^2 ratio at the RHIC and was argued to reflect the centrality dependence of fluctuations in the initial geometry [49].

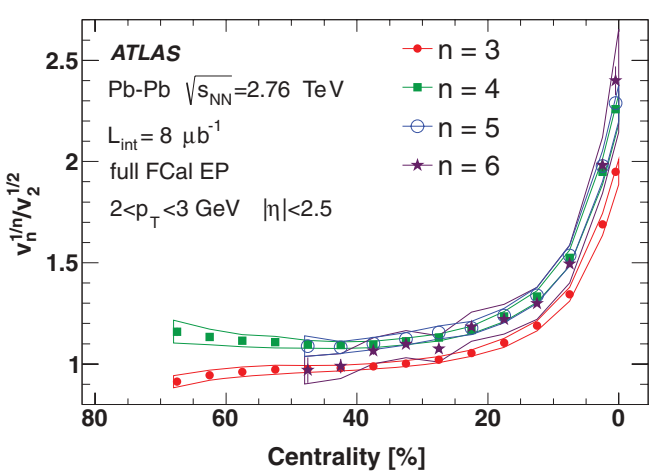

FIG. 7. (Color online) $v_n^{1/n}/v_2^{1/2}$ vs centrality for $2 < p_{\mathrm{T}} < 3$ GeV. Lines indicate systematic uncertainty bands, calculated by assuming that the uncertainties for different v_n are independent.

B. v_2–v_6 from the two-particle correlation method

Figure 8 shows the evolution of the 2D correlation function with centrality for particles with $2 < p_{\mathrm{T}} < 3$ GeV. While central events show structures that are long range in $\Delta\eta$ (the ridge and double-hump), the more peripheral events show a systematic disappearance of these long-range structures and the emergence of clear jet-related peaks on the away side. The magnitude of the long-range structures, measured as deviation from unity, exhibits a characteristic centrality dependence. Figure 8 shows that the near-side ridge (relative to unity) starts at about 0.015 in the 1% most central events, increases to 0.12 in 30%–50% midcentral events, and then decreases and disappears in the most peripheral (80%–90%) events. Because the harmonics for different n all contribute positively to the correlation function at $\Delta\phi = 0$, this nonmonotonic centrality dependence simply reflects the fact that v_n for $n \geqslant 2$ all reach their maxima in the 30%–50% centrality range for this p_{T} selection, as shown in Fig. 5. The away-side long-range structure exhibits a similar centrality dependence, but is complicated by the contribution from the recoil jet, which starts to dominate the away-side shape in the 60%–90% centrality range.

As discussed in Sec. IV B and shown in Fig. 2, each 2D correlation function is projected onto a set of 1D $\Delta\phi$ correlation functions in slices of $|\Delta\eta|$, and the Fourier coefficients $v_{n,n}$ and v_n are calculated from these distributions. Examples of such 1-D correlation functions are shown in Fig. 9 for pairs with $2 < |\Delta\eta| < 5$ and $3 < p_{\mathrm{T}} < 4$ GeV, together with individual contributions from the first six $v_{n,n}$ components. In a scenario where the Fourier coefficients are dominated by anisotropic flow, the value of the correlation function at $\Delta\phi \sim 0$ should be larger than its value at $\Delta\phi \sim \pi$ [see Eq. (3)]. This indeed is the case up to the 40%–50% centrality interval, but for centralities greater than 50% the trend reverses. This reversing of the asymmetry between the near- and away-side amplitudes correlates with a continuous decrease of $v_{1,1}$, which eventually becomes negative at around the 40%–50% centrality interval (also see top panel of Fig. 11). The correlation function in the 80%–90% centrality interval shows that a broad peak from the away-side jet predominantly generate a negative $v_{1,1}$ and a positive $v_{2,2}$. Therefore, they tend to cancel each other at the near side but add up at the away side. This behavior suggests that in peripheral collisions and at low p_{T}, the appearance of a large negative $v_{1,1}$ is a good indicator for a significant contribution of autocorrelations from jets to $v_{2,2}$.

Figure 10 shows Fourier decomposition of the correlation functions in the 0%–10% centrality interval for several p_{T} ranges. Again, a large pseudorapidity gap of $|\Delta\eta| > 2$ is required to suppress the near-side jet peak and to expose the long-range structures. At low p_{T}, the $v_{n,n}$ components are mainly driven by these long-range structures. However, for $p_{\mathrm{T}}^{\mathrm{a}}, p_{\mathrm{T}}^{\mathrm{b}} > 6$ GeV, they are dominated by the pronounced

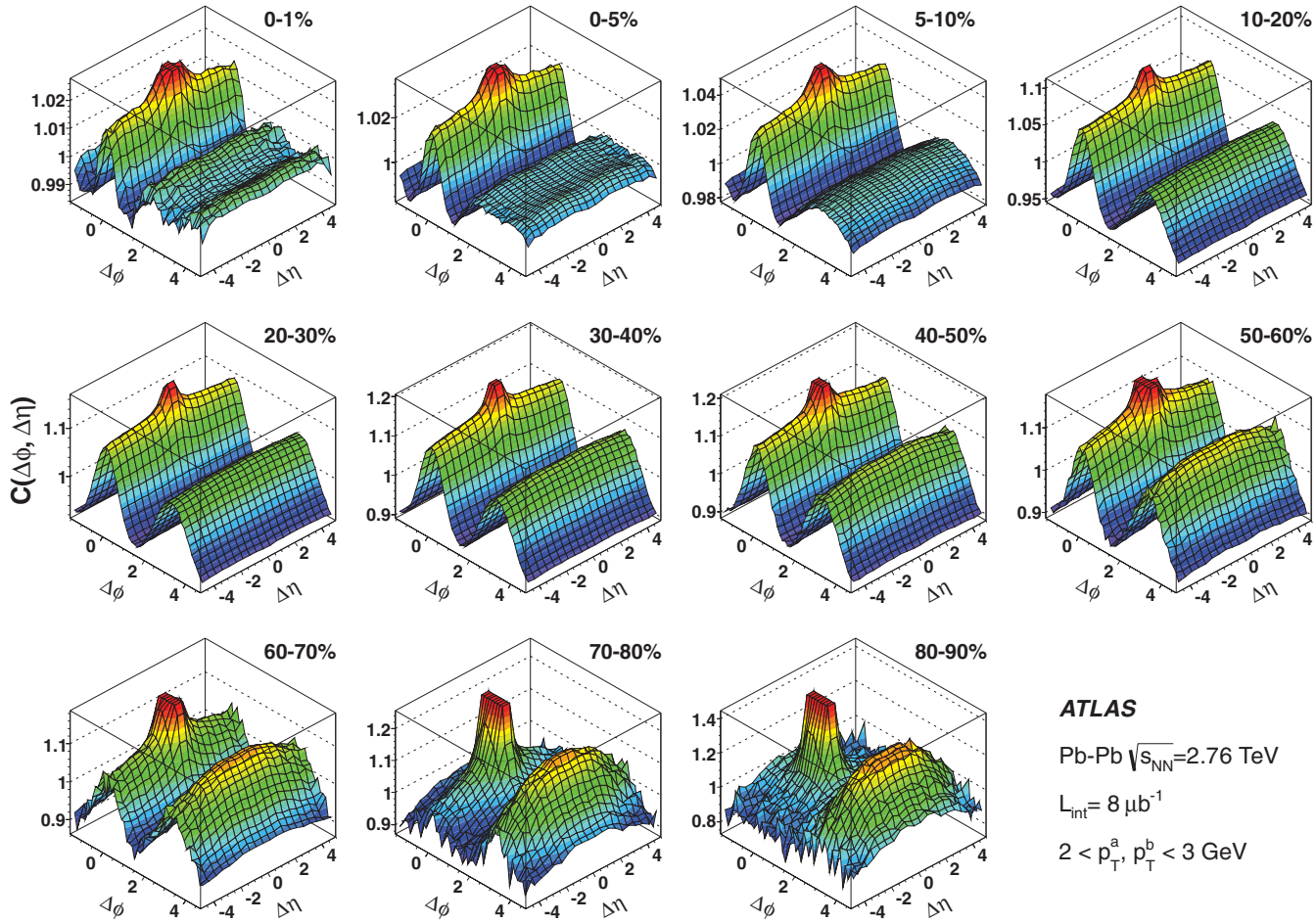

FIG. 8. (Color online) 2D correlations for $2 < p_T^a,\ p_T^b < 3$ GeV in several centrality intervals. The near-side jet peak is truncated from above to better reveal the long-range structures in $\Delta\eta$.

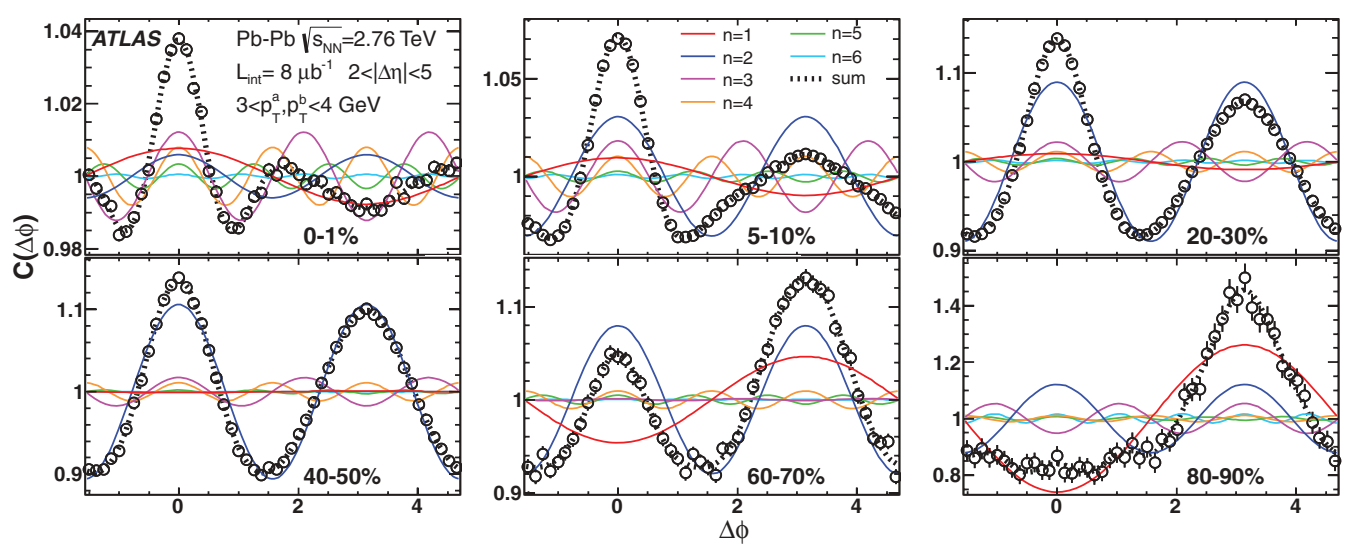

FIG. 9. (Color online) Centrality dependence of $\Delta\phi$ correlations for $3 < p_T^a,\ p_T^b < 4$ GeV. A rapidity gap of $2 < |\Delta\eta| < 5$ is required to isolate the long-range structures of the correlation functions; that is, the near-side peaks reflect the ridge instead of the autocorrelations from jet fragments. The error bars on the data points indicate the statistical uncertainty. The superimposed solid lines (thick dashed lines) indicate contributions from individual $v_{n,n}$ components (sum of the first six components).

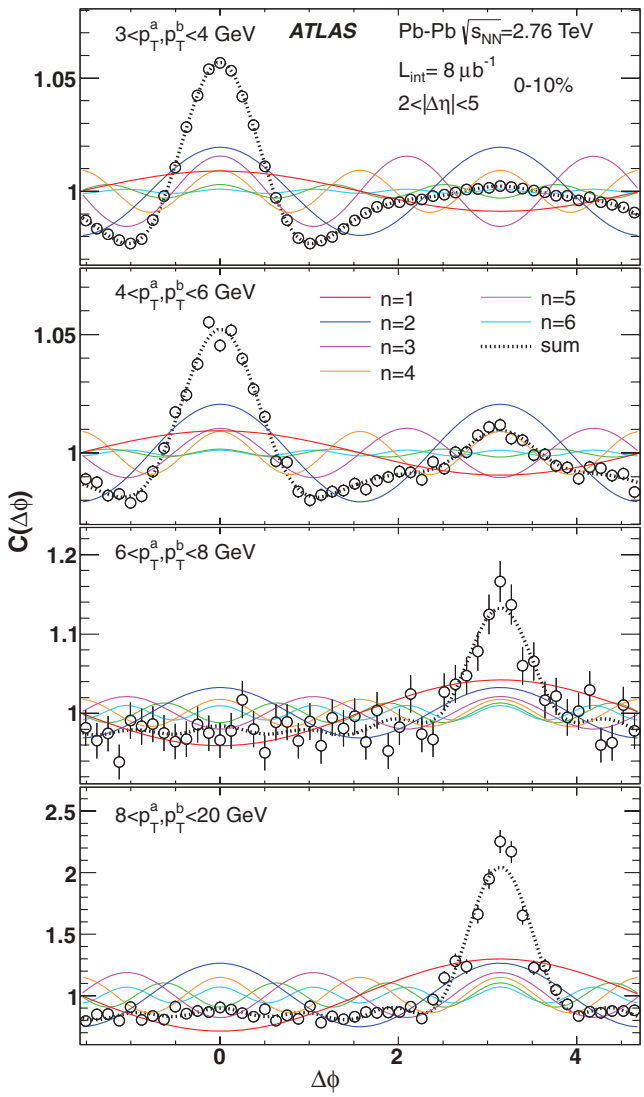

FIG. 10. (Color online) Fixed-p_T correlation function in the 0%–10% centrality interval for several p_T ranges. A rapidity gap of $2 < |\Delta\eta| < 5$ is required to isolate the long-range structures of the correlation functions. The error bars on the data points indicate the statistical uncertainty. The superimposed solid lines (thick dashed lines) indicate contributions from individual $v_{n,n}$ components (sum of the first six components).

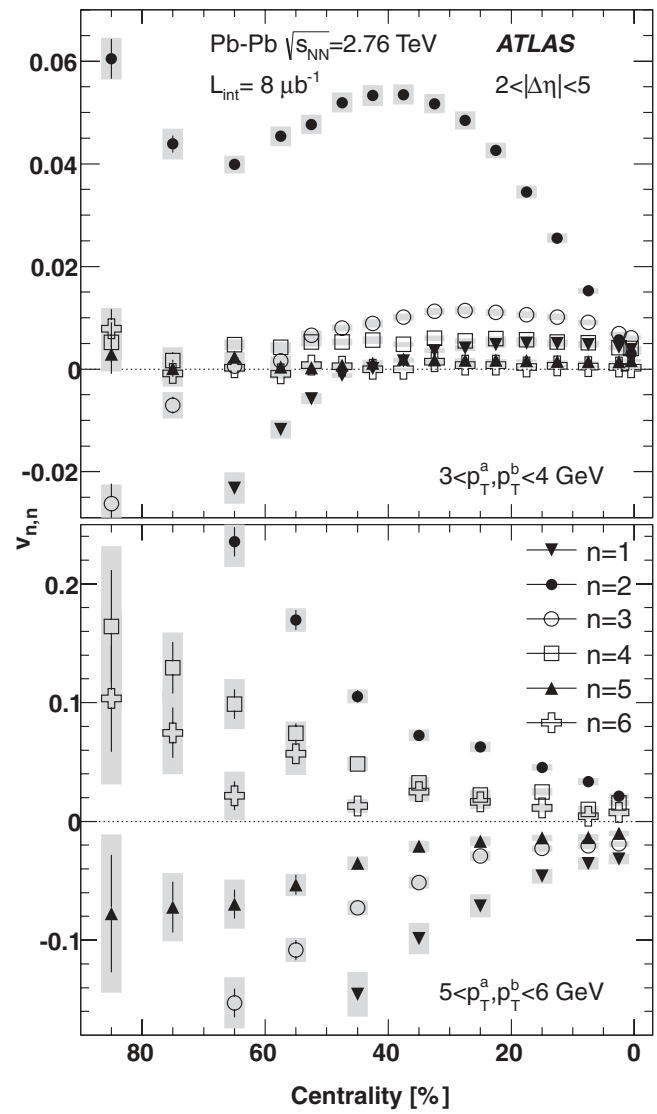

FIG. 11. $v_{n,n}$ vs centrality obtained from fixed-p_T correlations with $2 < |\Delta\eta| < 5$ for a low p_T interval (top) and a high p_T interval (bottom). The error bars (shaded bands) indicate the statistical (systematic) uncertainties.

away-side jet correlation centered at $\Delta\phi = \pi$, leading to $v_{n,n}$ values with alternating sign: $(-1)^n$. Figure 11 contrasts the centrality dependence of the $v_{n,n}$ for a low-p_T range (top panel) and a high-p_T range (bottom panel). It shows that at low p_T, the sign flipping of $v_{n,n}$ between even and odd n happens only for peripheral events; at high p_T the sign flipping happens over the entire centrality range. More details on the variation of the correlation functions and $v_{n,n}$ values as a function of p_T^a and p_T^b are shown in Figs. 29–36 in the Appendix.

As discussed in Sec. I, a necessary condition for the $v_{n,n}$ to reflect anisotropy associated with the initial spatial asymmetries is that it should factorize into the product of two single-particle v_n. A direct way to verify the factorization is to check whether the target $v_n(p_T^b)$ calculated as

$$v_n(p_T^b) = \frac{v_{n,n}(p_T^a, p_T^b)}{v_n(p_T^a)} = \frac{\sqrt{|v_{n,n}(p_T^a, p_T^a)|}\, v_{n,n}(p_T^a, p_T^b)}{v_{n,n}(p_T^a, p_T^a)}, \tag{17}$$

is independent of the reference p_T^a. Figure 12 shows one such study of $n = 1$–6 for $1 < p_T^b < 1.5$ GeV using four different reference p_T^a ranges. The $v_1(p_T^b)$ values calculated this way clearly change with the choice of p_T^a, indicating a breakdown of the factorization over the measured p_T range. This breakdown is mainly attributable to contributions from global momentum conservation for a system with finite multiplicity. More detailed discussions of the physics behind this breakdown and ways to separate different contributions

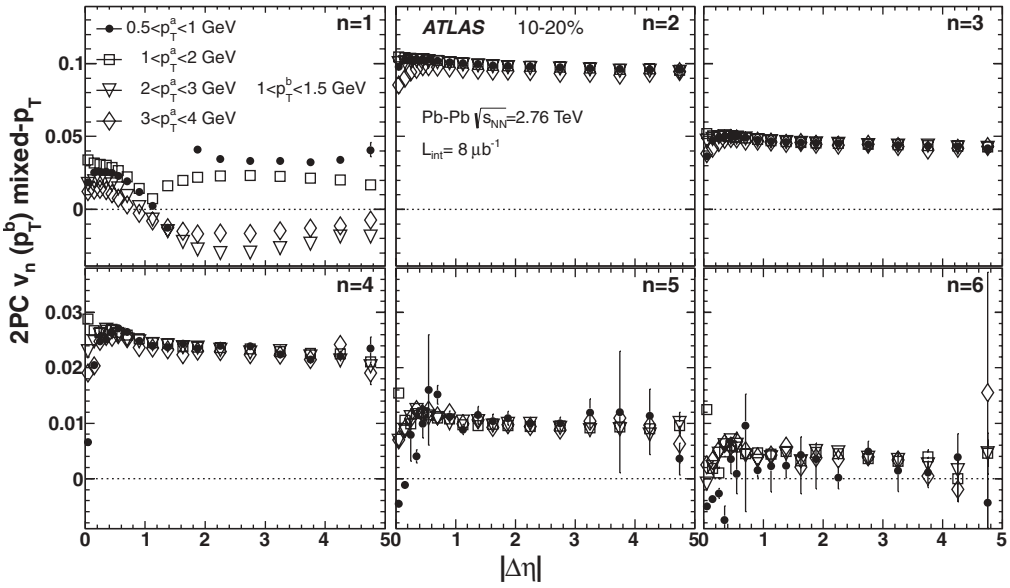

FIG. 12. $v_n(p_T^b) = \frac{v_{n,n}(p_T^a, p_T^b)}{v_n(p_T^a)}$ vs $|\Delta\eta|$ for $1 < p_T^b < 1.5$ GeV, calculated from a reference v_n in four p_T^a ranges (0.5–1, 1–2, 2–3, and 3–4 GeV). The error bars indicate the statistical uncertainties. As discussed in the text, the v_1 defined this way is strongly biased by global momentum conservation and should be distinguished from the collective v_1 discussed in Sec. V D.

and extract the v_1 associated with dipole asymmetry from $v_{1,1}$ are presented in Sec. V D.

Figure 12 shows that the factorization holds for $n = 2$–6 for $|\Delta\eta| > 1$. Despite a factor of three variation in the reference v_n value for the p_T ranges from 0.5–1 GeV to 3–4 GeV (see Fig. 4), the extracted $v_n(p_T^b)$ for $n = 2$–6 is constant within statistical uncertainties for $|\Delta\eta| > 1$. This factorization check is repeated for $n = 2$–6 for various ranges of p_T^a, p_T^b, and centrality. For correlations with the default choice of $|\Delta\eta| > 2$ used in this paper, factorization is found to hold at the 5%–10% level for $p_T < 3$–4 GeV in the 70% most central events. Further studies of this topic are presented in Sec. V C.

Figure 13 shows the extracted Fourier coefficients, v_n vs n, for several fixed-p_T correlations with $|\Delta\eta| > 2$ and for the 1% most central events. The $p_T^{a,b}$ ranges are restricted to below 4 GeV, where the factorization for v_2–v_6 works reasonably well. Significant signals are observed for $n \leqslant 6$, while the signals for $n > 6$ are consistent with zero within statistical and systematic uncertainties. Note that in cases where the uncertainty of $v_{n,n}$ is comparable to its own value, the v_n uncertainty becomes asymmetric and highly non-Gaussian. A complete compilation of the Fourier coefficients for other centrality intervals is included in Figs. 22–27 in the Appendix. Recent model comparisons indicate that these results can provide important constraints on the nature of initial geometry fluctuations and the shear viscosity of the created matter [34].

C. Comparison of v_2–v_6 from the two methods

Figure 14 compares the centrality dependence of v_n obtained from the 2PC method and the EP method at low p_T. They agree within 5% for v_2–v_4, 10% for v_5, and 15%

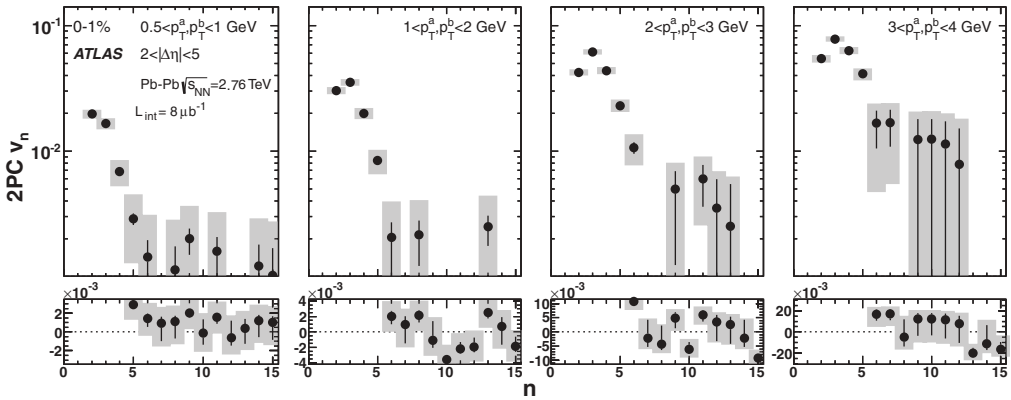

FIG. 13. v_n vs n for $n \geqslant 2$ in a 0%–1% centrality interval from four fixed-p_T correlations (0.5–1, 1–2, 2–3, and 3–4 GeV from left to right). The error bars and shaded bands indicate the statistical and total systematic uncertainties, respectively. In the top panels nonzero values of v_n are presented using a logarithmic scale, while v_n for large n are shown more precisely using a linear scale in the bottom panels.

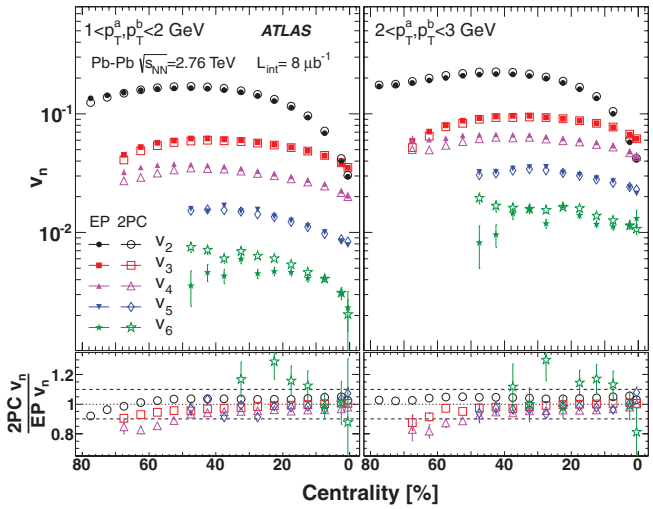

FIG. 14. (Color online) Comparison of v_n as a function of centrality between the fixed-p_T 2PC method with $2 < |\Delta\eta| < 5$ (open symbols) and the full FCal EP method (solid symbols). Results are shown for $1 < p_T < 2$ GeV (left panels) and $2 < p_T < 3$ GeV (right panels). The error bars represent statistical uncertainties only. The ratios of the 2PC to EP methods are shown in the bottom panels, where the dashed lines indicate a $\pm 10\%$ range to guide the eye.

for v_6 over a broad centrality range, well within the quoted systematic uncertainties for the two methods.

As the contribution of the away-side jet increases with p_T, the v_n values from the 2PC method are expected to deviate from the EP results. Figure 15 compares v_2–v_5 from the fixed-p_T 2PC method with those from the EP method in the 0%–10% centrality interval. The two methods agree within 5%–15% for v_2 and 5%–10% for v_3–v_5 for $p_T < 4$ GeV. Significant deviations are observed for $p_T > 4$–5 GeV, presumably owing to contributions from the away-side jet (see Fig. 10).

Figure 16 compares the v_2–v_5 obtained from the mixed-p_T 2PC method with those from the EP method in the 0%–10% centrality interval. The layout of this figure is similar to that of Fig. 15, except that the $v_n(p_T^b)$ are calculated using Eq. (17) for four reference p_T^a ranges. Because only one particle is chosen from high p_T, the influence of autocorrelations from jets is expected to be less than when both particles are chosen from high p_T. Indeed, when p_T^a is below 3 GeV, the deviations from the EP method are less than 5%–10% out to much higher p_T^b, when statistical precision allows. This behavior suggests that as long as the reference p_T^a is low, the factorization relation is valid and hence the v_n can be measured to high p_T via the 2PC method. It is also noticed that in central events, the agreement for v_2 is generally worse than that for the higher-order v_n: The differences for v_2 between the two methods reach >20% for $p_T^b > 4$ GeV and $3 < p_T^a < 4$ GeV, while the differences for the higher-order v_n are small and show no visible dependence on p_T^b for $p_T^a < 4$ GeV. Comparisons for several other centrality intervals are included in Fig. 28 in the Appendix. Good agreement is always observed for v_2–v_5 in noncentral events.

The agreement between the 2PC and EP methods implies that the structures of the two-particle correlation function

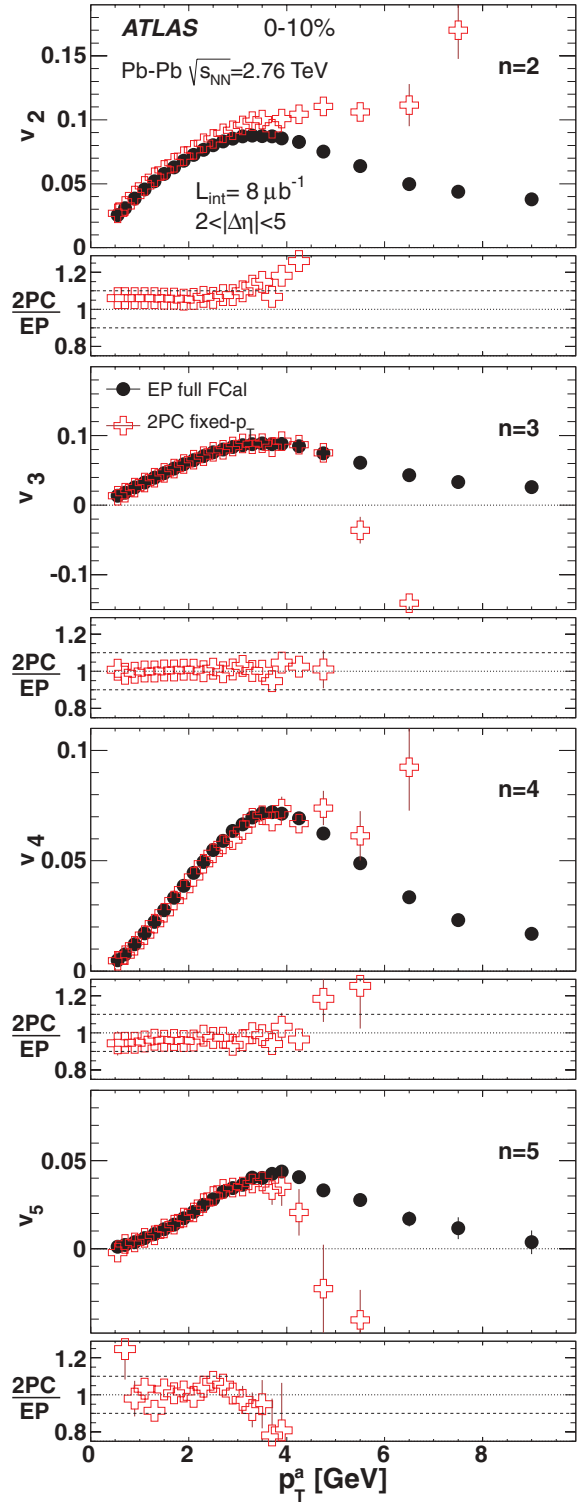

FIG. 15. (Color online) Comparision of $v_n(p_T)$ and the ratios between the fixed-p_T 2PC method and the EP method (v_2–v_5 from top row to bottom row) for the 0%–10% centrality interval. The error bars indicate the statistical uncertainties only. The dashed lines in the ratio plots indicate a $\pm 10\%$ band to guide eye.

at low p_T and large $|\Delta\eta|$ mainly reflect collective flow. This is verified explicitly by reconstructing the correlation

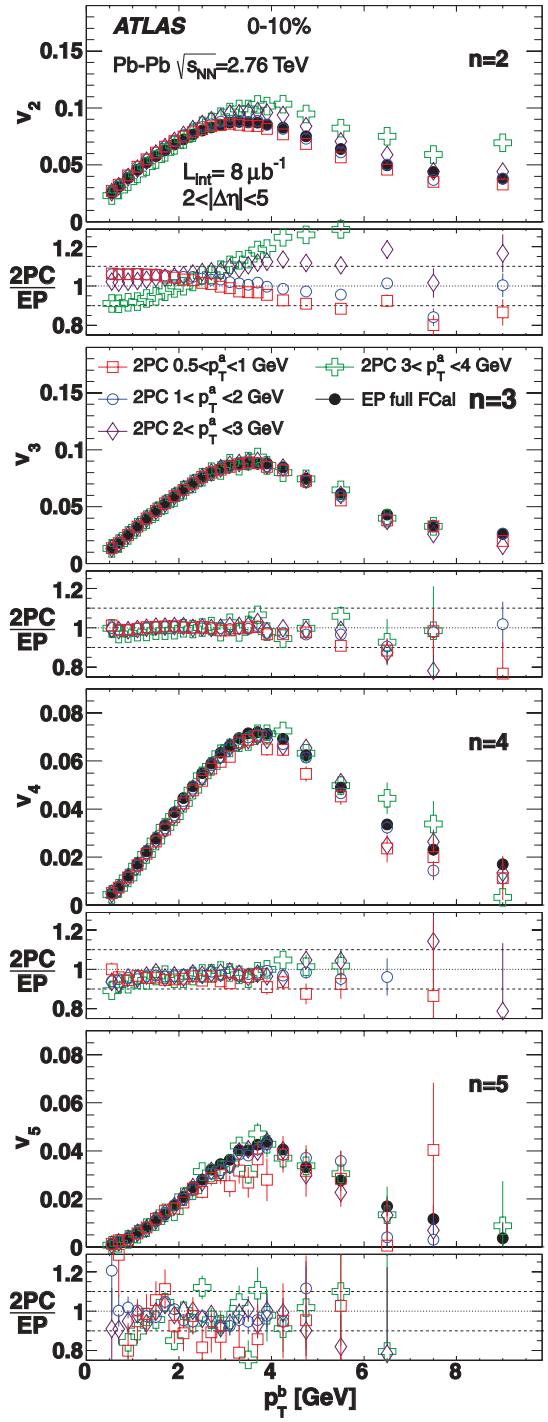

FIG. 16. (Color online) Comparison of $v_n(p_T)$ and ratios between the mixed-p_T 2PC method obtained for four reference p_T^a ranges (0.5–1, 1–2, 2–3, 3–4 GeV) and the EP method (v_2–v_5 from top row to bottom row) for the 0%–10% centrality interval. The error bars indicate the statistical uncertainties only. The dashed lines in the ratio plots indicate a ±10% band to guide eye.

function as

$$C(\Delta\phi) = b^{2PC}\left(1 + 2v_{1,1}^{2PC}\cos\Delta\phi + 2\sum_{n=2}^{6} v_n^{EP,a} v_n^{EP,b}\cos n\Delta\phi\right), \tag{18}$$

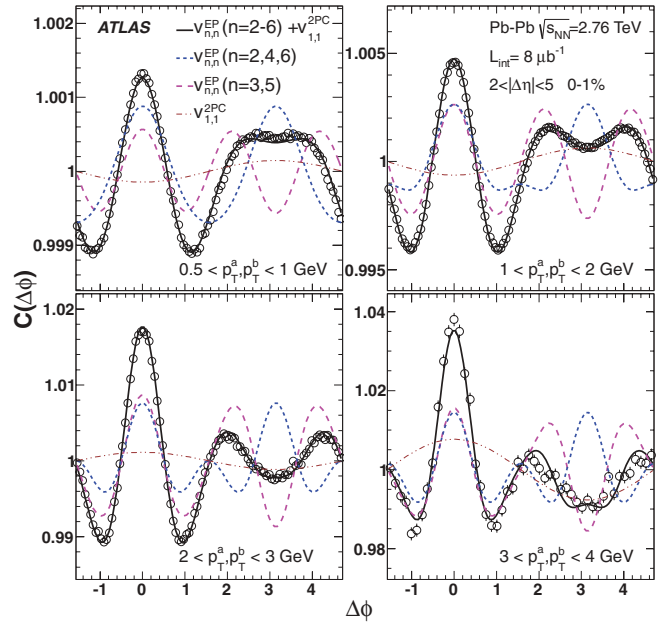

FIG. 17. (Color online) Measured correlation functions compared with those reconstructed from v_2–v_6 measured from the $FCal_{P(N)}$ method and $v_{1,1}$ from the 2PC method in 0%–1% centrality interval for four p_T ranges. The contributions from $n = 1$, $n = 3, 5$, and $n = 2, 4, 6$ are shown separately. The error bars indicate the statistical uncertainties.

where b^{2PC} and $v_{1,1}^{2PC}$ are the average of the correlation function and first harmonic coefficient from the 2PC analysis, and the remaining coefficients are calculated from the v_n measured by the $FCal_{P(N)}$ EP method. Figure 17 compares the measured correlation functions with those reconstructed using Eq. (18), and they are found to agree well. In general, the correlation functions are reproduced within 5% of their maximum variations for $p_T < 3$ GeV, with slightly larger residual differences for $3 < p_T < 4$ GeV. The $v_{1,1}$ term, not measured by the EP method, also plays a significant role, but it is not large enough to generate the near- and away-side structures in the correlation function.

Figure 17 also shows the separate contributions from odd harmonics v_3, v_5 and even harmonics v_2, v_4, v_6 measured by the $FCal_{P(N)}$ EP method. The motivation for doing this is that at $\Delta\phi \sim \pi$, the even harmonics all give positive contributions while the odd harmonics all give negative contributions. Thus, the relative magnitudes of these two contributions control the away-side shape. Figure 17 shows that the double-hump structure can be explained by the interplay between the odd and even harmonics.

D. $v_{1,1}$ from the two-particle correlation method and implications for the v_1 associated with the dipole asymmetry

The previous results show that the factorization properties of $v_{1,1}$ are quite different from those of the higher-order coefficients. The main reason for this is that $v_{1,1}$ is strongly influenced by global momentum conservation, while all higher-order coefficients conserve momentum owing to their multifold symmetries. One example of momentum

conservation effects comes from dijets in peripheral events, which tend to give a negative $v_{1,1}$ at large $|\Delta\eta|$ (see the $\cos\Delta\phi$ component in the bottom-right panel of Fig. 9). The influence of global momentum conservation on the two-particle correlation has been studied extensively [12,51,52,67,68] and was shown to explicitly break the factorization relation Eq. (4) [51,52]:

$$v_{1,1}(p_{\mathrm{T}}^{\mathrm{a}}, p_{\mathrm{T}}^{\mathrm{b}}, \eta_{\mathrm{a}}, \eta_{\mathrm{b}}) \approx v_1(p_{\mathrm{T}}^{\mathrm{a}}, \eta_{\mathrm{a}}) v_1(p_{\mathrm{T}}^{\mathrm{b}}, \eta_{\mathrm{b}}) - \frac{p_{\mathrm{T}}^{\mathrm{a}} p_{\mathrm{T}}^{\mathrm{b}}}{M\langle p_{\mathrm{T}}^2\rangle}, \quad (19)$$

where M and $\langle p_{\mathrm{T}}^2\rangle$ are the multiplicity and average squared transverse momentum for the whole event, respectively. The negative correction term is a leading-order approximation for momentum conservation. This approximation is expected to be valid when the correction term is much smaller than 1. The global momentum conservation effect is important in peripheral events and for high-p_{T} particles, but is diluted in central events owing to the large multiplicity.

The first term of Eq. (19) represents a contribution from v_1, whose dependence on pseudorapidity can be generally separated into a rapidity-odd component and a rapidity-even component. The rapidity-odd v_1 is thought to arise from the "sideward" deflection of the colliding ions [5] and changes sign going from negative η to positive η [53,54]. Because pairs with large $|\Delta\eta|$ separation typically select two particles from opposite hemispheres, the rapidity-odd v_1 contribution to $v_{1,1}$ is negative at large $|\Delta\eta|$. However, the rapidity-odd v_1 is found to be less than 0.005 for $|\eta| < 2$ at the LHC [69]. The corresponding contribution to $v_{1,1}$ ($<2.5 \times 10^{-5}$) is negligible compared to the typical $v_{1,1}$ values seen in the data (see below). The rapidity-even v_1 signal is believed to arise from the dipole asymmetry of the nuclear overlap owing to fluctuations in the initial geometry [11,68]. This spatial asymmetry results in a dipole anisotropy of the pressure gradient, which drives the v_1. If the rapidity-even v_1 depends weakly on η [68], similar to the higher-order v_n, its contribution to $v_{1,1}$ should be positive and vary weakly with $\Delta\eta$. In this case, Eq. (19) can be simplified to

$$v_{1,1}(p_{\mathrm{T}}^{\mathrm{a}}, p_{\mathrm{T}}^{\mathrm{b}}) \approx v_1(p_{\mathrm{T}}^{\mathrm{a}}) v_1(p_{\mathrm{T}}^{\mathrm{b}}) - \frac{p_{\mathrm{T}}^{\mathrm{a}} p_{\mathrm{T}}^{\mathrm{b}}}{M\langle p_{\mathrm{T}}^2\rangle}. \quad (20)$$

A previous analysis of published RHIC data supports the existence of a significant rapidity-even v_1 at lower beam energy [12]. Here the properties of the $v_{1,1}$ data are examined in detail, with the goal of understanding the relative contributions of v_1 and global momentum conservation.

Figure 18 shows the $|\Delta\eta|$ dependence of the $v_{1,1}$ extracted from two-particle fixed-p_{T} correlations for several centrality intervals (see discussions around Fig. 2). The $v_{1,1}$ values for $|\Delta\eta| < 0.5$ are always positive, presumably owing to contributions from the near-side jet or other short-range correlations. The $v_{1,1}$ values at large $|\Delta\eta|$, however, have a more complex dependence on centrality and p_{T}. In peripheral events, the $v_{1,1}$ values are always negative at $|\Delta\eta| > 1$, and their absolute values increase up to $|\Delta\eta| \sim 1.6$ and then decrease for larger $|\Delta\eta|$. This trend is consistent with the gradual falloff of the away-side jet contribution at large $|\Delta\eta|$ seen in 2D correlation function, for example, the last panel of Fig. 8. In central and midcentral events, the $v_{1,1}$ values at

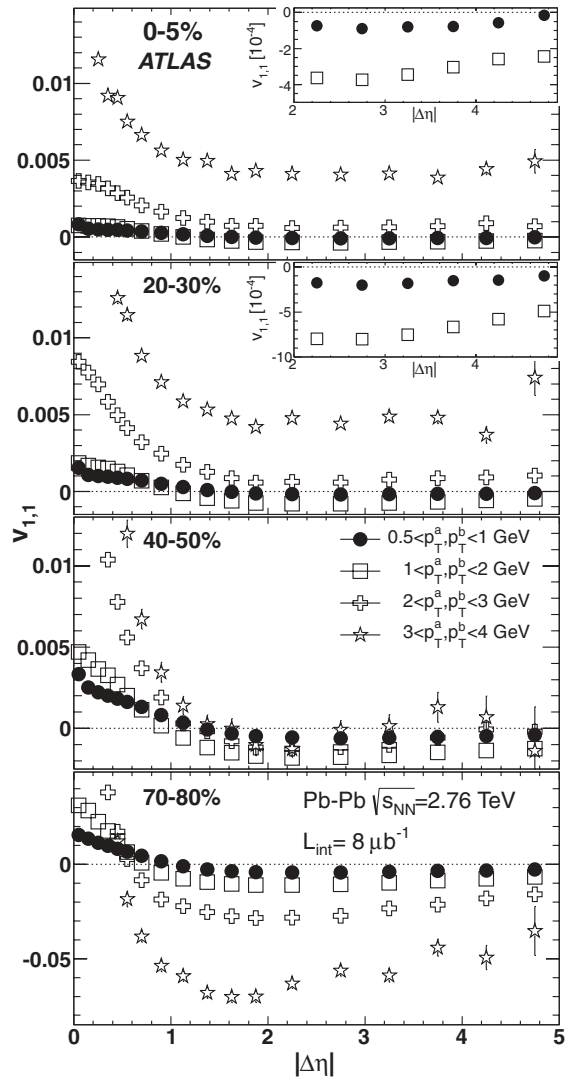

FIG. 18. $v_{1,1}$ vs $|\Delta\eta|$ for four p_{T} ranges in several centrality intervals. The error bars represent the statistical uncertainties. The inset panels show a magnified view of the region $|\Delta\eta| > 2$.

$|\Delta\eta| > 1$ are negative for $p_{\mathrm{T}}^{\mathrm{a}}, p_{\mathrm{T}}^{\mathrm{b}} < 2$ GeV, but they become positive and relatively independent of $|\Delta\eta|$ at higher p_{T}, consistent with the contribution from a rapidity-even v_1 that varies weakly with η.

Given that the $|\Delta\eta|$ dependence of Fig. 18 is generally weak at large $|\Delta\eta|$, $v_{1,1}$ is integrated over $2 < |\Delta\eta| < 5$ to obtain one value for each $p_{\mathrm{T}}^{\mathrm{a}}$ and $p_{\mathrm{T}}^{\mathrm{b}}$ combination. The $v_{1,1}(p_{\mathrm{T}}^{\mathrm{a}}, p_{\mathrm{T}}^{\mathrm{b}})$ functions are then shown in Fig. 19 for various centrality intervals. In peripheral events, the $v_{1,1}$ values are always negative and their absolute values increase nearly linearly with $p_{\mathrm{T}}^{\mathrm{a}}$ and $p_{\mathrm{T}}^{\mathrm{b}}$, presumably dominated by autocorrelations from the away-side jet. In more central events, the absolute value of this negative $v_{1,1}$ component is smaller, reflecting a dilution of the momentum conservation term by the large event multiplicity. Furthermore, Fig. 19 clearly suggests that a positive $v_{1,1}$ component sets in for $2 \lesssim p_{\mathrm{T}} \lesssim 6$ GeV. Its magnitude increases for more central events and eventually drives $v_{1,1}$ into the positive region. The $v_{1,1}$ values reach a

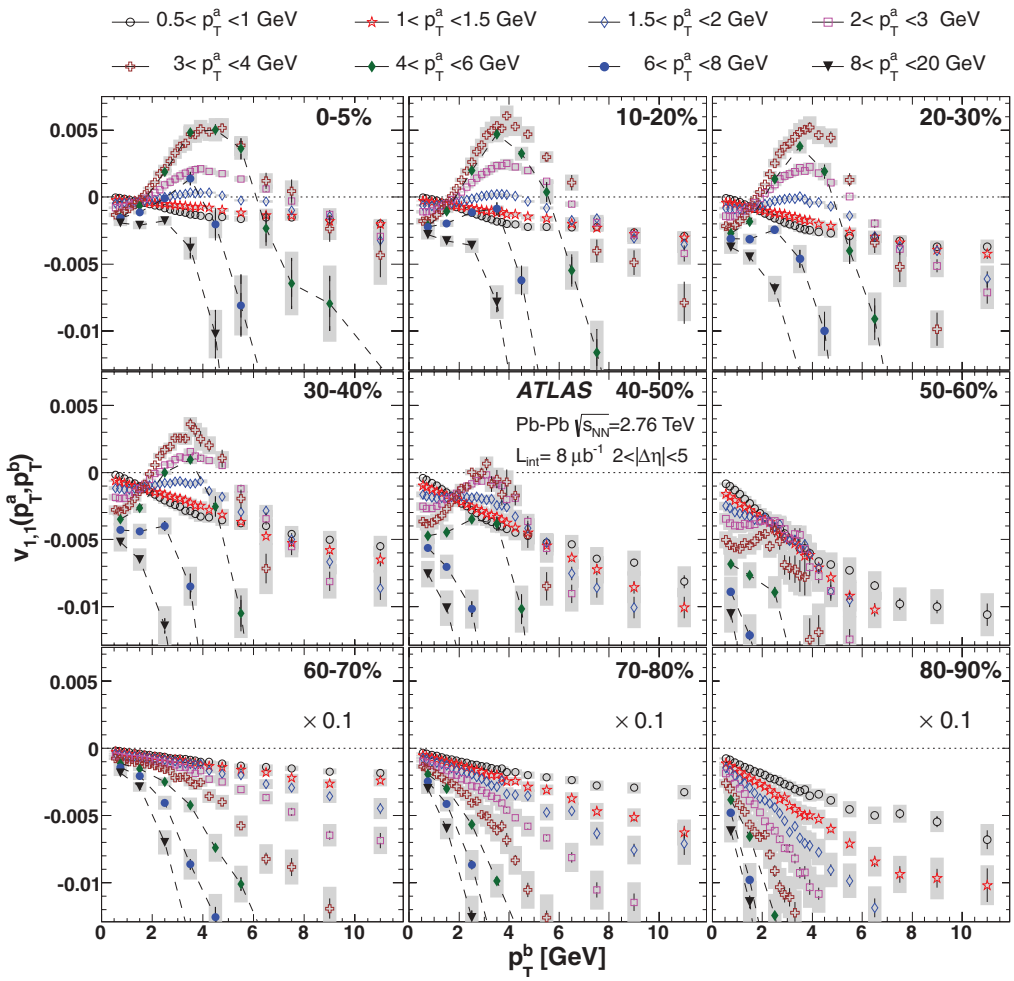

FIG. 19. (Color online) $v_{1,1}(p_T^a, p_T^b)$ for $2 < |\Delta\eta| < 5$ vs p_T^b for different p_T^a ranges. Each panel presents results in one centrality interval. The error bars and shaded bands represent statistical and systematic uncertainties, respectively. The data points for the three highest p_T^a intervals have coarser binning in p_T^b, hence are connected by dashed lines to guide the eye. The data in the bottom three panels are scaled down by a factor of ten to fit within the same vertical range.

maximum at around 4 GeV, similar to those for the higher-order harmonic coefficients (see Fig. 4).

To validate the two-component model of Eq. (20) as a reasonable interpretation of the $v_{1,1}$ data and to extract the v_1, a least-squares fit of the $v_{1,1}$ data is performed for each centrality interval with the following form:

$$\chi^2 = \sum_{a,b} \frac{\left\{v_{1,1}(p_T^a, p_T^b) - \left[v_1^{Fit}(p_T^a)v_1^{Fit}(p_T^b) - c p_T^a p_T^b\right]\right\}^2}{\left(\sigma_{a,b}^{stat}\right)^2 + \left(\sigma_{a,b}^{sys,p2p}\right)^2}, \tag{21}$$

where $\sigma_{a,b}^{stat}$ and $\sigma_{a,b}^{sys,p2p}$ denote the statistical and point-to-point systematic uncertainties for $v_{1,1}(p_T^a, p_T^b)$, respectively (see Sec. IV B). The $v_1^{Fit}(p_T)$ function is defined via a smooth interpolation of its values at m discrete p_T points, $v_1^{Fit}(p_{T,i})|_{i=1}^m$, and these together with the parameter c constitute a total of $m + 1$ fit parameters. An interpolation procedure is used because the functional form of $v_1^{Fit}(p_T)$ is, *a priori*, unknown, yet it is expected to vary smoothly with p_T.

In the default setup, the $v_{1,1}$ data used in the fit are restricted to $p_T^a < 6$ GeV and $p_T^b < 10$ GeV, giving a total of 129 data

TABLE VII. Quality of the fit χ^2/DOF, fit parameter c, and corresponding multiplicity scaled values $c\frac{dN}{d\eta}_{|\eta=0}$ for various centrality intervals. The uncertainty of $c\frac{dN}{d\eta}_{|\eta=0}$ is calculated as the quadrature sum of uncertainties from c and $\frac{dN}{d\eta}_{|\eta=0}$ of Ref. [57]. The bottom row lists the 15 p_T interpolation points used in the default fit.

Centrality	χ^2/DOF	$c(\times 0.001\text{GeV}^{-2})$	$c\frac{dN}{d\eta}_{\|\eta=0}(\times\text{GeV}^{-2})$
0%–5%	159/113	0.24 ± 0.02	0.39 ± 0.04
5%–10%	133/113	0.28 ± 0.02	0.37 ± 0.04
10%–20%	165/113	0.35 ± 0.03	0.36 ± 0.04
20%–30%	134/113	0.50 ± 0.04	0.34 ± 0.03
30%–40%	188/113	0.75 ± 0.05	0.33 ± 0.03
40%–50%	181/113	1.16 ± 0.09	0.32 ± 0.03
15 interpolation points used in the default fit: 0.5, 0.7, 0.9, 1.1, 1.3, 1.5, 2.0, 2.5, 3.0, 3.5, 4.5, 5.5, 6.5, 7.5, 9.0 GeV			

points for each centrality interval. A cubic-spline interpolation procedure is used, and the number of interpolation points is chosen to be $m = 15$ (listed in Table VII). To account for the p_T-correlated uncertainty ($\sigma_{a,b}^{sys,corr}$, see Sec. IV B), the least-squares minimization is repeated after varying all the $v_{1,1}$ data points up or down by $\sigma_{a,b}^{sys,corr}$. Because $v_{1,1}(p_T^a, p_T^b)$ is symmetric with respect to p_T^a and p_T^b, data points for $p_T^a < p_T^b$ are correlated with those for $p_T^a > p_T^b$. The effect of this correlation is evaluated by repeating the fit using only $v_{1,1}$ data for $p_T^a \leqslant p_T^b$ or $v_{1,1}$ data for $p_T^a \geqslant p_T^b$. The variations from the default fit are included in the systematic uncertainties.

Figure 20 shows the fit to the $v_{1,1}$ data from Fig. 19 for the 0%–5% and 40%–50% centrality intervals. The $v_{1,1}$ data are plotted as a function of p_T^b for six intervals of p_T^a. The seemingly complex patterns of the $v_{1,1}$ data are well described by the two-component fit across broad ranges of p_T^a and p_T^b, with the dot-dashed lines indicating the estimated contributions from the global momentum conservation. The typical χ^2/DOF of the fit is between one and two depending on the centrality, as shown in Table VII. The deviations of the data from the fit, as shown in the bottom section of each panel, are less than 10^{-4} for $p_T < 5$ GeV. Above that p_T and in more peripheral events the deviations increase, possibly reflecting the limitation of the leading-order approximation for the momentum conservation term in Eq. (20), or the two-component assumption in general. In this paper, the study is restricted to the 0%–50% most central events, for which the first term in Eq. (20) is comparable or larger than the second term and the statistical uncertainty of the fit is not too large.

The stability of the least-square minimization procedure is checked for three types of variations: (1) the interpolation

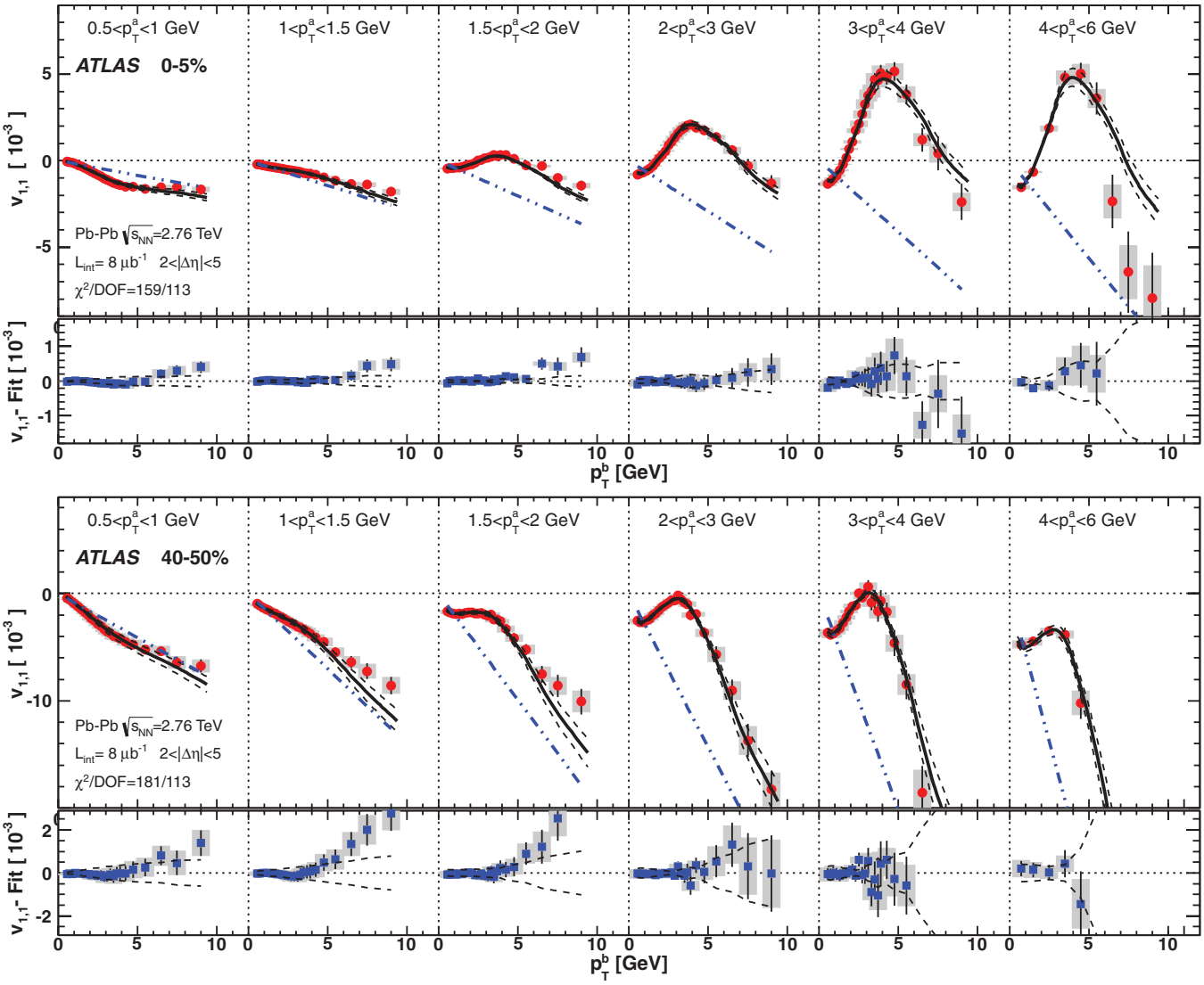

FIG. 20. (Color online) Global fit [via Eq. (21)] to the $v_{1,1}$ data for the 0%–5% centrality interval (top) and the (40%–50%) centrality interval (bottom). The fit is performed simultaneously over all $v_{1,1}$ data points in a given centrality interval, which are organized as a function of p_T^b for various p_T^a ranges (indicated at the top of each panel), with shaded bars indicating the correlated systematic uncertainties. The fit function and the associated systematic uncertainties are indicated by the thick solid lines and surrounding dashed lines, respectively. The dot-dashed lines intercepting each dataset (with negative slope) indicate estimated contributions from the momentum conservation component. The lower part of each panel shows the difference between the data and fit (solid points), as well as the systematic uncertainties of the fit (dashed lines).

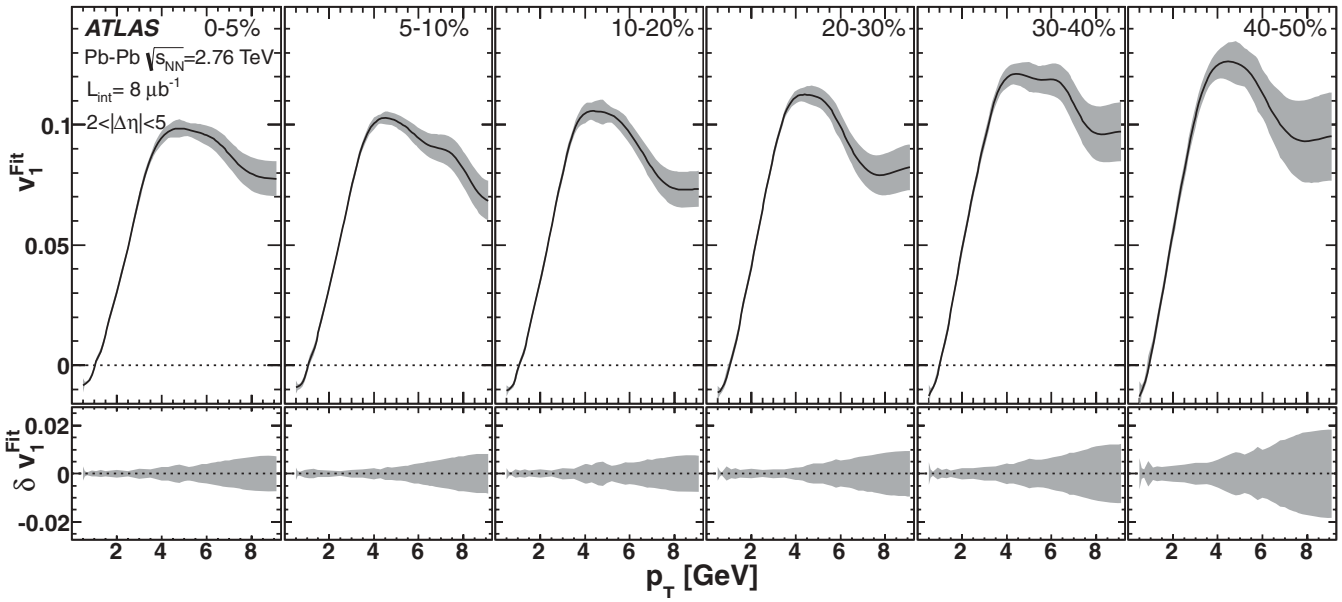

FIG. 21. $v_1^{\rm Fit}$ vs $p_{\rm T}$ for various centrality intervals. The shaded bands indicate the total uncertainty. The uncertainty bands are reproduced on their own at the bottom of the figure for clarity.

function is varied from cubic-spline interpolation to a linear interpolation, (2) the number of interpolation points is varied from 9 to 21, and (3) the $p_{\rm T}$ range of the fit is varied from $p_{\rm T}^{\rm a}, p_{\rm T}^{\rm b} < 5$ GeV to $p_{\rm T}^{\rm a}, p_{\rm T}^{\rm b} < 10$ GeV. The systematic uncertainties of the minimization procedure are calculated as the rms sum of these three variations. They are small in central events but become substantial in peripheral events and are important sources of uncertainties at intermediate $p_{\rm T}$. The statistical uncertainty of the fit dominates at high $p_{\rm T}$, while the fit uncertainty from $\sigma_{\rm a,b}^{\rm sys,corr}$ dominates at low $p_{\rm T}$. The total absolute uncertainty of $v_1^{\rm Fit}$ is $\delta v_1^{\rm Fit} = 0.001$–$0.004$ for $p_{\rm T} < 3$ GeV and increases rapidly for higher $p_{\rm T}$ owing to the greater statistical uncertainty.

Figure 21 shows $v_1^{\rm Fit}(p_{\rm T})$ for various centrality intervals. A significant $v_1^{\rm Fit}$ signal is observed for all cases. It reaches a maximum between 4 and 5 GeV and then falls at higher $p_{\rm T}$. This falloff may indicate the onset of path-length-dependent jet energy loss, which correlates with the dipole asymmetry in the initial geometry similar to higher-order v_n. The magnitude of the $v_1^{\rm Fit}$ is large: Its peak value is comparable to that for the v_3 shown in Fig. 4, and the peak value increases by about 20% over the measured centrality range. These results imply that the rapidity-even collective v_1 is an important component of the two-particle correlation at intermediate $p_{\rm T}$. For example, the large positive $v_{1,1}$ harmonic seen in the bottom-right panel of Fig. 17 is mainly attributable to collective v_1: Its contribution to $v_{1,1}$ is about three times larger than the negative momentum conservation term estimated by the global fit (top panel of Fig. 20). $v_1^{\rm Fit}(p_{\rm T})$ is negative for $p_{\rm T} \lesssim 1.0$ GeV, confirming a generic feature expected for collective v_1, as suggested by hydrodynamic model calculations [11,68]. This behavior, together with the fact that $v_{1,1}$ data show little $|\Delta\eta|$ dependence for $|\Delta\eta| > 2$ (Fig. 18), is consistent with a rapidity-even v_1 that is almost independent of η.

If the two-component ansatz of Eq. (20) is valid, the fit parameter c should be inversely proportional to multiplicity M and $\langle p_{\rm T}^2\rangle$ of the whole event. This ansatz is checked by calculating the product of c and the charged hadron multiplicity at midrapidity $\frac{dN}{d\eta}_{|\eta=0}$ from [57], with the assumption that $\frac{dN}{d\eta}_{|\eta=0}$ is proportional to M. The results are summarized in Table VII for each centrality interval. Because $\langle p_{\rm T}^2\rangle$ for the whole event is expected to vary weakly with centrality (the $\langle p_{\rm T}\rangle$ for charged pions at midrapidity only varies by $\sim$5% within the 0%–50% centrality interval at the LHC [70]), the product is also expected to vary weakly with centrality. Table VII shows that this is indeed the case, supporting the assumptions underlying Eq. (20).

VI. CONCLUSION

In summary, differential measurements of harmonic coefficients v_1–v_6 for the azimuthal distributions of charged particles are presented for lead-lead collisions at $\sqrt{s_{NN}} = 2.76$ TeV, based on an integrated luminosity of approximately 8 μb^{-1} recorded by ATLAS. The v_n values are measured for $n = 2$–6 using an event plane method and are also derived for $n = 1$–6 from the $v_{n,n}$ measured in a two-particle correlation method.

In the event plane method, v_2–v_6 are extracted as a function of transverse momentum ($0.5 < p_{\rm T} < 20$ GeV), pseudorapidity ($|\eta| < 2.5$), and centrality (0%–80%) by correlating tracks with the event plane determined at large rapidity. The v_n values exhibit a weak η dependence, slightly decreasing toward larger $|\eta|$. The v_n values show a similar $p_{\rm T}$ dependence, namely, increasing with $p_{\rm T}$ to a maximum around 3–4 GeV and then decreasing for higher $p_{\rm T}$. The higher-order coefficients exhibit stronger $p_{\rm T}$ variations. They follow an approximate scaling relation, $v_n^{1/n}(p_{\rm T}) \propto v_2^{1/2}(p_{\rm T})$, except in the top 5% most central collisions. Furthermore, the coefficients v_3–v_6 show little dependence on centrality, consistent with an anisotropy

primarily associated with fluctuations in the initial geometry. In contrast, v_2 varies strongly with centrality, reflecting an anisotropy mainly associated with a change in the average elliptic geometry with centrality.

In the two-particle azimuthal correlation method, harmonic coefficients for the distributions of the charged particle pairs in $\Delta\phi$, $v_{n,n} = \langle \cos n\Delta\phi \rangle$ are extracted over a broad range of p_{T}, relative pseudorapidity ($|\Delta\eta| < 5$) and centrality. For pairs of charged particles with a large pseudorapidity gap ($|\Delta\eta| > 2$) and one particle at $p_{\mathrm{T}} < 3$ GeV, the $v_{2,2}$–$v_{6,6}$ are found to factorize into the product of corresponding v_n harmonics, that is, $v_{n,n}(p_{\mathrm{T}}^{\mathrm{a}}, p_{\mathrm{T}}^{\mathrm{b}}) \approx v_n(p_{\mathrm{T}}^{\mathrm{a}})v_n(p_{\mathrm{T}}^{\mathrm{b}})$, in central and midcentral events. This suggests that these values of $v_{2,2}$–$v_{6,6}$ are consistent with the response of the created matter to fluctuations in the geometry of the initial state. This factorization does not describe the $v_{2,2}$–$v_{6,6}$ data in more peripheral collisions or at higher p_{T}, primarily owing to autocorrelations from dijets. The factorization relation is also found to fail for $v_{1,1}$ over the entire p_{T} range. A detailed investigation of the $v_{1,1}(|\Delta\eta|, p_{\mathrm{T}}^{\mathrm{a}}, p_{\mathrm{T}}^{\mathrm{b}})$ data suggests that they are consistent with the combined contributions from a rapidity-even v_1 component, and a global momentum conservation component that increases linearly with the $p_{\mathrm{T}}^{\mathrm{a}} \times p_{\mathrm{T}}^{\mathrm{b}}$ and is inversely proportional to the event multiplicity. Motivated by this observation, a two-component fit is used to extract v_1. The derived signal is negative at low p_{T}, changes sign at $p_{\mathrm{T}} \approx 1.0$ GeV, reaches a maximum at around 4–5 GeV and then decreases at higher p_{T}. The magnitude of v_1 at the peak is comparable to that of v_3.

At low p_{T} where single-particle anisotropy is dominated by collective flow, the two-particle correlation functions are found to be well reproduced by combining the contributions of v_2–v_6 from the event plane method and the $v_{1,1}$ [Eq. (18)]. This implies that the main structures of the low p_{T} two-particle correlation for $|\Delta\eta| > 2$ largely reflect higher-order collective flow ($n \geqslant 2$), together with a $\cos\Delta\phi$ term that contains contributions from both a rapidity-even v_1 and the global momentum conservation. Therefore, the low p_{T} correlation functions do not allow significant contributions from jet-induced medium responses. The fluctuations in the initial geometry together with the low viscosity of the created matter are potentially responsible for these $v_{n,n}$ coefficients. A detailed comparison of the comprehensive v_n and $v_{n,n}$ data presented in this paper with viscous hydrodynamic model calculations at low p_{T} [25,26,32,34,71,72] and jet energy loss model calculations at high p_{T} [27,29,73,74] may help elucidate the nature of these fluctuations and better constrain the transport properties of the medium.

ACKNOWLEDGMENTS

We thank CERN for the very successful operation of the LHC, as well as the support staff from our institutions without whom ATLAS could not be operated efficiently. We acknowledge the support of ANPCyT, Argentina; YerPhI, Armenia; ARC, Australia; BMWF, Austria; ANAS, Azerbaijan; SSTC, Belarus; CNPq and FAPESP, Brazil; NSERC, NRC, and CFI, Canada; CERN; CONICYT, Chile; CAS, MOST, and NSFC, China; COLCIENCIAS, Colombia; MSMT CR, MPO CR, and VSC CR, Czech Republic; DNRF, DNSRC, and Lundbeck Foundation, Denmark; ARTEMIS and ERC, European Union; IN2P3-CNRS, CEA-DSM/IRFU, France; GNAS, Georgia; BMBF, DFG, HGF, MPG, and AvH Foundation, Germany; GSRT, Greece; ISF, MINERVA, GIF, DIP, and Benoziyo Center, Israel; INFN, Italy; MEXT and JSPS, Japan; CNRST, Morocco; FOM and NWO, Netherlands; RCN, Norway; MNiSW, Poland; GRICES and FCT, Portugal; MERYS (MECTS), Romania; MES of Russia and ROSATOM, Russian Federation; JINR; MSTD, Serbia; MSSR, Slovakia; ARRS and MVZT, Slovenia; DST/NRF, South Africa; MICINN, Spain; SRC and Wallenberg Foundation, Sweden; SER, SNSF, and Cantons of Bern and Geneva, Switzerland; NSC, Taiwan; TAEK, Turkey; STFC, the Royal Society and Leverhulme Trust, United Kingdom; DOE and NSF, United States of America. The crucial computing support from all WLCG partners is acknowledged gratefully, in particular from CERN and the ATLAS Tier-1 facilities at TRIUMF (Canada), NDGF (Denmark, Norway, Sweden), CC-IN2P3 (France), KIT/GridKA (Germany), INFN-CNAF (Italy), NL-T1 (Netherlands), PIC (Spain), ASGC (Taiwan), RAL (UK), and BNL (USA) and in the Tier-2 facilities worldwide.

APPENDIX: COMPREHENSIVE DATA PLOTS FROM TWO-PARTICLE CORRELATION

Section V B presents the results only from selected centrality or p_{T} intervals. One of the primary goals of this paper is the detailed study in a wide range of centrality and p_{T} of the $v_{n,n}$ and v_n, obtained from the 2PC in $\Delta\phi$ with a large pseudorapidity gap. For completeness, the v_n coefficients for several fixed-p_{T} correlations and for centrality intervals other than that shown in Fig. 13 are presented in Figs. 22–27.

One important study of the factorization properties of v_2–v_6 is the comparison between the EP method and mixed-p_{T} 2PC method. This comparison is shown in Fig. 16 for the 0%–10% centrality interval. Figure 28 extends this comparison to several centrality intervals. Good consistency is observed for v_2–v_6 in noncentral collisions.

Figures 29–31 present the full set of the $\Delta\phi$ correlation functions with $2 < |\Delta\eta| < 5$ for one central, one midcentral, and one peripheral centrality interval. These correlation functions are the inputs for the $v_{n,n}$ and v_n spectra. They provide the complete picture of how the structures of the correlation functions are influenced, as a function of $p_{\mathrm{T}}^{\mathrm{a}}$ and $p_{\mathrm{T}}^{\mathrm{b}}$, by the anisotropies related to the initial geometry and autocorrelations from the away-side jets, as well as how these influences map onto the strength and sign of the $v_{n,n}$ coefficients. Note that the correlation functions are symmetric with respect to $p_{\mathrm{T}}^{\mathrm{a}}$ and $p_{\mathrm{T}}^{\mathrm{b}}$. For example, the correlation for $1 < p_{\mathrm{T}}^{\mathrm{a}} < 2$ GeV and $2 < p_{\mathrm{T}}^{\mathrm{b}} < 3$ GeV (denoted as [1–2, 2–3] GeV) is the same as that for $2 < p_{\mathrm{T}}^{\mathrm{a}} < 3$ GeV and $1 < p_{\mathrm{T}}^{\mathrm{b}} < 2$ GeV (denoted as [2–3, 1–2] GeV).

Figures 32–36 shows the dependence of $v_{2,2}$–$v_{6,6}$ on $p_{\mathrm{T}}^{\mathrm{a}}$ and $p_{\mathrm{T}}^{\mathrm{b}}$. Together with Fig. 19, they provide a concise summary of $v_{n,n}$ spectra for all the 1D correlation functions such as those in Figs. 29–31 for $2 < |\Delta\eta| < 5$. Because the sum of the $v_{1,1}$–$v_{6,6}$ components almost exhaust the shape of the correlation functions, these data provide almost equivalent information as the correlation functions themselves over broad ranges of $p_{\mathrm{T}}^{\mathrm{a}}$ and $p_{\mathrm{T}}^{\mathrm{b}}$.

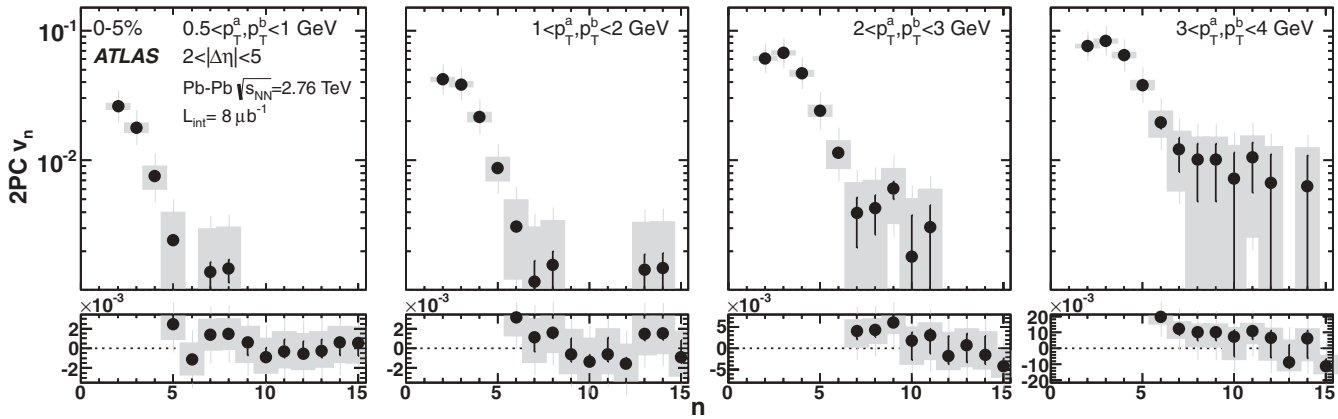

FIG. 22. v_n vs n for $n \geqslant 2$ in the 0%–5% centrality interval for four fixed-p_{T} correlations (0.5–1, 1–2, 2–3, and 3–4 GeV from left to right). The error bars and shaded bands indicate the statistical and total systematic uncertainties, respectively.

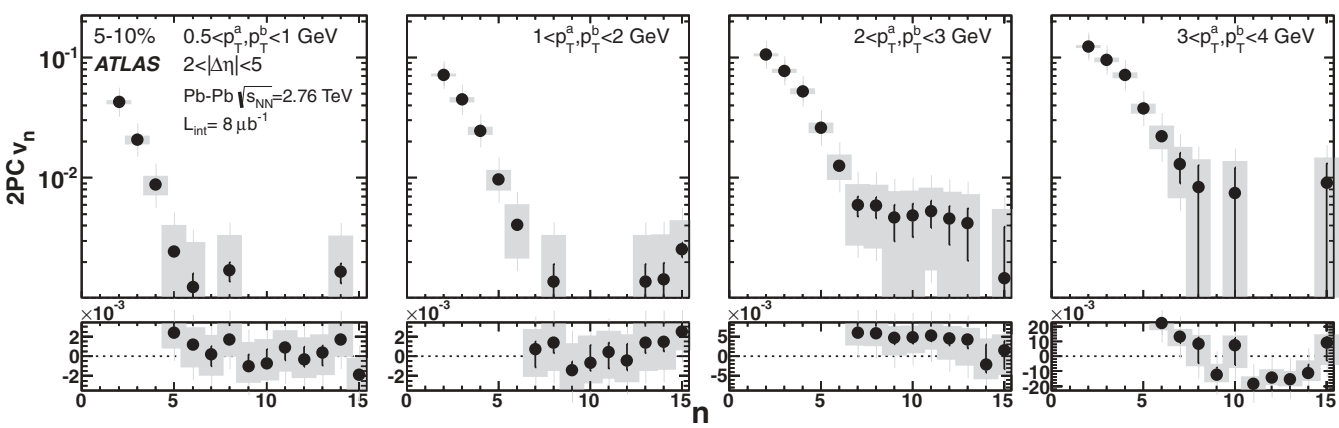

FIG. 23. v_n vs n for $n \geqslant 2$ in the 5%–10% centrality interval for four fixed-p_{T} correlations (0.5–1, 1–2, 2–3, and 3–4 GeV from left to right). The error bars and shaded bands indicate the statistical and total systematic uncertainties, respectively.

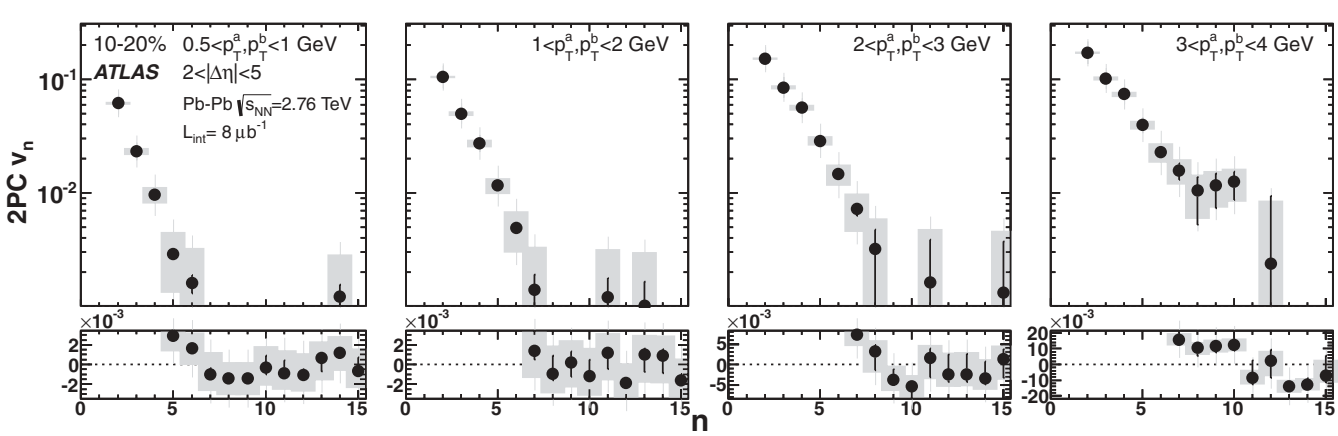

FIG. 24. v_n vs n for $n \geqslant 2$ in 10%–20% centrality interval for four fixed-p_{T} correlations (0.5–1, 1–2, 2–3, and 3–4 GeV from left to right). The error bars and shaded bands indicate the statistical and total systematic uncertainties, respectively.

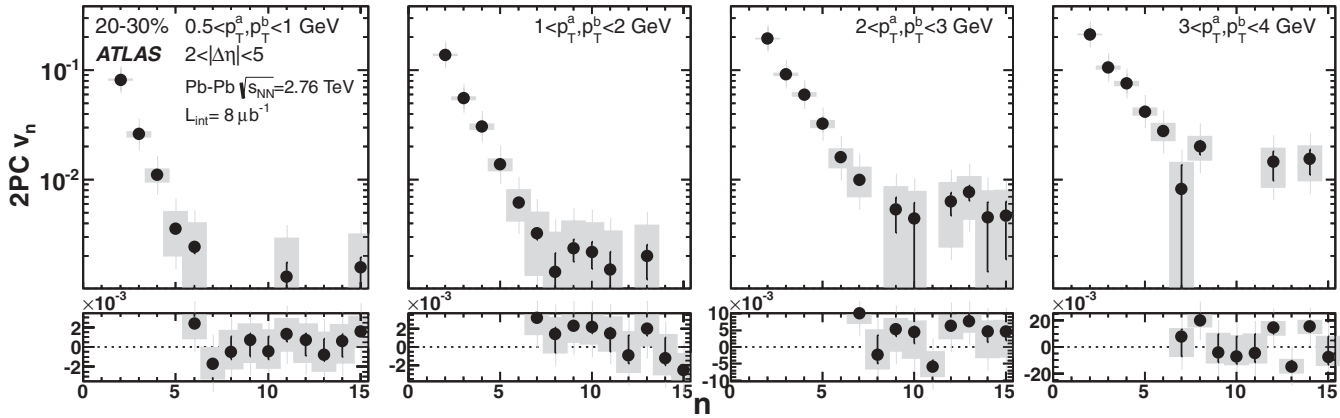

FIG. 25. v_n vs n for $n \geqslant 2$ in the 20%–30% centrality interval for four fixed-p_{T} correlations (0.5–1, 1–2, 2–3, and 3–4 GeV from left to right). The error bars and shaded bands indicate the statistical and total systematic uncertainties, respectively.

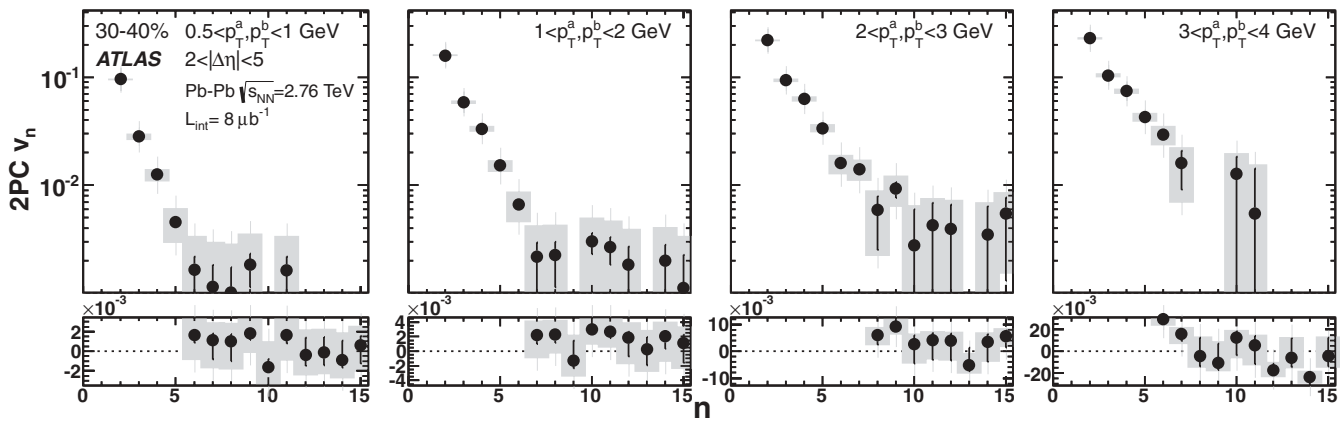

FIG. 26. v_n vs n for $n \geqslant 2$ in the 30%–40% centrality interval for four fixed-p_{T} correlations (0.5–1, 1–2, 2–3, and 3–4 GeV from left to right). The error bars and shaded bands indicate the statistical and total systematic uncertainties, respectively.

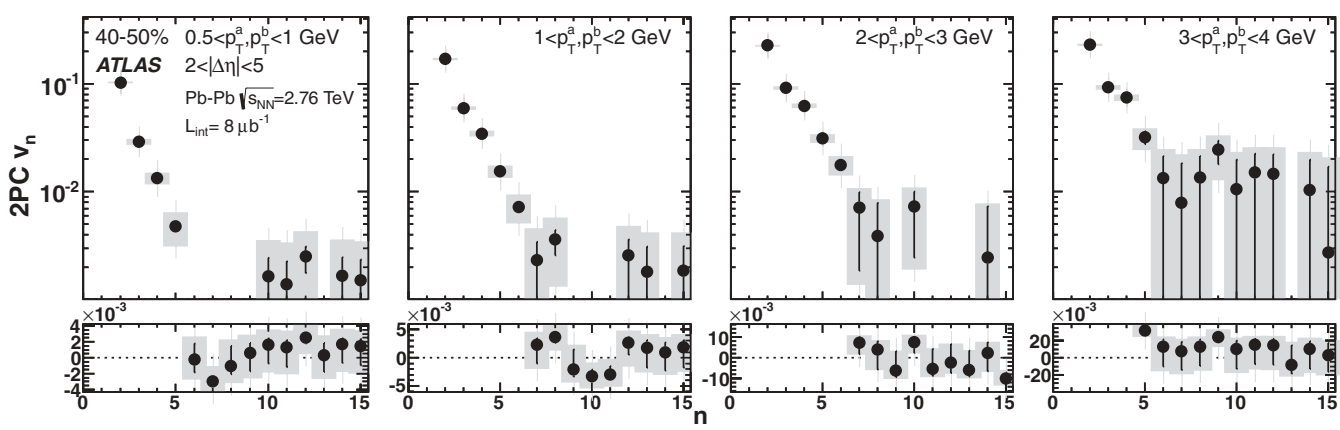

FIG. 27. v_n vs n for $n \geqslant 2$ in the 40%–50% centrality interval for four fixed-p_{T} correlations (0.5–1, 1–2, 2–3, and 3–4 GeV from left to right). The error bars and shaded bands indicate the statistical and total systematic uncertainties, respectively.

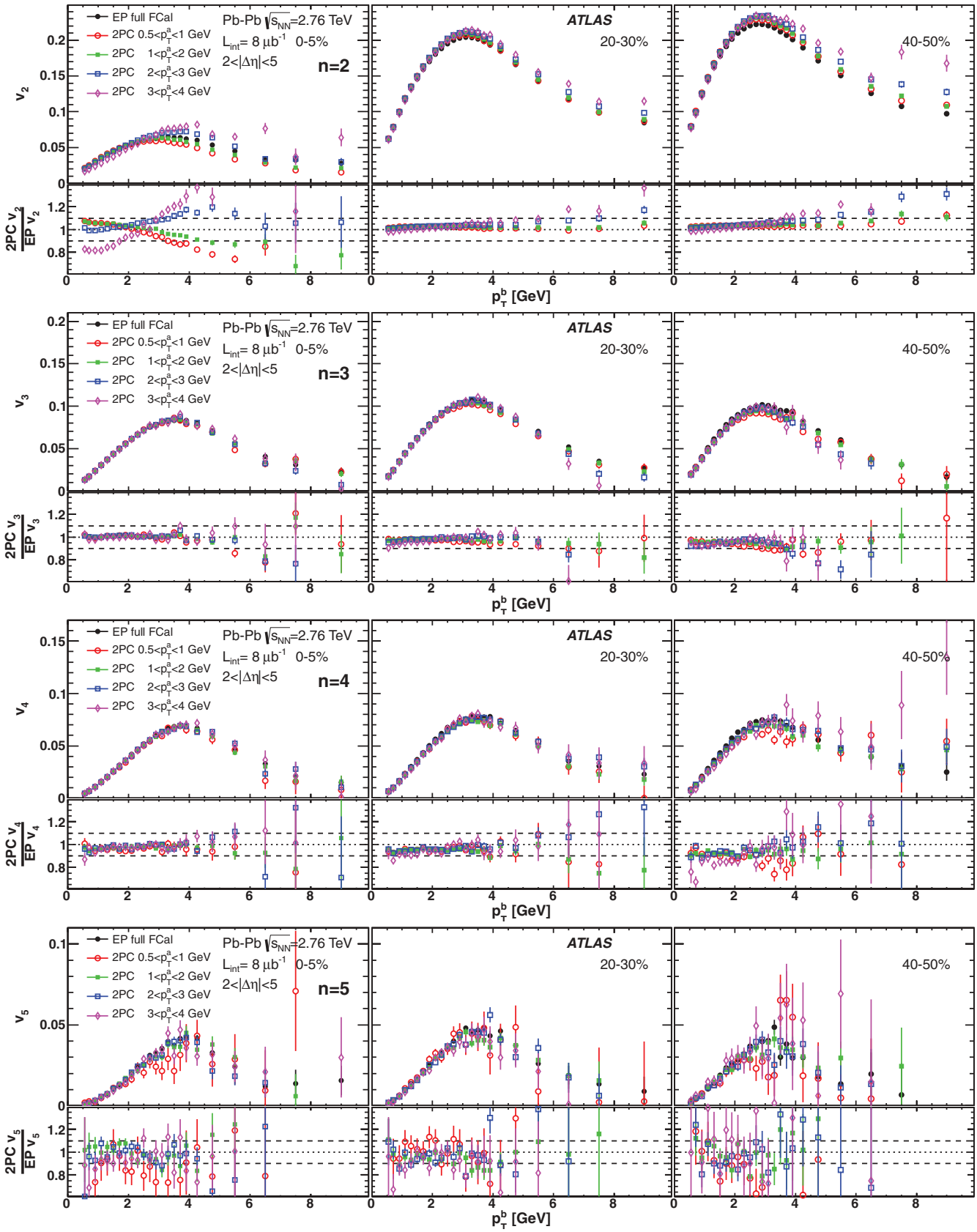

FIG. 28. (Color online) Comparison of v_n as a function of p_T (v_2–v_5 from top to bottom) between mixed-p_T 2PC method and the EP method for the 0%–5% (left panels), 20%–30% (middle panels), and 40%–50% (right panels) centrality intervals. The error bars indicate the statistical uncertainties only. The dashed lines in the ratio plots indicate a ±10% band to guide the eye.

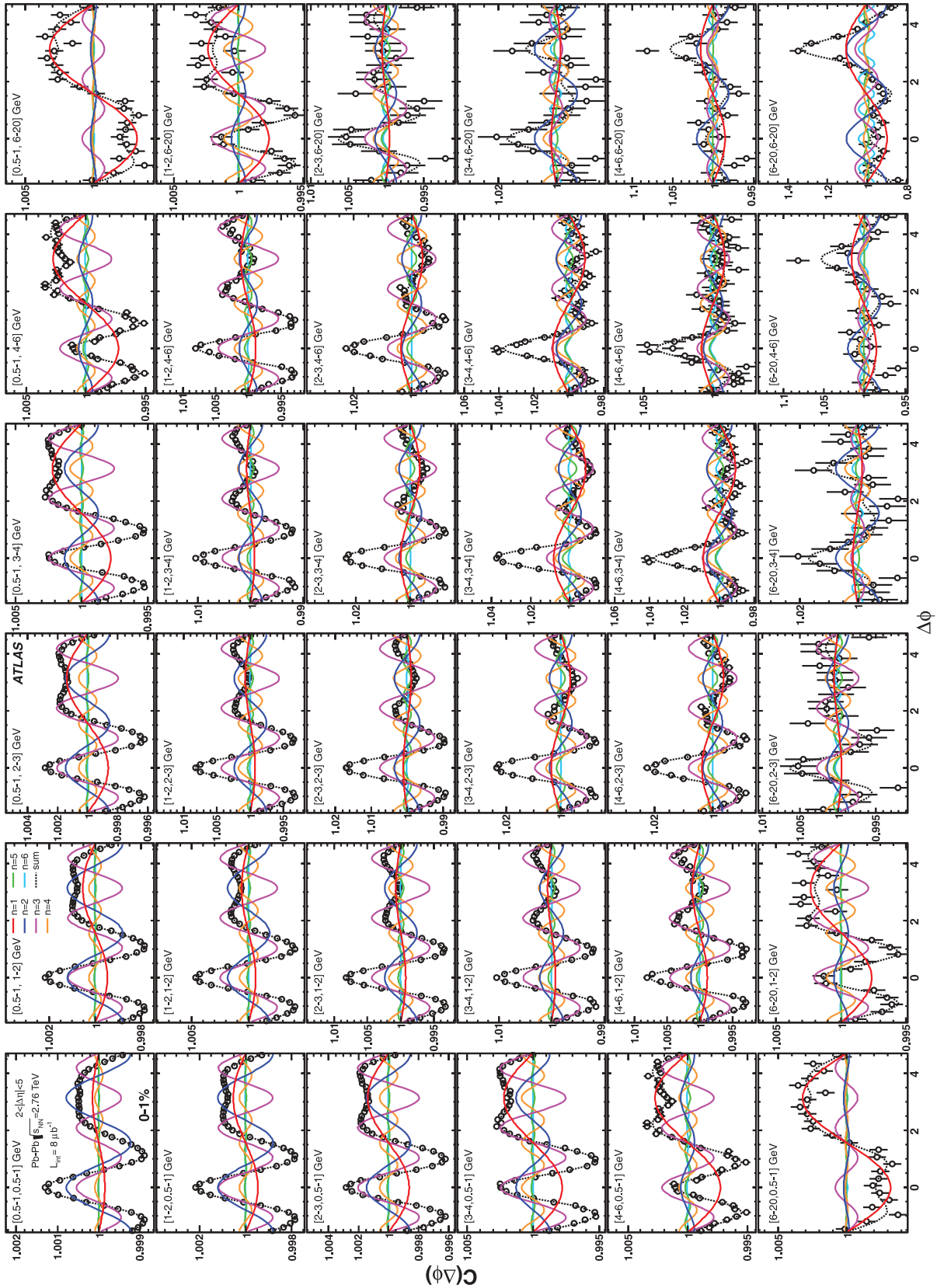

FIG. 29. (Color online) $\Delta\phi$ correlation functions for various combinations of $p_{\mathrm{T}}^{\mathrm{a}}$ and $p_{\mathrm{T}}^{\mathrm{b}}$ for the 0%–1% centrality interval. The superimposed solid lines (dashed lines) indicate the contributions from individual $v_{n,n}$ (sum of the first six components).

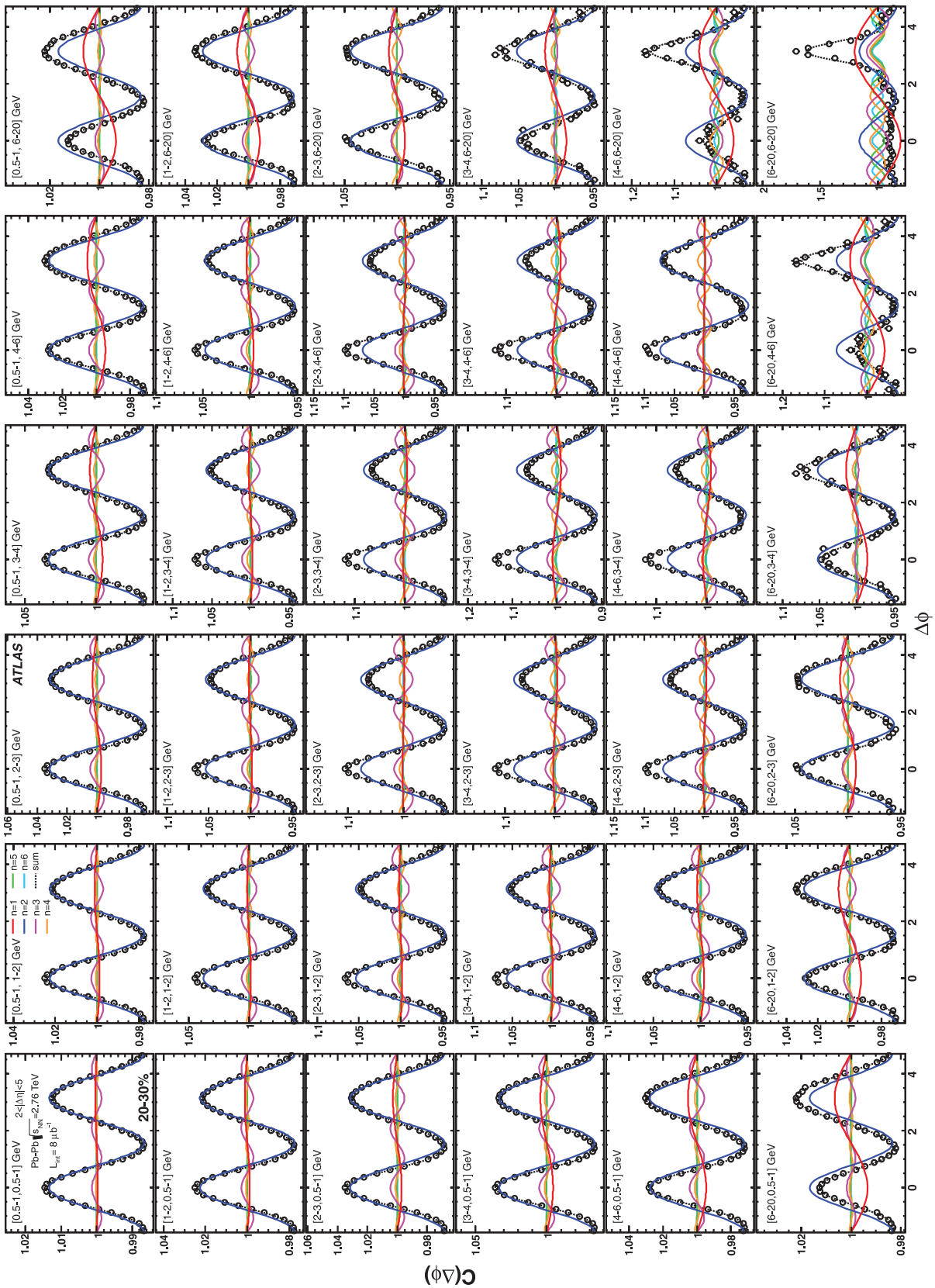

FIG. 30. (Color online) $\Delta\phi$ correlation functions for various combinations of p_T^a and p_T^b for the 20%–30% centrality interval. The superimposed solid lines (dashed lines) indicate the contributions from individual $v_{n,n}$ (sum of the first six components).

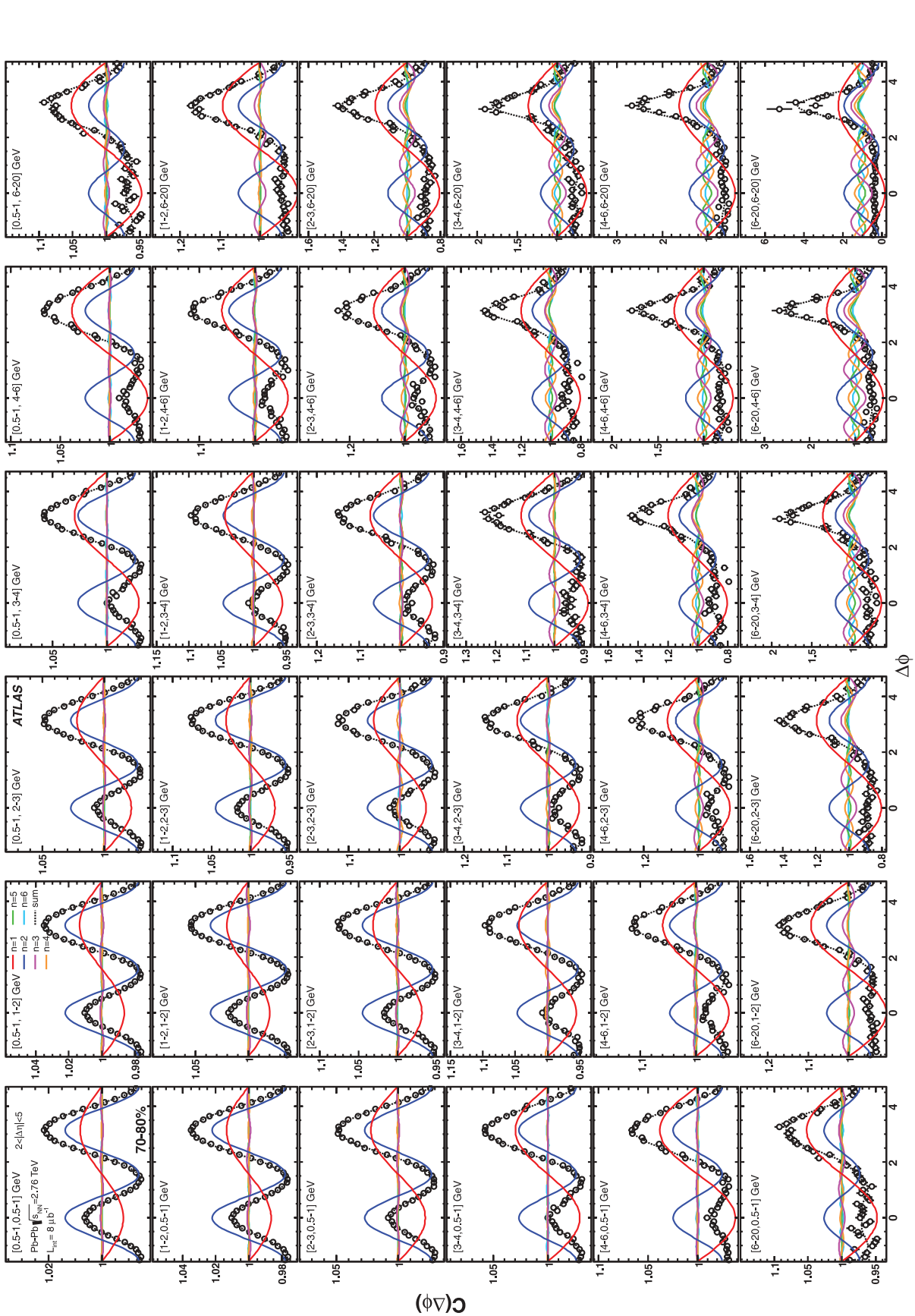

FIG. 31. (Color online) $\Delta\phi$ correlations for various combinations of $p_{\mathrm{T}}^{\mathrm{a}}$ and $p_{\mathrm{T}}^{\mathrm{b}}$ for the 70%–80% centrality interval. The superimposed solid lines (dashed lines) indicate the contributions from individual $v_{n,n}$ (sum of the first six components).

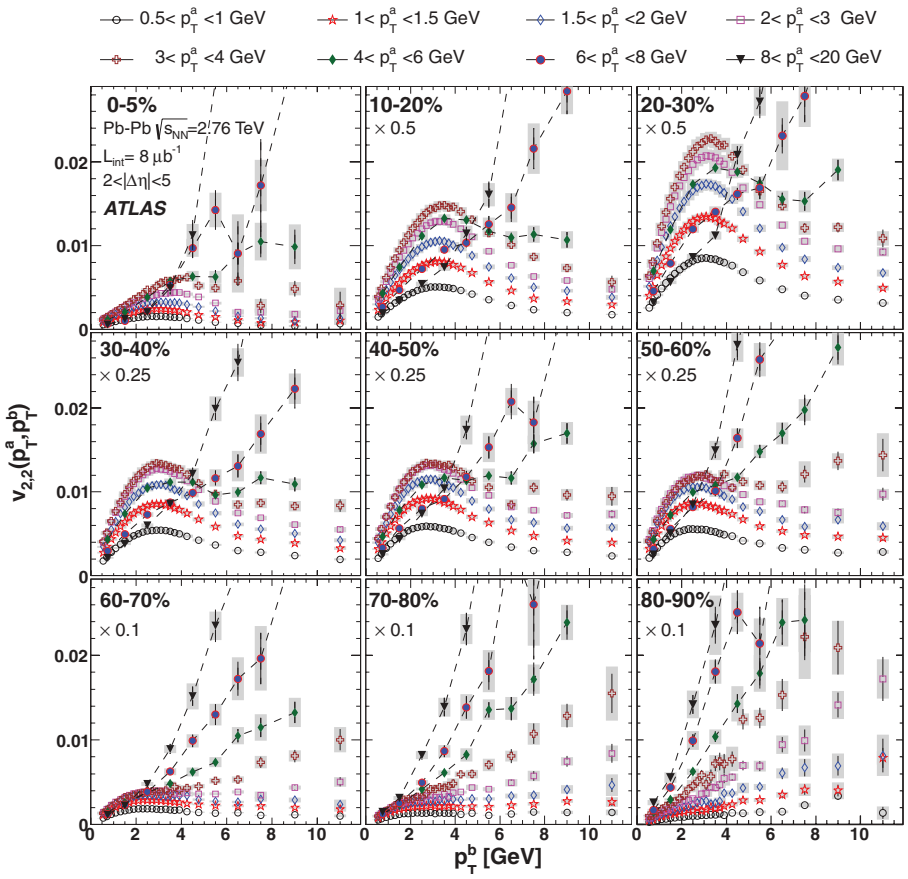

FIG. 32. (Color online) $v_{2,2}(p_T^a, p_T^b)$ for $2 < |\Delta\eta| < 5$ vs p_T^b for different p_T^a ranges. Each panel presents results in one centrality interval. The error bars and shaded bands represent statistical and systematic uncertainties, respectively. The data points for three highest p_T^a intervals have coarser binning in p_T^b, hence are connected by dashed lines to guide the eye. The data in some panels are rescaled to fit within the same vertical range.

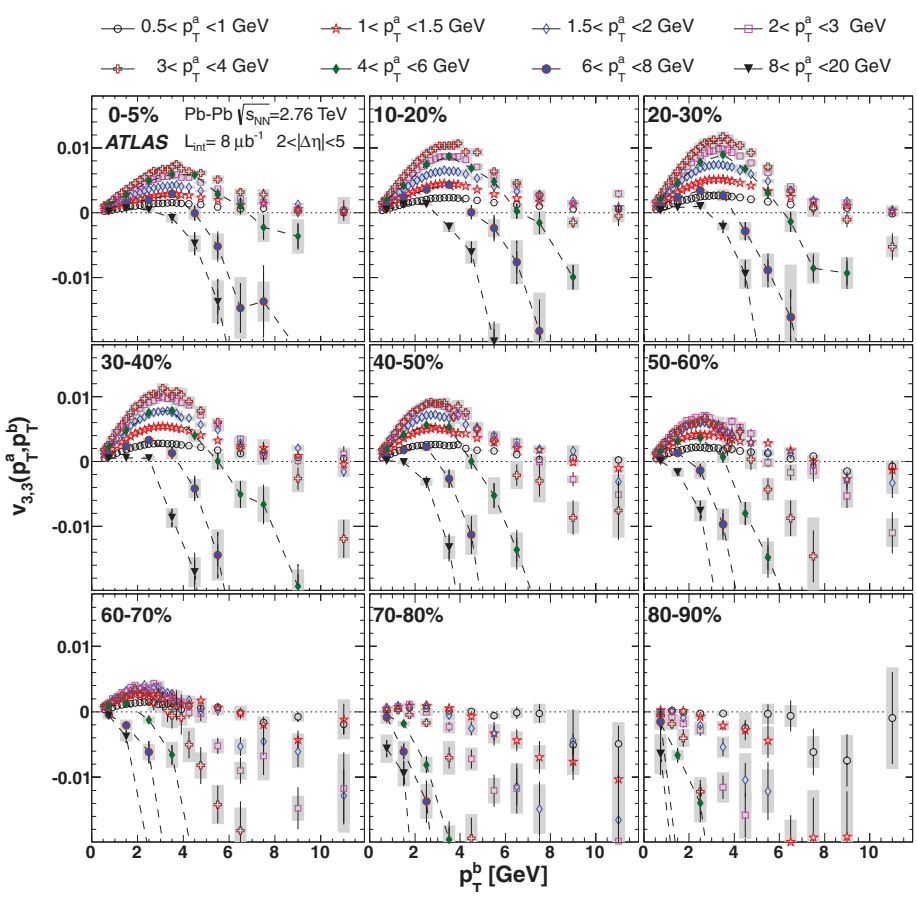

FIG. 33. (Color online) $v_{3,3}(p_T^a, p_T^b)$ for $2 < |\Delta\eta| < 5$ vs p_T^b for different p_T^a ranges. Each panel presents results in one centrality interval. The error bars and shaded bands represent statistical and systematic uncertainties, respectively. The data points for three highest p_T^a intervals have coarser binning in p_T^b, hence are connected by dashed lines to guide the eye.

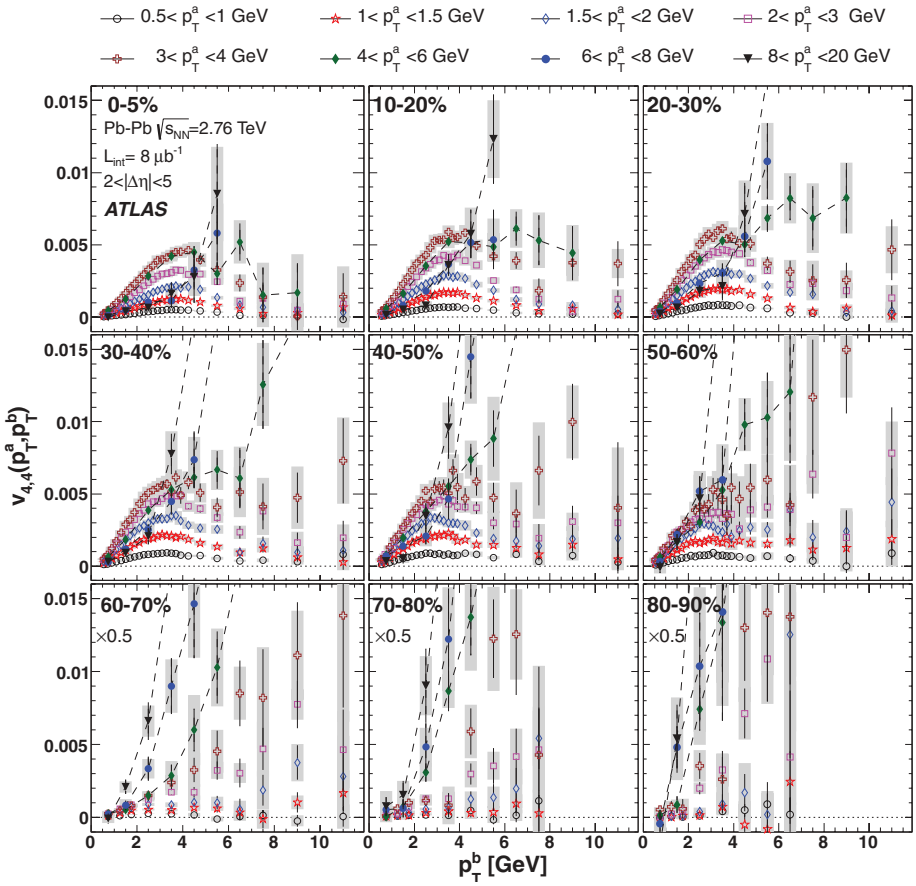

FIG. 34. (Color online) $v_{4,4}(p_T^a, p_T^b)$ for $2 < |\Delta\eta| < 5$ vs p_T^b for different p_T^a ranges. Each panel presents results in one centrality interval. The error bars and shaded bands represent statistical and systematic uncertainties, respectively. The data points for three highest p_T^a intervals have coarser binning in p_T^b, hence are connected by dashed lines to guide the eye. The data in some panels are rescaled to fit within the same vertical range.

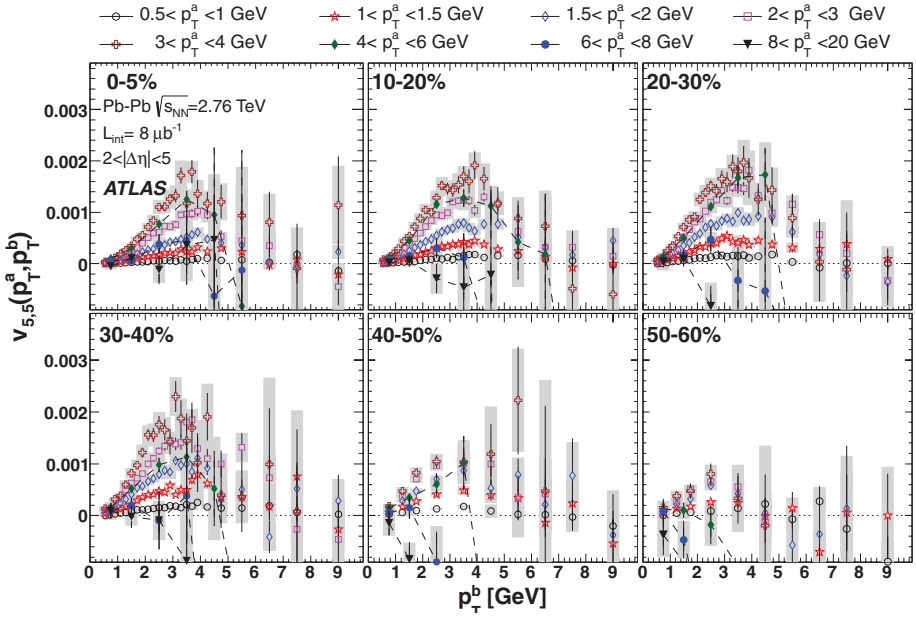

FIG. 35. (Color online) $v_{5,5}(p_T^a, p_T^b)$ for $2 < |\Delta\eta| < 5$ vs p_T^b for different p_T^a ranges. Each panel presents results in one centrality interval. The error bars and shaded bands represent statistical and systematic uncertainties, respectively. The data points for three highest p_T^a intervals have coarser binning in p_T^b, hence are connected by dashed lines to guide the eye.

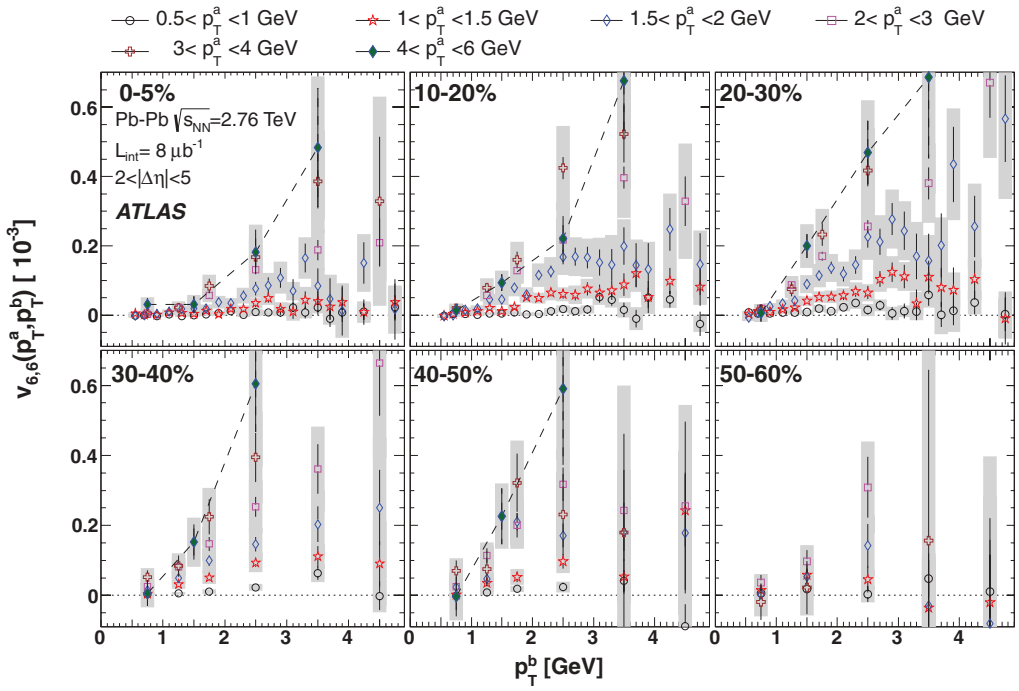

FIG. 36. (Color online) $v_{6,6}(p_T^a, p_T^b)$ for $2 < |\Delta\eta| < 5$ vs p_T^b for different p_T^a ranges. Each panel presents results in one centrality interval. The error bars and shaded bands represent statistical and systematic uncertainties, respectively. The data points for three highest p_T^a intervals have coarser binning in p_T^b, hence are connected by dashed lines to guide the eye.

[1] J. Y. Ollitrault, Phys. Rev. D **46**, 229 (1992).
[2] M. Gyulassy, I. Vitev, and X. N. Wang, Phys. Rev. Lett. **86**, 2537 (2001).
[3] S. Voloshin and Y. Zhang, Z. Phys. C **70**, 665 (1996).
[4] A. M. Poskanzer and S. A. Voloshin, Phys. Rev. C **58**, 1671 (1998).
[5] S. A. Voloshin, A. M. Poskanzer, and R. Snellings, arXiv:0809.2949 [nucl-ex].
[6] U. W. Heinz, arXiv:0901.4355 [nucl-th].
[7] D. A. Teaney, arXiv:0905.2433 [nucl-th].
[8] B. Alver and G. Roland, Phys. Rev. C **81**, 054905 (2010); **82**, 039903 (2010).
[9] B. H. Alver, C. Gombeaud, M. Luzum, and J.-Y. Ollitrault, Phys. Rev. C **82**, 034913 (2010).
[10] P. Staig and E. Shuryak, Phys. Rev. C **84**, 034908 (2011).
[11] D. Teaney and L. Yan, Phys. Rev. C **83**, 064904 (2011).
[12] M. Luzum and J. Y. Ollitrault, Phys. Rev. Lett. **106**, 102301 (2011).
[13] K. H. Ackermann *et al.* (STAR Collaboration), Phys. Rev. Lett. **86**, 402 (2001).
[14] K. Adcox *et al.*, Nucl. Phys. A **757**, 184 (2005); J. Adams *et al.*, *ibid.* **757**, 102 (2005); B. B. Back *et al.*, *ibid.* **757**, 28 (2005); I. Arsene *et al.*, *ibid.* **757**, 1 (2005).
[15] K. Aamodt *et al.* (ALICE Collaboration), Phys. Rev. Lett. **105**, 252302 (2010).
[16] G. Aad *et al.* (ATLAS Collaboration), Phys. Lett. B **707**, 330 (2012).
[17] M. Gyulassy, arXiv:nucl-th/0403032.
[18] E. Shuryak, Physics **3**, 105 (2010).
[19] D. Teaney, Phys. Rev. C **68**, 034913 (2003).
[20] P. Romatschke and U. Romatschke, Phys. Rev. Lett. **99**, 172301 (2007).
[21] H. Song, S. A. Bass, U. Heinz, T. Hirano, and C. Shen, Phys. Rev. C **83**, 054910 (2011).
[22] G. Policastro, D. T. Son, and A. O. Starinets, Phys. Rev. Lett. **87**, 081601 (2001).
[23] P. K. Kovtun, D. T. Son, and A. O. Starinets, Phys. Rev. Lett. **94**, 111601 (2005).
[24] H. Song and U. W. Heinz, J. Phys. G **36**, 064033 (2009).
[25] G. Y. Qin, H. Petersen, S. A. Bass, and B. Muller, Phys. Rev. C **82**, 064903 (2010).
[26] B. Schenke, S. Jeon, and C. Gale, Phys. Rev. C **85**, 024901 (2012).
[27] S. A. Bass, C. Gale, A. Majumder, C. Nonaka, G.-Y. Qin, T. Renk, and J. Ruppert, Phys. Rev. C **79**, 024901 (2009).
[28] A. Adare *et al.* (PHENIX Collaboration), Phys. Rev. Lett. **105**, 142301 (2010).
[29] B. Betz, M. Gyulassy, and G. Torrieri, Phys. Rev. C **84**, 024913 (2011).
[30] A. Adare *et al.* (PHENIX Collaboration), Phys. Rev. Lett. **107**, 252301 (2011).
[31] K. Aamodt *et al.* (ALICE Collaboration), Phys. Rev. Lett. **107**, 032301 (2011).
[32] Z. Qiu, C. Shen, and U. W. Heinz, Phys. Lett. B **707**, 151 (2012).
[33] J. Jia and R. Wei, Phys. Rev. C **82**, 024902 (2010).
[34] P. Staig and E. Shuryak, Phys. Rev. C **84**, 044912 (2011).
[35] G.-Y. Qin and B. Müller, Phys. Rev. C **85**, 061901 (2012).
[36] H. Petersen, R. La Placa, and S. A. Bass, J. Phys. G **39**, 055102 (2012).

[37] A. Adare *et al.* (PHENIX Collaboration), Phys. Rev. C **78**, 014901 (2008).
[38] K. Adcox *et al.* (PHENIX Collaboration), Phys. Rev. Lett. **89**, 212301 (2002).
[39] K. Aamodt *et al.* (ALICE Collaboration), Phys. Lett. B **708**, 249 (2012).
[40] S. Chatrchyan *et al.* (CMS Collaboration), Eur. Phys. J. C **72**, 2012 (2012).
[41] B. I. Abelev *et al.* (STAR Collaboration), Phys. Rev. C **80**, 064912 (2009).
[42] B. Alver *et al.* (PHOBOS Collaboration), Phys. Rev. Lett. **104**, 062301 (2010).
[43] S. S. Adler *et al.* (PHENIX Collaboration), Phys. Rev. Lett. **97**, 052301 (2006).
[44] J. Casalderrey-Solana, E. V. Shuryak, and D. Teaney, J. Phys.: Conf. Ser. **27**, 22 (2005).
[45] N. Armesto, C. A. Salgado, and U. A. Wiedemann, Phys. Rev. Lett. **93**, 242301 (2004).
[46] B. I. Abelev *et al.* (STAR Collaboration), Phys. Rev. C **77**, 054901 (2008).
[47] B. Alver *et al.* (PHOBOS Collaboration), Phys. Rev. Lett. **98**, 242302 (2007).
[48] J. Adams *et al.* (STAR Collaboration), Phys. Rev. Lett. **92**, 062301 (2004).
[49] A. Adare *et al.* (PHENIX Collaboration), Phys. Rev. Lett. **105**, 062301 (2010).
[50] E. Retinskaya, M. Luzum, and J.-Y. Ollitrault, Phys. Rev. Lett. **108**, 252302 (2012).
[51] N. Borghini, P. M. Dinh, and J.-Y. Ollitrault, Phys. Rev. C **62**, 034902 (2000).
[52] N. Borghini, P. M. Dinh, J.-Y. Ollitrault, A. M. Poskanzer, and S. A. Voloshin, Phys. Rev. C **66**, 014901 (2002).
[53] B. B. Back *et al.* (PHOBOS Collaboration), Phys. Rev. Lett. **97**, 012301 (2006).
[54] B. I. Abelev *et al.* (STAR Collaboration), Phys. Rev. Lett. **101**, 252301 (2008).
[55] G. Aad *et al.* (ATLAS Collaboration), J. Instrum. **3**, S08003 (2008).
[56] M. Chiu, A. Denisov, E. Garcia, J. Katzy, A. Makeev, M. Murray, and S. N. White, Phys. Rev. Lett. **89**, 012302 (2002).
[57] G. Aad *et al.* (ATLAS Collaboration), Phys. Lett. B **710**, 363, (2012).
[58] M. L. Miller, K. Reygers, S. J. Sanders, and P. Steinberg, Annu. Rev. Nucl. Part. Sci. **57**, 205 (2007).
[59] G. Aad *et al.* (ATLAS Collaboration), Phys. Lett. B **688**, 21 (2010).
[60] M. Gyulassy and X.-N. Wang, Comput. Phys. Commun. **83**, 307 (1994).
[61] S. Agostinelli *et al.*, Nucl. Instrum. Meth. A **506**, 250 (2003).
[62] S. Afanasiev *et al.* (PHENIX Collaboration), Phys. Rev. C **80**, 024909 (2009).
[63] J. Barrette *et al.* (E877 Collaboration), Phys. Rev. C **56**, 3254 (1997).
[64] B. B. Back *et al.* (PHOBOS Collaboration), Phys. Rev. C **72**, 051901 (2005).
[65] J. Adams *et al.* (STAR Collaboration), Phys. Rev. Lett. **93**, 252301 (2004).
[66] N. Borghini and J.-Y. Ollitrault, Phys. Lett. B **642**, 227 (2006).
[67] N. Borghini, Phys. Rev. C **75**, 021904 (2007).
[68] F. G. Gardim, F. Grassi, Y. Hama, M. Luzum, and J.-Y. Ollitrault, Phys. Rev. C **83**, 064901 (2011).
[69] I. Selyuzhenkov *et al.* (ALICE Collaboration), J. Phys. G **38**, 124167 (2011).
[70] R. Preghenella *et al.* (ALICE Collaboration), arXiv:1111.0763 [nucl-ex].
[71] B. Schenke, S. Jeon, and C. Gale, Phys. Lett. B **702**, 59 (2011).
[72] Z. Qiu and U. W. Heinz, Phys. Rev. C **84**, 024911 (2011).
[73] A. Majumder and M. Van Leeuwen, Prog. Part. Nucl. Phys. A **66**, 41 (2011).
[74] W. A. Horowitz and M. Gyulassy, J. Phys. G **38**, 124114 (2011).

G. Aad,[47] B. Abbott,[109] J. Abdallah,[11] S. Abdel Khalek,[113] A. A. Abdelalim,[48] A. Abdesselam,[116] O. Abdinov,[10] B. Abi,[110] M. Abolins,[86] O. S. AbouZeid,[156] H. Abramowicz,[151] H. Abreu,[113] E. Acerbi,[87a,87b] B. S. Acharya,[162a,162b] L. Adamczyk,[37] D. L. Adams,[24] T. N. Addy,[55] J. Adelman,[173] M. Aderholz,[97] S. Adomeit,[96] P. Adragna,[73] T. Adye,[127] S. Aefsky,[22] J. A. Aguilar-Saavedra,[122b,a] M. Aharrouche,[79] S. P. Ahlen,[21] F. Ahles,[47] A. Ahmad,[146] M. Ahsan,[40] G. Aielli,[131a,131b] T. Akdogan,[18a] T. P. A. Åkesson,[77] G. Akimoto,[153] A. V. Akimov,[92] A. Akiyama,[65] M. S. Alam,[1] M. A. Alam,[74] J. Albert,[167] S. Albrand,[54] M. Aleksa,[29] I. N. Aleksandrov,[63] F. Alessandria,[87a] C. Alexa,[25a] G. Alexander,[151] G. Alexandre,[48] T. Alexopoulos,[9] M. Alhroob,[20] M. Aliev,[15] G. Alimonti,[87a] J. Alison,[118] M. Aliyev,[10] B. M. M. Allbrooke,[17] P. P. Allport,[71] S. E. Allwood-Spiers,[52] J. Almond,[80] A. Aloisio,[100a,100b] R. Alon,[169] A. Alonso,[77] B. Alvarez Gonzalez,[86] M. G. Alviggi,[100a,100b] K. Amako,[64] P. Amaral,[29] C. Amelung,[22] V. V. Ammosov,[126] A. Amorim,[122a,b] G. Amorós,[165] N. Amram,[151] C. Anastopoulos,[29] L. S. Ancu,[16] N. Andari,[113] T. Andeen,[34] C. F. Anders,[20] G. Anders,[57a] K. J. Anderson,[30] A. Andreazza,[87a,87b] V. Andrei,[57a] M-L. Andrieux,[54] X. S. Anduaga,[68] A. Angerami,[34] F. Anghinolfi,[29] A. Anisenkov,[105] N. Anjos,[122a] A. Annovi,[46] A. Antonaki,[8] M. Antonelli,[46] A. Antonov,[94] J. Antos,[142b] F. Anulli,[130a] S. Aoun,[81] L. Aperio Bella,[4] R. Apolle,[116,c] G. Arabidze,[86] I. Aracena,[141] Y. Arai,[64] A. T. H. Arce,[44] S. Arfaoui,[146] J-F. Arguin,[14] E. Arik,[18a,*] M. Arik,[18a] A. J. Armbruster,[85] O. Arnaez,[79] V. Arnal,[78] C. Arnault,[113] A. Artamonov,[93] G. Artoni,[130a,130b] D. Arutinov,[20] S. Asai,[153] R. Asfandiyarov,[170] S. Ask,[27] B. Åsman,[144a,144b] L. Asquith,[5] K. Assamagan,[24] A. Astbury,[167] A. Astvatsatourov,[51] B. Aubert,[4] E. Auge,[113] K. Augsten,[125] M. Aurousseau,[143a] G. Avolio,[161] R. Avramidou,[9] D. Axen,[166] C. Ay,[53] G. Azuelos,[91,d] Y. Azuma,[153] M. A. Baak,[29] G. Baccaglioni,[87a] C. Bacci,[132a,132b] A. M. Bach,[14] H. Bachacou,[134] K. Bachas,[29] M. Backes,[48] M. Backhaus,[20] E. Badescu,[25a] P. Bagnaia,[130a,130b] S. Bahinipati,[2] Y. Bai,[32a] D. C. Bailey,[156] T. Bain,[156] J. T. Baines,[127] O. K. Baker,[173] M. D. Baker,[24] S. Baker,[75] E. Banas,[38] P. Banerjee,[91] Sw. Banerjee,[170] D. Banfi,[29] A. Bangert,[148] V. Bansal,[167] H. S. Bansil,[17] L. Barak,[169] S. P. Baranov,[92] A. Barashkou,[63] A. Barbaro Galtieri,[14] T. Barber,[47] E. L. Barberio,[84]

D. Barberis,[49a,49b] M. Barbero,[20] D. Y. Bardin,[63] T. Barillari,[97] M. Barisonzi,[172] T. Barklow,[141] N. Barlow,[27] B. M. Barnett,[127] R. M. Barnett,[14] A. Baroncelli,[132a] G. Barone,[48] A. J. Barr,[116] F. Barreiro,[78] J. Barreiro Guimarães da Costa,[56] P. Barrillon,[113] R. Bartoldus,[141] A. E. Barton,[69] V. Bartsch,[147] R. L. Bates,[52] L. Batkova,[142a] J. R. Batley,[27] A. Battaglia,[16] M. Battistin,[29] F. Bauer,[134] H. S. Bawa,[141,e] S. Beale,[96] T. Beau,[76] P. H. Beauchemin,[159] R. Beccherle,[49a] P. Bechtle,[20] H. P. Beck,[16] S. Becker,[96] M. Beckingham,[136] K. H. Becks,[172] A. J. Beddall,[18c] A. Beddall,[18c] S. Bedikian,[173] V. A. Bednyakov,[63] C. P. Bee,[81] M. Begel,[24] S. Behar Harpaz,[150] P. K. Behera,[61] M. Beimforde,[97] C. Belanger-Champagne,[83] P. J. Bell,[48] W. H. Bell,[48] G. Bella,[151] L. Bellagamba,[19a] F. Bellina,[29] M. Bellomo,[29] A. Belloni,[56] O. Beloborodova,[105,f] K. Belotskiy,[94] O. Beltramello,[29] O. Benary,[151] D. Benchekroun,[133a] M. Bendel,[79] N. Benekos,[163] Y. Benhammou,[151] E. Benhar Noccioli,[48] J. A. Benitez Garcia,[157b] D. P. Benjamin,[44] M. Benoit,[113] J. R. Bensinger,[22] K. Benslama,[128] S. Bentvelsen,[103] D. Berge,[29] E. Bergeaas Kuutmann,[41] N. Berger,[4] F. Berghaus,[167] E. Berglund,[103] J. Beringer,[14] P. Bernat,[75] R. Bernhard,[47] C. Bernius,[24] T. Berry,[74] C. Bertella,[81] A. Bertin,[19a,19b] F. Bertinelli,[29] F. Bertolucci,[120a,120b] M. I. Besana,[87a,87b] N. Besson,[134] S. Bethke,[97] W. Bhimji,[45] R. M. Bianchi,[29] M. Bianco,[70a,70b] O. Biebel,[96] S. P. Bieniek,[75] K. Bierwagen,[53] J. Biesiada,[14] M. Biglietti,[132a] H. Bilokon,[46] M. Bindi,[19a,19b] S. Binet,[113] A. Bingul,[18c] C. Bini,[130a,130b] C. Biscarat,[175] U. Bitenc,[47] K. M. Black,[21] R. E. Blair,[5] J.-B. Blanchard,[134] G. Blanchot,[29] T. Blazek,[142a] C. Blocker,[22] J. Blocki,[38] A. Blondel,[48] W. Blum,[79] U. Blumenschein,[53] G. J. Bobbink,[103] V. B. Bobrovnikov,[105] S. S. Bocchetta,[77] A. Bocci,[44] C. R. Boddy,[116] M. Boehler,[41] J. Boek,[172] N. Boelaert,[35] J. A. Bogaerts,[29] A. Bogdanchikov,[105] A. Bogouch,[88,*] C. Bohm,[144a] J. Bohm,[123] V. Boisvert,[74] T. Bold,[37] V. Boldea,[25a] N. M. Bolnet,[134] M. Bomben,[76] M. Bona,[73] V. G. Bondarenko,[94] M. Bondioli,[161] M. Boonekamp,[134] C. N. Booth,[137] S. Bordoni,[76] C. Borer,[16] A. Borisov,[126] G. Borissov,[69] I. Borjanovic,[12a] M. Borri,[80] S. Borroni,[85] V. Bortolotto,[132a,132b] K. Bos,[103] D. Boscherini,[19a] M. Bosman,[11] H. Boterenbrood,[103] D. Botterill,[127] J. Bouchami,[91] J. Boudreau,[121] E. V. Bouhova-Thacker,[69] D. Boumediene,[33] C. Bourdarios,[113] N. Bousson,[81] A. Boveia,[30] J. Boyd,[29] I. R. Boyko,[63] N. I. Bozhko,[126] I. Bozovic-Jelisavcic,[12b] J. Bracinik,[17] A. Braem,[29] P. Branchini,[132a] G. W. Brandenburg,[56] A. Brandt,[7] G. Brandt,[116] O. Brandt,[53] U. Bratzler,[154] B. Brau,[82] J. E. Brau,[112] H. M. Braun,[172] B. Brelier,[156] J. Bremer,[29] K. Brendlinger,[118] R. Brenner,[164] S. Bressler,[169] D. Britton,[52] F. M. Brochu,[27] I. Brock,[20] R. Brock,[86] T. J. Brodbeck,[69] E. Brodet,[151] F. Broggi,[87a] C. Bromberg,[86] J. Bronner,[97] G. Brooijmans,[34] W. K. Brooks,[31b] G. Brown,[80] H. Brown,[7] P. A. Bruckman de Renstrom,[38] D. Bruncko,[142b] R. Bruneliere,[47] S. Brunet,[59] A. Bruni,[19a] G. Bruni,[19a] M. Bruschi,[19a] T. Buanes,[13] Q. Buat,[54] F. Bucci,[48] J. Buchanan,[116] N. J. Buchanan,[2] P. Buchholz,[139] R. M. Buckingham,[116] A. G. Buckley,[45] S. I. Buda,[25a] I. A. Budagov,[63] B. Budick,[106] V. Büscher,[79] L. Bugge,[115] O. Bulekov,[94] M. Bunse,[42] T. Buran,[115] H. Burckhart,[29] S. Burdin,[71] T. Burgess,[13] S. Burke,[127] E. Busato,[33] P. Bussey,[52] C. P. Buszello,[164] F. Butin,[29] B. Butler,[141] J. M. Butler,[21] C. M. Buttar,[52] J. M. Butterworth,[75] W. Buttinger,[27] S. Cabrera Urbán,[165] D. Caforio,[19a,19b] O. Cakir,[3a] P. Calafiura,[14] G. Calderini,[76] P. Calfayan,[96] R. Calkins,[104] L. P. Caloba,[23a] R. Caloi,[130a,130b] D. Calvet,[33] S. Calvet,[33] R. Camacho Toro,[33] P. Camarri,[131a,131b] M. Cambiaghi,[117a,117b] D. Cameron,[115] L. M. Caminada,[14] S. Campana,[29] M. Campanelli,[75] V. Canale,[100a,100b] F. Canelli,[30,g] A. Canepa,[157a] J. Cantero,[78] L. Capasso,[100a,100b] M. D. M. Capeans Garrido,[29] I. Caprini,[25a] M. Caprini,[25a] D. Capriotti,[97] M. Capua,[36a,36b] R. Caputo,[79] R. Cardarelli,[131a] T. Carli,[29] G. Carlino,[100a] L. Carminati,[87a,87b] B. Caron,[83] S. Caron,[102] E. Carquin,[31b] G. D. Carrillo Montoya,[170] A. A. Carter,[73] J. R. Carter,[27] J. Carvalho,[122a,h] D. Casadei,[106] M. P. Casado,[11] M. Cascella,[120a,120b] C. Caso,[49a,49b,*] A. M. Castaneda Hernandez,[170] E. Castaneda-Miranda,[170] V. Castillo Gimenez,[165] N. F. Castro,[122a] G. Cataldi,[70a] A. Catinaccio,[29] J. R. Catmore,[29] A. Cattai,[29] G. Cattani,[131a,131b] S. Caughron,[86] D. Cauz,[162a,162c] P. Cavalleri,[76] D. Cavalli,[87a] M. Cavalli-Sforza,[11] V. Cavasinni,[120a,120b] F. Ceradini,[132a,132b] A. S. Cerqueira,[23b] A. Cerri,[29] L. Cerrito,[73] F. Cerutti,[46] S. A. Cetin,[18b] F. Cevenini,[100a,100b] A. Chafaq,[133a] D. Chakraborty,[104] K. Chan,[2] B. Chapleau,[83] J. D. Chapman,[27] J. W. Chapman,[85] E. Chareyre,[76] D. G. Charlton,[17] V. Chavda,[80] C. A. Chavez Barajas,[29] S. Cheatham,[83] S. Chekanov,[5] S. V. Chekulaev,[157a] G. A. Chelkov,[63] M. A. Chelstowska,[102] C. Chen,[62] H. Chen,[24] S. Chen,[32c] T. Chen,[32c] X. Chen,[170] S. Cheng,[32a] A. Cheplakov,[63] V. F. Chepurnov,[63] R. Cherkaoui El Moursli,[133e] V. Chernyatin,[24] E. Cheu,[6] S. L. Cheung,[156] L. Chevalier,[134] G. Chiefari,[100a,100b] L. Chikovani,[50a] J. T. Childers,[29] A. Chilingarov,[69] G. Chiodini,[70a] A. S. Chisholm,[17] R. T. Chislett,[75] M. V. Chizhov,[63] G. Choudalakis,[30] S. Chouridou,[135] I. A. Christidi,[75] A. Christov,[47] D. Chromek-Burckhart,[29] M. L. Chu,[149] J. Chudoba,[123] G. Ciapetti,[130a,130b] A. K. Ciftci,[3a] R. Ciftci,[3a] D. Cinca,[33] V. Cindro,[72] M. D. Ciobotaru,[161] C. Ciocca,[19a] A. Ciocio,[14] M. Cirilli,[85] M. Citterio,[87a] M. Ciubancan,[25a] A. Clark,[48] P. J. Clark,[45] W. Cleland,[121] J. C. Clemens,[81] B. Clement,[54] C. Clement,[144a,144b] R. W. Clifft,[127] Y. Coadou,[81] M. Cobal,[162a,162c] A. Coccaro,[170] J. Cochran,[62] P. Coe,[116] J. G. Cogan,[141] J. Coggeshall,[163] E. Cogneras,[175] J. Colas,[4] A. P. Colijn,[103] N. J. Collins,[17] C. Collins-Tooth,[52] J. Collot,[54] G. Colon,[82] P. Conde Muiño,[122a] E. Coniavitis,[116] M. C. Conidi,[11] M. Consonni,[102] S. M. Consonni,[87a,87b] V. Consorti,[47] S. Constantinescu,[25a] C. Conta,[117a,117b] G. Conti,[56] F. Conventi,[100a,i] J. Cook,[29] M. Cooke,[14] B. D. Cooper,[75] A. M. Cooper-Sarkar,[116] K. Copic,[14] T. Cornelissen,[172] M. Corradi,[19a] F. Corriveau,[83,j] A. Cortes-Gonzalez,[163] G. Cortiana,[97] G. Costa,[87a] M. J. Costa,[165] D. Costanzo,[137] T. Costin,[30] D. Côté,[29] R. Coura Torres,[23a] L. Courneyea,[167] G. Cowan,[74] C. Cowden,[27] B. E. Cox,[80] K. Cranmer,[106] F. Crescioli,[120a,120b] M. Cristinziani,[20] G. Crosetti,[36a,36b] R. Crupi,[70a,70b] S. Crépé-Renaudin,[54] C.-M. Cuciuc,[25a] C. Cuenca Almenar,[173] T. Cuhadar Donszelmann,[137] M. Curatolo,[46] C. J. Curtis,[17] C. Cuthbert,[148] P. Cwetanski,[59] H. Czirr,[139] P. Czodrowski,[43] Z. Czyczula,[173] S. D'Auria,[52] M. D'Onofrio,[71] A. D'Orazio,[130a,130b] P. V. M. Da Silva,[23a] C. Da Via,[80] W. Dabrowski,[37] A. Dafinca,[116] T. Dai,[85] C. Dallapiccola,[82] M. Dam,[35] M. Dameri,[49a,49b] D. S. Damiani,[135] H. O. Danielsson,[29] D. Dannheim,[97] V. Dao,[48] G. Darbo,[49a] G. L. Darlea,[25b] W. Davey,[20] T. Davidek,[124] N. Davidson,[84] R. Davidson,[69] E. Davies,[116,c] M. Davies,[91] A. R. Davison,[75] Y. Davygora,[57a] E. Dawe,[140] I. Dawson,[137] J. W. Dawson,[5,*] R. K. Daya-Ishmukhametova,[22] K. De,[7] R. de

Asmundis,[100a] S. De Castro,[19a,19b] P. E. De Castro Faria Salgado,[24] S. De Cecco,[76] J. de Graat,[96] N. De Groot,[102] P. de Jong,[103] C. De La Taille,[113] H. De la Torre,[78] B. De Lotto,[162a,162c] L. de Mora,[69] L. De Nooij,[103] D. De Pedis,[130a] A. De Salvo,[130a] U. De Sanctis,[162a,162c] A. De Santo,[147] J. B. De Vivie De Regie,[113] G. De Zorzi,[130a,130b] S. Dean,[75] W. J. Dearnaley,[69] R. Debbe,[24] C. Debenedetti,[45] B. Dechenaux,[54] D. V. Dedovich,[63] J. Degenhardt,[118] M. Dehchar,[116] C. Del Papa,[162a,162c] J. Del Peso,[78] T. Del Prete,[120a,120b] T. Delemontex,[54] M. Deliyergiyev,[72] A. Dell'Acqua,[29] L. Dell'Asta,[21] M. Della Pietra,[100a,i] D. della Volpe,[100a,100b] M. Delmastro,[4] N. Delruelle,[29] P. A. Delsart,[54] C. Deluca,[146] S. Demers,[173] M. Demichev,[63] B. Demirkoz,[11,k] J. Deng,[161] S. P. Denisov,[126] D. Derendarz,[38] J. E. Derkaoui,[133d] F. Derue,[76] P. Dervan,[71] K. Desch,[20] E. Devetak,[146] P. O. Deviveiros,[103] A. Dewhurst,[127] B. DeWilde,[146] S. Dhaliwal,[156] R. Dhullipudi,[24,l] A. Di Ciaccio,[131a,131b] L. Di Ciaccio,[4] A. Di Girolamo,[29] B. Di Girolamo,[29] S. Di Luise,[132a,132b] A. Di Mattia,[170] B. Di Micco,[29] R. Di Nardo,[46] A. Di Simone,[131a,131b] R. Di Sipio,[19a,19b] M. A. Diaz,[31a] F. Diblen,[18c] E. B. Diehl,[85] J. Dietrich,[41] T. A. Dietzsch,[57a] S. Diglio,[84] K. Dindar Yagci,[39] J. Dingfelder,[20] C. Dionisi,[130a,130b] P. Dita,[25a] S. Dita,[25a] F. Dittus,[29] F. Djama,[81] T. Djobava,[50b] M. A. B. do Vale,[23c] A. Do Valle Wemans,[122a] T. K. O. Doan,[4] M. Dobbs,[83] R. Dobinson,[29,*] D. Dobos,[29] E. Dobson,[29,m] J. Dodd,[34] C. Doglioni,[48] T. Doherty,[52] Y. Doi,[64,*] J. Dolejsi,[124] I. Dolenc,[72] Z. Dolezal,[124] B. A. Dolgoshein,[94,*] T. Dohmae,[153] M. Donadelli,[23d] M. Donega,[118] J. Donini,[33] J. Dopke,[29] A. Doria,[100a] A. Dos Anjos,[170] M. Dosil,[11] A. Dotti,[120a,120b] M. T. Dova,[68] A. D. Doxiadis,[103] A. T. Doyle,[52] Z. Drasal,[124] J. Drees,[172] N. Dressnandt,[118] H. Drevermann,[29] C. Driouichi,[35] M. Dris,[9] J. Dubbert,[97] S. Dube,[14] E. Duchovni,[169] G. Duckeck,[96] A. Dudarev,[29] F. Dudziak,[62] M. Dührssen,[29] I. P. Duerdoth,[80] L. Duflot,[113] M.-A. Dufour,[83] M. Dunford,[29] H. Duran Yildiz,[3a] R. Duxfield,[137] M. Dwuznik,[37] F. Dydak,[29] M. Düren,[51] W. L. Ebenstein,[44] J. Ebke,[96] S. Eckweiler,[79] K. Edmonds,[79] C. A. Edwards,[74] N. C. Edwards,[52] W. Ehrenfeld,[41] T. Ehrich,[97] T. Eifert,[141] G. Eigen,[13] K. Einsweiler,[14] E. Eisenhandler,[73] T. Ekelof,[164] M. El Kacimi,[133c] M. Ellert,[164] S. Elles,[4] F. Ellinghaus,[79] K. Ellis,[73] N. Ellis,[29] J. Elmsheuser,[96] M. Elsing,[29] D. Emeliyanov,[127] R. Engelmann,[146] A. Engl,[96] B. Epp,[60] A. Eppig,[85] J. Erdmann,[53] A. Ereditato,[16] D. Eriksson,[144a] J. Ernst,[1] M. Ernst,[24] J. Ernwein,[134] D. Errede,[163] S. Errede,[163] E. Ertel,[79] M. Escalier,[113] C. Escobar,[121] X. Espinal Curull,[11] B. Esposito,[46] F. Etienne,[81] A. I. Etienvre,[134] E. Etzion,[151] D. Evangelakou,[53] H. Evans,[59] L. Fabbri,[19a,19b] C. Fabre,[29] R. M. Fakhrutdinov,[126] S. Falciano,[130a] Y. Fang,[170] M. Fanti,[87a,87b] A. Farbin,[7] A. Farilla,[132a] J. Farley,[146] T. Farooque,[156] S. Farrell,[161] S. M. Farrington,[116] P. Farthouat,[29] P. Fassnacht,[29] D. Fassouliotis,[8] B. Fatholahzadeh,[156] A. Favareto,[87a,87b] L. Fayard,[113] S. Fazio,[36a,36b] R. Febbraro,[33] P. Federic,[142a] O. L. Fedin,[119] W. Fedorko,[86] M. Fehling-Kaschek,[47] L. Feligioni,[81] D. Fellmann,[5] C. Feng,[32d] E. J. Feng,[30] A. B. Fenyuk,[126] J. Ferencei,[142b] J. Ferland,[91] W. Fernando,[107] S. Ferrag,[52] J. Ferrando,[52] V. Ferrara,[41] A. Ferrari,[164] P. Ferrari,[103] R. Ferrari,[117a] D. E. Ferreira de Lima,[52] A. Ferrer,[165] M. L. Ferrer,[46] D. Ferrere,[48] C. Ferretti,[85] A. Ferretto Parodi,[49a,49b] M. Fiascaris,[30] F. Fiedler,[79] A. Filipčič,[72] A. Filippas,[9] F. Filthaut,[102] M. Fincke-Keeler,[167] M. C. N. Fiolhais,[122a,h] L. Fiorini,[165] A. Firan,[39] G. Fischer,[41] P. Fischer,[20] M. J. Fisher,[107] M. Flechl,[47] I. Fleck,[139] J. Fleckner,[79] P. Fleischmann,[171] S. Fleischmann,[172] T. Flick,[172] A. Floderus,[77] L. R. Flores Castillo,[170] M. J. Flowerdew,[97] M. Fokitis,[9] T. Fonseca Martin,[16] D. A. Forbush,[136] A. Formica,[134] A. Forti,[80] D. Fortin,[157a] J. M. Foster,[80] D. Fournier,[113] A. Foussat,[29] A. J. Fowler,[44] K. Fowler,[135] H. Fox,[69] P. Francavilla,[11] S. Franchino,[117a,117b] D. Francis,[29] T. Frank,[169] M. Franklin,[56] S. Franz,[29] M. Fraternali,[117a,117b] S. Fratina,[118] S. T. French,[27] F. Friedrich,[43] R. Froeschl,[29] D. Froidevaux,[29] J. A. Frost,[27] C. Fukunaga,[154] E. Fullana Torregrosa,[29] J. Fuster,[165] C. Gabaldon,[29] O. Gabizon,[169] T. Gadfort,[24] S. Gadomski,[48] G. Gagliardi,[49a,49b] P. Gagnon,[59] C. Galea,[96] E. J. Gallas,[116] V. Gallo,[16] B. J. Gallop,[127] P. Gallus,[123] K. K. Gan,[107] Y. S. Gao,[141,e] V. A. Gapienko,[126] A. Gaponenko,[14] F. Garberson,[173] M. Garcia-Sciveres,[14] C. García,[165] J. E. García Navarro,[165] R. W. Gardner,[30] N. Garelli,[29] H. Garitaonandia,[103] V. Garonne,[29] J. Garvey,[17] C. Gatti,[46] G. Gaudio,[117a] B. Gaur,[139] L. Gauthier,[134] P. Gauzzi,[130a,130b] I. L. Gavrilenko,[92] C. Gay,[166] G. Gaycken,[20] J-C. Gayde,[29] E. N. Gazis,[9] P. Ge,[32d] C. N. P. Gee,[127] D. A. A. Geerts,[103] Ch. Geich-Gimbel,[20] K. Gellerstedt,[144a,144b] C. Gemme,[49a] A. Gemmell,[52] M. H. Genest,[54] S. Gentile,[130a,130b] M. George,[53] S. George,[74] P. Gerlach,[172] A. Gershon,[151] C. Geweniger,[57a] H. Ghazlane,[133b] N. Ghodbane,[33] B. Giacobbe,[19a] S. Giagu,[130a,130b] V. Giakoumopoulou,[8] V. Giangiobbe,[11] F. Gianotti,[29] B. Gibbard,[24] A. Gibson,[156] S. M. Gibson,[29] L. M. Gilbert,[116] V. Gilewsky,[89] D. Gillberg,[28] A. R. Gillman,[127] D. M. Gingrich,[2,d] J. Ginzburg,[151] N. Giokaris,[8] M. P. Giordani,[162c] R. Giordano,[100a,100b] F. M. Giorgi,[15] P. Giovannini,[97] P. F. Giraud,[134] D. Giugni,[87a] M. Giunta,[91] P. Giusti,[19a] B. K. Gjelsten,[115] L. K. Gladilin,[95] C. Glasman,[78] J. Glatzer,[47] A. Glazov,[41] K. W. Glitza,[172] G. L. Glonti,[63] J. R. Goddard,[73] J. Godfrey,[140] J. Godlewski,[29] M. Goebel,[41] T. Göpfert,[43] C. Goeringer,[79] C. Gössling,[42] T. Göttfert,[97] S. Goldfarb,[85] T. Golling,[173] A. Gomes,[122a,b] L. S. Gomez Fajardo,[41] R. Gonçalo,[74] J. Goncalves Pinto Firmino Da Costa,[41] L. Gonella,[20] A. Gonidec,[29] S. Gonzalez,[170] S. González de la Hoz,[165] G. Gonzalez Parra,[11] M. L. Gonzalez Silva,[26] S. Gonzalez-Sevilla,[48] J. J. Goodson,[146] L. Goossens,[29] P. A. Gorbounov,[93] H. A. Gordon,[24] I. Gorelov,[101] G. Gorfine,[172] B. Gorini,[29] E. Gorini,[70a,70b] A. Gorišek,[72] E. Gornicki,[38] V. N. Goryachev,[126] B. Gosdzik,[41] M. Gosselink,[103] M. I. Gostkin,[63] I. Gough Eschrich,[161] M. Gouighri,[133a] D. Goujdami,[133c] M. P. Goulette,[48] A. G. Goussiou,[136] C. Goy,[4] S. Gozpinar,[22] I. Grabowska-Bold,[37] P. Grafström,[29] K-J. Grahn,[41] F. Grancagnolo,[70a] S. Grancagnolo,[15] V. Grassi,[146] V. Gratchev,[119] N. Grau,[34] H. M. Gray,[29] J. A. Gray,[146] E. Graziani,[132a] O. G. Grebenyuk,[119] T. Greenshaw,[71] Z. D. Greenwood,[24,l] K. Gregersen,[35] I. M. Gregor,[41] P. Grenier,[141] J. Griffiths,[136] N. Grigalashvili,[63] A. A. Grillo,[135] S. Grinstein,[11] Y. V. Grishkevich,[95] J.-F. Grivaz,[113] M. Groh,[97] E. Gross,[169] J. Grosse-Knetter,[53] J. Groth-Jensen,[169] K. Grybel,[139] V. J. Guarino,[5] D. Guest,[173] C. Guicheney,[33] A. Guida,[70a,70b] S. Guindon,[53] H. Guler,[83,n] J. Gunther,[123] B. Guo,[156] J. Guo,[34] A. Gupta,[30] Y. Gusakov,[63] V. N. Gushchin,[126] P. Gutierrez,[109] N. Guttman,[151] O. Gutzwiller,[170] C. Guyot,[134] C. Gwenlan,[116] C. B. Gwilliam,[71] A. Haas,[141] S. Haas,[29] C. Haber,[14] H. K. Hadavand,[39] D. R. Hadley,[17] P. Haefner,[97] F. Hahn,[29] S. Haider,[29] Z. Hajduk,[38] H. Hakobyan,[174] D. Hall,[116] J. Haller,[53]

K. Hamacher,[172] P. Hamal,[111] M. Hamer,[53] A. Hamilton,[143b,o] S. Hamilton,[159] H. Han,[32a] L. Han,[32b] K. Hanagaki,[114] K. Hanawa,[158] M. Hance,[14] C. Handel,[79] P. Hanke,[57a] J. R. Hansen,[35] J. B. Hansen,[35] J. D. Hansen,[35] P. H. Hansen,[35] P. Hansson,[141] K. Hara,[158] G. A. Hare,[135] T. Harenberg,[172] S. Harkusha,[88] D. Harper,[85] R. D. Harrington,[45] O. M. Harris,[136] K. Harrison,[17] J. Hartert,[47] F. Hartjes,[103] T. Haruyama,[64] A. Harvey,[55] S. Hasegawa,[99] Y. Hasegawa,[138] S. Hassani,[134] M. Hatch,[29] D. Hauff,[97] S. Haug,[16] M. Hauschild,[29] R. Hauser,[86] M. Havranek,[20] B. M. Hawes,[116] C. M. Hawkes,[17] R. J. Hawkings,[29] A. D. Hawkins,[77] D. Hawkins,[161] T. Hayakawa,[65] T. Hayashi,[158] D. Hayden,[74] H. S. Hayward,[71] S. J. Haywood,[127] E. Hazen,[21] M. He,[32d] S. J. Head,[17] V. Hedberg,[77] L. Heelan,[7] S. Heim,[86] B. Heinemann,[14] S. Heisterkamp,[35] L. Helary,[4] C. Heller,[96] M. Heller,[29] S. Hellman,[144a,144b] D. Hellmich,[20] C. Helsens,[11] R. C. W. Henderson,[69] M. Henke,[57a] A. Henrichs,[53] A. M. Henriques Correia,[29] S. Henrot-Versille,[113] F. Henry-Couannier,[81] C. Hensel,[53] T. Henß,[172] C. M. Hernandez,[7] Y. Hernández Jiménez,[165] R. Herrberg,[15] A. D. Hershenhorn,[150] G. Herten,[47] R. Hertenberger,[96] L. Hervas,[29] G. G. Hesketh,[75] N. P. Hessey,[103] E. Higón-Rodriguez,[165] D. Hill,[5,*] J. C. Hill,[27] N. Hill,[5] K. H. Hiller,[41] S. Hillert,[20] S. J. Hillier,[17] I. Hinchliffe,[14] E. Hines,[118] M. Hirose,[114] F. Hirsch,[42] D. Hirschbuehl,[172] J. Hobbs,[146] N. Hod,[151] M. C. Hodgkinson,[137] P. Hodgson,[137] A. Hoecker,[29] M. R. Hoeferkamp,[101] J. Hoffman,[39] D. Hoffmann,[81] M. Hohlfeld,[79] M. Holder,[139] S. O. Holmgren,[144a] T. Holy,[125] J. L. Holzbauer,[86] Y. Homma,[65] T. M. Hong,[118] L. Hooft van Huysduynen,[106] T. Horazdovsky,[125] C. Horn,[141] S. Horner,[47] J-Y. Hostachy,[54] S. Hou,[149] M. A. Houlden,[71] A. Hoummada,[133a] J. Howarth,[80] D. F. Howell,[116] I. Hristova,[15] J. Hrivnac,[113] I. Hruska,[123] T. Hryn'ova,[4] P. J. Hsu,[79] S.-C. Hsu,[14] G. S. Huang,[109] Z. Hubacek,[125] F. Hubaut,[81] F. Huegging,[20] A. Huettmann,[41] T. B. Huffman,[116] E. W. Hughes,[34] G. Hughes,[69] R. E. Hughes-Jones,[80] M. Huhtinen,[29] P. Hurst,[56] M. Hurwitz,[14] U. Husemann,[41] N. Huseynov,[63,p] J. Huston,[86] J. Huth,[56] G. Iacobucci,[48] G. Iakovidis,[9] M. Ibbotson,[80] I. Ibragimov,[139] R. Ichimiya,[65] L. Iconomidou-Fayard,[113] J. Idarraga,[113] P. Iengo,[100a] O. Igonkina,[103] Y. Ikegami,[64] M. Ikeno,[64] Y. Ilchenko,[39] D. Iliadis,[152] N. Ilic,[156] M. Imori,[153] T. Ince,[20] J. Inigo-Golfin,[29] P. Ioannou,[8] M. Iodice,[132a] V. Ippolito,[130a,130b] A. Irles Quiles,[165] C. Isaksson,[164] A. Ishikawa,[65] M. Ishino,[66] R. Ishmukhametov,[39] C. Issever,[116] S. Istin,[18a] A. V. Ivashin,[126] W. Iwanski,[38] H. Iwasaki,[64] J. M. Izen,[40] V. Izzo,[100a] B. Jackson,[118] J. N. Jackson,[71] P. Jackson,[141] M. R. Jaekel,[29] V. Jain,[59] K. Jakobs,[47] S. Jakobsen,[35] J. Jakubek,[125] D. K. Jana,[109] E. Jansen,[75] H. Jansen,[29] A. Jantsch,[97] M. Janus,[47] G. Jarlskog,[77] L. Jeanty,[56] K. Jelen,[37] I. Jen-La Plante,[30] P. Jenni,[29] A. Jeremie,[4] P. Jež,[35] S. Jézéquel,[4] M. K. Jha,[19a] H. Ji,[170] W. Ji,[79] J. Jia,[146] Y. Jiang,[32b] M. Jimenez Belenguer,[41] G. Jin,[32b] S. Jin,[32a] O. Jinnouchi,[155] M. D. Joergensen,[35] D. Joffe,[39] L. G. Johansen,[13] M. Johansen,[144a,144b] K. E. Johansson,[144a] P. Johansson,[137] S. Johnert,[41] K. A. Johns,[6] K. Jon-And,[144a,144b] G. Jones,[116] R. W. L. Jones,[69] T. W. Jones,[75] T. J. Jones,[71] O. Jonsson,[29] C. Joram,[29] P. M. Jorge,[122a] J. Joseph,[14] K. D. Joshi,[80] J. Jovicevic,[145] T. Jovin,[12b] X. Ju,[170] C. A. Jung,[42] R. M. Jungst,[29] V. Juranek,[123] P. Jussel,[60] A. Juste Rozas,[11] V. V. Kabachenko,[126] S. Kabana,[16] M. Kaci,[165] A. Kaczmarska,[38] P. Kadlecik,[35] M. Kado,[113] H. Kagan,[107] M. Kagan,[56] S. Kaiser,[97] E. Kajomovitz,[150] S. Kalinin,[172] L. V. Kalinovskaya,[63] S. Kama,[39] N. Kanaya,[153] M. Kaneda,[29] S. Kaneti,[27] T. Kanno,[155] V. A. Kantserov,[94] J. Kanzaki,[64] B. Kaplan,[173] A. Kapliy,[30] J. Kaplon,[29] D. Kar,[43] M. Karagounis,[20] M. Karagoz,[116] M. Karnevskiy,[41] V. Kartvelishvili,[69] A. N. Karyukhin,[126] L. Kashif,[170] G. Kasieczka,[57b] R. D. Kass,[107] A. Kastanas,[13] M. Kataoka,[4] Y. Kataoka,[153] E. Katsoufis,[9] J. Katzy,[41] V. Kaushik,[6] K. Kawagoe,[65] T. Kawamoto,[153] G. Kawamura,[79] M. S. Kayl,[103] V. A. Kazanin,[105] M. Y. Kazarinov,[63] R. Keeler,[167] R. Kehoe,[39] M. Keil,[53] G. D. Kekelidze,[63] J. S. Keller,[136] J. Kennedy,[96] M. Kenyon,[52] O. Kepka,[123] N. Kerschen,[29] B. P. Kerševan,[72] S. Kersten,[172] K. Kessoku,[153] J. Keung,[156] F. Khalil-zada,[10] H. Khandanyan,[163] A. Khanov,[110] D. Kharchenko,[63] A. Khodinov,[94] A. G. Kholodenko,[126] A. Khomich,[57a] T. J. Khoo,[27] G. Khoriauli,[20] A. Khoroshilov,[172] N. Khovanskiy,[63] V. Khovanskiy,[93] E. Khramov,[63] J. Khubua,[50b] H. Kim,[144a,144b] M. S. Kim,[2] S. H. Kim,[158] N. Kimura,[168] O. Kind,[15] B. T. King,[71] M. King,[65] R. S. B. King,[116] J. Kirk,[127] L. E. Kirsch,[22] A. E. Kiryunin,[97] T. Kishimoto,[65] D. Kisielewska,[37] T. Kittelmann,[121] A. M. Kiver,[126] E. Kladiva,[142b] M. Klein,[71] U. Klein,[71] K. Kleinknecht,[79] M. Klemetti,[83] A. Klier,[169] P. Klimek,[144a,144b] A. Klimentov,[24] R. Klingenberg,[42] J. A. Klinger,[80] E. B. Klinkby,[35] T. Klioutchnikova,[29] P. F. Klok,[102] S. Klous,[103] E.-E. Kluge,[57a] T. Kluge,[71] P. Kluit,[103] S. Kluth,[97] N. S. Knecht,[156] E. Kneringer,[60] J. Knobloch,[29] E. B. F. G. Knoops,[81] A. Knue,[53] B. R. Ko,[44] T. Kobayashi,[153] M. Kobel,[43] M. Kocian,[141] P. Kodys,[124] K. Köneke,[29] A. C. König,[102] S. Koenig,[79] L. Köpke,[79] F. Koetsveld,[102] P. Koevesarki,[20] T. Koffas,[28] E. Koffeman,[103] L. A. Kogan,[116] F. Kohn,[53] Z. Kohout,[125] T. Kohriki,[64] T. Koi,[141] T. Kokott,[20] G. M. Kolachev,[105] H. Kolanoski,[15] V. Kolesnikov,[63] I. Koletsou,[87a] J. Koll,[86] M. Kollefrath,[47] S. D. Kolya,[80] A. A. Komar,[92] Y. Komori,[153] T. Kondo,[64] T. Kono,[41,q] A. I. Kononov,[47] R. Konoplich,[106,r] N. Konstantinidis,[75] A. Kootz,[172] S. Koperny,[37] K. Korcyl,[38] K. Kordas,[152] V. Koreshev,[126] A. Korn,[116] A. Korol,[105] I. Korolkov,[11] E. V. Korolkova,[137] V. A. Korotkov,[126] O. Kortner,[97] S. Kortner,[97] V. V. Kostyukhin,[20] M. J. Kotamäki,[29] S. Kotov,[97] V. M. Kotov,[63] A. Kotwal,[44] C. Kourkoumelis,[8] V. Kouskoura,[152] A. Koutsman,[157a] R. Kowalewski,[167] T. Z. Kowalski,[37] W. Kozanecki,[134] A. S. Kozhin,[126] V. Kral,[125] V. A. Kramarenko,[95] G. Kramberger,[72] M. W. Krasny,[76] A. Krasznahorkay,[106] J. Kraus,[86] J. K. Kraus,[20] A. Kreisel,[151] F. Krejci,[125] J. Kretzschmar,[71] N. Krieger,[53] P. Krieger,[156] K. Kroeninger,[53] H. Kroha,[97] J. Kroll,[118] J. Kroseberg,[20] J. Krstic,[12a] U. Kruchonak,[63] H. Krüger,[20] T. Kruker,[16] N. Krumnack,[62] Z. V. Krumshteyn,[63] A. Kruth,[20] T. Kubota,[84] S. Kuday,[3a] S. Kuehn,[47] A. Kugel,[57c] T. Kuhl,[41] D. Kuhn,[60] V. Kukhtin,[63] Y. Kulchitsky,[88] S. Kuleshov,[31b] C. Kummer,[96] M. Kuna,[76] N. Kundu,[116] J. Kunkle,[118] A. Kupco,[123] H. Kurashige,[65] M. Kurata,[158] Y. A. Kurochkin,[88] V. Kus,[123] E. S. Kuwertz,[145] M. Kuze,[155] J. Kvita,[140] R. Kwee,[15] A. La Rosa,[48] L. La Rotonda,[36a,36b] L. Labarga,[78] J. Labbe,[4] S. Lablak,[133a] C. Lacasta,[165] F. Lacava,[130a,130b] H. Lacker,[15] D. Lacour,[76] V. R. Lacuesta,[165] E. Ladygin,[63] R. Lafaye,[4] B. Laforge,[76] T. Lagouri,[78] S. Lai,[47] E. Laisne,[54] M. Lamanna,[29] L. Lambourne,[75] C. L. Lampen,[6] W. Lampl,[6] E. Lancon,[134] U. Landgraf,[47] M. P. J. Landon,[73] J. L. Lane,[80] C. Lange,[41] A. J. Lankford,[161]

F. Lanni,[24] K. Lantzsch,[172] S. Laplace,[76] C. Lapoire,[20] J. F. Laporte,[134] T. Lari,[87a] A. V. Larionov,[126] A. Larner,[116] C. Lasseur,[29] M. Lassnig,[29] P. Laurelli,[46] V. Lavorini,[36a,36b] W. Lavrijsen,[14] P. Laycock,[71] A. B. Lazarev,[63] O. Le Dortz,[76] E. Le Guirriec,[81] C. Le Maner,[156] E. Le Menedeu,[9] C. Lebel,[91] T. LeCompte,[5] F. Ledroit-Guillon,[54] H. Lee,[103] J. S. H. Lee,[114] S. C. Lee,[149] L. Lee,[173] M. Lefebvre,[167] M. Legendre,[134] A. Leger,[48] B. C. LeGeyt,[118] F. Legger,[96] C. Leggett,[14] M. Lehmacher,[20] G. Lehmann Miotto,[29] X. Lei,[6] M. A. L. Leite,[23d] R. Leitner,[124] D. Lellouch,[169] M. Leltchouk,[34] B. Lemmer,[53] V. Lendermann,[57a] K. J. C. Leney,[143b] T. Lenz,[103] G. Lenzen,[172] B. Lenzi,[29] K. Leonhardt,[43] S. Leontsinis,[9] C. Leroy,[91] J.-R. Lessard,[167] J. Lesser,[144a] C. G. Lester,[27] A. Leung Fook Cheong,[170] J. Levêque,[4] D. Levin,[85] L. J. Levinson,[169] M. S. Levitski,[126] A. Lewis,[116] G. H. Lewis,[106] A. M. Leyko,[20] M. Leyton,[15] B. Li,[81] H. Li,[170,s] S. Li,[32b,t] X. Li,[85] Z. Liang,[116,u] H. Liao,[33] B. Liberti,[131a] P. Lichard,[29] M. Lichtnecker,[96] K. Lie,[163] W. Liebig,[13] C. Limbach,[20] A. Limosani,[84] M. Limper,[61] S. C. Lin,[149,v] F. Linde,[103] J. T. Linnemann,[86] E. Lipeles,[118] L. Lipinsky,[123] A. Lipniacka,[13] T. M. Liss,[163] D. Lissauer,[24] A. Lister,[48] A. M. Litke,[135] C. Liu,[28] D. Liu,[149] H. Liu,[85] J. B. Liu,[85] M. Liu,[32b] Y. Liu,[32b] M. Livan,[117a,117b] S. S. A. Livermore,[116] A. Lleres,[54] J. Llorente Merino,[78] S. L. Lloyd,[73] E. Lobodzinska,[41] P. Loch,[6] W. S. Lockman,[135] T. Loddenkoetter,[20] F. K. Loebinger,[80] A. Loginov,[173] C. W. Loh,[166] T. Lohse,[15] K. Lohwasser,[47] M. Lokajicek,[123] J. Loken,[116] V. P. Lombardo,[4] R. E. Long,[69] L. Lopes,[122a] D. Lopez Mateos,[56] J. Lorenz,[96] N. Lorenzo Martinez,[113] M. Losada,[160] P. Loscutoff,[14] F. Lo Sterzo,[130a,130b] M. J. Losty,[157a] X. Lou,[40] A. Lounis,[113] K. F. Loureiro,[160] J. Love,[21] P. A. Love,[69] A. J. Lowe,[141,e] F. Lu,[32a] H. J. Lubatti,[136] C. Luci,[130a,130b] A. Lucotte,[54] A. Ludwig,[43] D. Ludwig,[41] I. Ludwig,[47] J. Ludwig,[47] F. Luehring,[59] G. Luijckx,[103] W. Lukas,[60] D. Lumb,[47] L. Luminari,[130a] E. Lund,[115] B. Lund-Jensen,[145] B. Lundberg,[77] J. Lundberg,[144a,144b] J. Lundquist,[35] M. Lungwitz,[79] G. Lutz,[97] D. Lynn,[24] J. Lys,[14] E. Lytken,[77] H. Ma,[24] L. L. Ma,[170] J. A. Macana Goia,[91] G. Maccarrone,[46] A. Macchiolo,[97] B. Maček,[72] J. Machado Miguens,[122a] R. Mackeprang,[35] R. J. Madaras,[14] W. F. Mader,[43] R. Maenner,[57c] T. Maeno,[24] P. Mättig,[172] S. Mättig,[41] L. Magnoni,[29] E. Magradze,[53] Y. Mahalalel,[151] K. Mahboubi,[47] S. Mahmoud,[71] G. Mahout,[17] C. Maiani,[130a,130b] C. Maidantchik,[23a] A. Maio,[122a,b] S. Majewski,[24] Y. Makida,[64] N. Makovec,[113] P. Mal,[134] B. Malaescu,[29] Pa. Malecki,[38] P. Malecki,[38] V. P. Maleev,[119] F. Malek,[54] U. Mallik,[61] D. Malon,[5] C. Malone,[141] S. Maltezos,[9] V. Malyshev,[105] S. Malyukov,[29] R. Mameghani,[96] J. Mamuzic,[12b] A. Manabe,[64] L. Mandelli,[87a] I. Mandić,[72] R. Mandrysch,[15] J. Maneira,[122a] P. S. Mangeard,[86] L. Manhaes de Andrade Filho,[23a] I. D. Manjavidze,[63] A. Mann,[53] P. M. Manning,[135] A. Manousakis-Katsikakis,[8] B. Mansoulie,[134] A. Manz,[97] A. Mapelli,[29] L. Mapelli,[29] L. March,[78] J. F. Marchand,[28] F. Marchese,[131a,131b] G. Marchiori,[76] M. Marcisovsky,[123] C. P. Marino,[167] F. Marroquim,[23a] R. Marshall,[80] Z. Marshall,[29] F. K. Martens,[156] S. Marti-Garcia,[165] A. J. Martin,[173] B. Martin,[29] B. Martin,[86] F. F. Martin,[118] J. P. Martin,[91] Ph. Martin,[54] T. A. Martin,[17] V. J. Martin,[45] B. Martin dit Latour,[48] S. Martin-Haugh,[147] M. Martinez,[11] V. Martinez Outschoorn,[56] A. C. Martyniuk,[167] M. Marx,[80] F. Marzano,[130a] A. Marzin,[109] L. Masetti,[79] T. Mashimo,[153] R. Mashinistov,[92] J. Masik,[80] A. L. Maslennikov,[105] I. Massa,[19a,19b] G. Massaro,[103] N. Massol,[4] P. Mastrandrea,[130a,130b] A. Mastroberardino,[36a,36b] T. Masubuchi,[153] P. Matricon,[113] H. Matsumoto,[153] H. Matsunaga,[153] T. Matsushita,[65] C. Mattravers,[116,c] J. M. Maugain,[29] J. Maurer,[81] S. J. Maxfield,[71] D. A. Maximov,[105,f] E. N. May,[5] A. Mayne,[137] R. Mazini,[149] M. Mazur,[20] M. Mazzanti,[87a] S. P. Mc Kee,[85] A. McCarn,[163] R. L. McCarthy,[146] T. G. McCarthy,[28] N. A. McCubbin,[127] K. W. McFarlane,[55] J. A. Mcfayden,[137] H. McGlone,[52] G. Mchedlidze,[50b] R. A. McLaren,[29] T. Mclaughlan,[17] S. J. McMahon,[127] R. A. McPherson,[167,j] A. Meade,[82] J. Mechnich,[103] M. Mechtel,[172] M. Medinnis,[41] R. Meera-Lebbai,[109] T. Meguro,[114] R. Mehdiyev,[91] S. Mehlhase,[35] A. Mehta,[71] K. Meier,[57a] B. Meirose,[77] C. Melachrinos,[30] B. R. Mellado Garcia,[170] L. Mendoza Navas,[160] Z. Meng,[149,s] A. Mengarelli,[19a,19b] S. Menke,[97] C. Menot,[29] E. Meoni,[11] K. M. Mercurio,[56] P. Mermod,[48] L. Merola,[100a,100b] C. Meroni,[87a] F. S. Merritt,[30] H. Merritt,[107] A. Messina,[29] J. Metcalfe,[101] A. S. Mete,[62] C. Meyer,[79] C. Meyer,[30] J.-P. Meyer,[134] J. Meyer,[171] J. Meyer,[53] T. C. Meyer,[29] W. T. Meyer,[62] J. Miao,[32d] S. Michal,[29] L. Micu,[25a] R. P. Middleton,[127] S. Migas,[71] L. Mijović,[41] G. Mikenberg,[169] M. Mikestikova,[123] M. Mikuž,[72] D. W. Miller,[30] R. J. Miller,[86] W. J. Mills,[166] C. Mills,[56] A. Milov,[169] D. A. Milstead,[144a,144b] D. Milstein,[169] A. A. Minaenko,[126] M. Miñano Moya,[165] I. A. Minashvili,[63] A. I. Mincer,[106] B. Mindur,[37] M. Mineev,[63] Y. Ming,[170] L. M. Mir,[11] G. Mirabelli,[130a] L. Miralles Verge,[11] A. Misiejuk,[74] J. Mitrevski,[135] G. Y. Mitrofanov,[126] V. A. Mitsou,[165] S. Mitsui,[64] P. S. Miyagawa,[137] K. Miyazaki,[65] J. U. Mjörnmark,[77] T. Moa,[144a,144b] P. Mockett,[136] S. Moed,[56] V. Moeller,[27] K. Mönig,[41] N. Möser,[20] S. Mohapatra,[146] W. Mohr,[47] S. Mohrdieck-Möck,[97] R. Moles-Valls,[165] J. Molina-Perez,[29] J. Monk,[75] E. Monnier,[81] S. Montesano,[87a,87b] F. Monticelli,[68] S. Monzani,[19a,19b] R. W. Moore,[2] G. F. Moorhead,[84] C. Mora Herrera,[48] A. Moraes,[52] N. Morange,[134] J. Morel,[53] G. Morello,[36a,36b] D. Moreno,[79] M. Moreno Llácer,[165] P. Morettini,[49a] M. Morgenstern,[43] M. Morii,[56] J. Morin,[73] A. K. Morley,[29] G. Mornacchi,[29] S. V. Morozov,[94] J. D. Morris,[73] L. Morvaj,[99] H. G. Moser,[97] M. Mosidze,[50b] J. Moss,[107] R. Mount,[141] E. Mountricha,[9,w] S. V. Mouraviev,[92] E. J. W. Moyse,[82] M. Mudrinic,[12b] F. Mueller,[57a] J. Mueller,[121] K. Mueller,[20] T. A. Müller,[96] T. Mueller,[79] D. Muenstermann,[29] A. Muir,[166] Y. Munwes,[151] W. J. Murray,[127] I. Mussche,[103] E. Musto,[100a,100b] A. G. Myagkov,[126] M. Myska,[123] J. Nadal,[11] K. Nagai,[158] K. Nagano,[64] A. Nagarkar,[107] Y. Nagasaka,[58] M. Nagel,[97] A. M. Nairz,[29] Y. Nakahama,[29] K. Nakamura,[153] T. Nakamura,[153] I. Nakano,[108] G. Nanava,[20] A. Napier,[159] R. Narayan,[57b] M. Nash,[75,c] N. R. Nation,[21] T. Nattermann,[20] T. Naumann,[41] G. Navarro,[160] H. A. Neal,[85] E. Nebot,[78] P. Yu. Nechaeva,[92] T. J. Neep,[80] A. Negri,[117a,117b] G. Negri,[29] S. Nektarijevic,[48] A. Nelson,[161] T. K. Nelson,[141] S. Nemecek,[123] P. Nemethy,[106] A. A. Nepomuceno,[23a] M. Nessi,[29,x] M. S. Neubauer,[163] A. Neusiedl,[79] R. M. Neves,[106] P. Nevski,[24] P. R. Newman,[17] V. Nguyen Thi Hong,[134] R. B. Nickerson,[116] R. Nicolaidou,[134] L. Nicolas,[137] B. Nicquevert,[29] F. Niedercorn,[113] J. Nielsen,[135] T. Niinikoski,[29] N. Nikiforou,[34] A. Nikiforov,[15] V. Nikolaenko,[126] K. Nikolaev,[63] I. Nikolic-Audit,[76] K. Nikolics,[48] K. Nikolopoulos,[24] H. Nilsen,[47] P. Nilsson,[7] Y. Ninomiya,[153] A. Nisati,[130a] T. Nishiyama,[65] R. Nisius,[97] L. Nodulman,[5]

M. Nomachi,[114] I. Nomidis,[152] M. Nordberg,[29] B. Nordkvist,[144a,144b] P. R. Norton,[127] J. Novakova,[124] M. Nozaki,[64] L. Nozka,[111] I. M. Nugent,[157a] A.-E. Nuncio-Quiroz,[20] G. Nunes Hanninger,[84] T. Nunnemann,[96] E. Nurse,[75] B. J. O'Brien,[45] S. W. O'Neale,[17,*] D. C. O'Neil,[140] V. O'Shea,[52] L. B. Oakes,[96] F. G. Oakham,[28,d] H. Oberlack,[97] J. Ocariz,[76] A. Ochi,[65] S. Oda,[153] S. Odaka,[64] J. Odier,[81] H. Ogren,[59] A. Oh,[80] S. H. Oh,[44] C. C. Ohm,[144a,144b] T. Ohshima,[99] H. Ohshita,[138] S. Okada,[65] H. Okawa,[161] Y. Okumura,[99] T. Okuyama,[153] A. Olariu,[25a] M. Olcese,[49a] A. G. Olchevski,[63] S. A. Olivares Pino,[31a] M. Oliveira,[122a,h] D. Oliveira Damazio,[24] E. Oliver Garcia,[165] D. Olivito,[118] A. Olszewski,[38] J. Olszowska,[38] C. Omachi,[65] A. Onofre,[122a,y] P. U. E. Onyisi,[30] C. J. Oram,[157a] M. J. Oreglia,[30] Y. Oren,[151] D. Orestano,[132a,132b] N. Orlando,[70a,70b] I. Orlov,[105] C. Oropeza Barrera,[52] R. S. Orr,[156] B. Osculati,[49a,49b] R. Ospanov,[118] C. Osuna,[11] G. Otero y Garzon,[26] J. P. Ottersbach,[103] M. Ouchrif,[133d] E. A. Ouellette,[167] F. Ould-Saada,[115] A. Ouraou,[134] Q. Ouyang,[32a] A. Ovcharova,[14] M. Owen,[80] S. Owen,[137] V. E. Ozcan,[18a] N. Ozturk,[7] A. Pacheco Pages,[11] C. Padilla Aranda,[11] S. Pagan Griso,[14] E. Paganis,[137] F. Paige,[24] P. Pais,[82] K. Pajchel,[115] G. Palacino,[157b] C. P. Paleari,[6] S. Palestini,[29] D. Pallin,[33] A. Palma,[122a] J. D. Palmer,[17] Y. B. Pan,[170] E. Panagiotopoulou,[9] B. Panes,[31a] N. Panikashvili,[85] S. Panitkin,[24] D. Pantea,[25a] M. Panuskova,[123] V. Paolone,[121] A. Papadelis,[144a] Th. D. Papadopoulou,[9] A. Paramonov,[5] D. Paredes Hernandez,[33] W. Park,[24,z] M. A. Parker,[27] F. Parodi,[49a,49b] J. A. Parsons,[34] U. Parzefall,[47] S. Pashapour,[53] E. Pasqualucci,[130a] S. Passaggio,[49a] A. Passeri,[132a] F. Pastore,[132a,132b] Fr. Pastore,[74] G. Pásztor,[48,aa] S. Pataraia,[172] N. Patel,[148] J. R. Pater,[80] S. Patricelli,[100a,100b] T. Pauly,[29] M. Pecsy,[142a] M. I. Pedraza Morales,[170] S. V. Peleganchuk,[105] H. Peng,[32b] B. Penning,[30] A. Penson,[34] J. Penwell,[59] M. Perantoni,[23a] K. Perez,[34,bb] T. Perez Cavalcanti,[41] E. Perez Codina,[11] M. T. Pérez García-Estañ,[165] V. Perez Reale,[34] L. Perini,[87a,87b] H. Pernegger,[29] R. Perrino,[70a] P. Perrodo,[4] S. Persembe,[3a] V. D. Peshekhonov,[63] K. Peters,[29] B. A. Petersen,[29] J. Petersen,[29] T. C. Petersen,[35] E. Petit,[4] A. Petridis,[152] C. Petridou,[152] E. Petrolo,[130a] F. Petrucci,[132a,132b] D. Petschull,[41] M. Petteni,[140] R. Pezoa,[31b] A. Phan,[84] P. W. Phillips,[127] G. Piacquadio,[29] A. Picazio,[48] E. Piccaro,[73] M. Piccinini,[19a,19b] S. M. Piec,[41] R. Piegaia,[26] D. T. Pignotti,[107] J. E. Pilcher,[30] A. D. Pilkington,[80] J. Pina,[122a,b] M. Pinamonti,[162a,162c] A. Pinder,[116] J. L. Pinfold,[2] J. Ping,[32c] B. Pinto,[122a] O. Pirotte,[29] C. Pizio,[87a,87b] M. Plamondon,[167] M.-A. Pleier,[24] A. V. Pleskach,[126] E. Plotnikova,[63] A. Poblaguev,[24] S. Poddar,[57a] F. Podlyski,[33] L. Poggioli,[113] T. Poghosyan,[20] M. Pohl,[48] F. Polci,[54] G. Polesello,[117a] A. Policicchio,[36a,36b] A. Polini,[19a] J. Poll,[73] V. Polychronakos,[24] D. M. Pomarede,[134] D. Pomeroy,[22] K. Pommès,[29] L. Pontecorvo,[130a] B. G. Pope,[86] G. A. Popeneciu,[25a] D. S. Popovic,[12a] A. Poppleton,[29] X. Portell Bueso,[29] C. Posch,[21] G. E. Pospelov,[97] S. Pospisil,[125] I. N. Potrap,[97] C. J. Potter,[147] C. T. Potter,[112] G. Poulard,[29] J. Poveda,[170] V. Pozdnyakov,[63] R. Prabhu,[75] P. Pralavorio,[81] A. Pranko,[14] S. Prasad,[29] R. Pravahan,[7] S. Prell,[62] K. Pretzl,[16] L. Pribyl,[29] D. Price,[59] J. Price,[71] L. E. Price,[5] M. J. Price,[29] D. Prieur,[121] M. Primavera,[70a] K. Prokofiev,[106] F. Prokoshin,[31b] S. Protopopescu,[24] J. Proudfoot,[5] X. Prudent,[43] M. Przybycien,[37] H. Przysiezniak,[4] S. Psoroulas,[20] E. Ptacek,[112] E. Pueschel,[82] J. Purdham,[85] M. Purohit,[24,z] P. Puzo,[113] Y. Pylypchenko,[61] J. Qian,[85] Z. Qian,[81] Z. Qin,[41] A. Quadt,[53] D. R. Quarrie,[14] W. B. Quayle,[170] F. Quinonez,[31a] M. Raas,[102] V. Radescu,[41] B. Radics,[20] P. Radloff,[112] T. Rador,[18a] F. Ragusa,[87a,87b] G. Rahal,[175] A. M. Rahimi,[107] D. Rahm,[24] S. Rajagopalan,[24] M. Rammensee,[47] M. Rammes,[139] A. S. Randle-Conde,[39] K. Randrianarivony,[28] P. N. Ratoff,[69] F. Rauscher,[96] T. C. Rave,[47] M. Raymond,[29] A. L. Read,[115] D. M. Rebuzzi,[117a,117b] A. Redelbach,[171] G. Redlinger,[24] R. Reece,[118] K. Reeves,[40] A. Reichold,[103] E. Reinherz-Aronis,[151] A. Reinsch,[112] I. Reisinger,[42] C. Rembser,[29] Z. L. Ren,[149] A. Renaud,[113] M. Rescigno,[130a] S. Resconi,[87a] B. Resende,[134] P. Reznicek,[96] R. Rezvani,[156] A. Richards,[75] R. Richter,[97] E. Richter-Was,[4,cc] M. Ridel,[76] M. Rijpstra,[103] M. Rijssenbeek,[146] A. Rimoldi,[117a,117b] L. Rinaldi,[19a] R. R. Rios,[39] I. Riu,[11] G. Rivoltella,[87a,87b] F. Rizatdinova,[110] E. Rizvi,[73] S. H. Robertson,[83,j] A. Robichaud-Veronneau,[116] D. Robinson,[27] J. E. M. Robinson,[75] A. Robson,[52] J. G. Rocha de Lima,[104] C. Roda,[120a,120b] D. Roda Dos Santos,[29] D. Rodriguez,[160] A. Roe,[53] S. Roe,[29] O. Røhne,[115] V. Rojo,[1] S. Rolli,[159] A. Romaniouk,[94] M. Romano,[19a,19b] V. M. Romanov,[63] G. Romeo,[26] E. Romero Adam,[165] L. Roos,[76] E. Ros,[165] S. Rosati,[130a] K. Rosbach,[48] A. Rose,[147] M. Rose,[74] G. A. Rosenbaum,[156] E. I. Rosenberg,[62] P. L. Rosendahl,[13] O. Rosenthal,[139] L. Rosselet,[48] V. Rossetti,[11] E. Rossi,[130a,130b] L. P. Rossi,[49a] M. Rotaru,[25a] I. Roth,[169] J. Rothberg,[136] D. Rousseau,[113] C. R. Royon,[134] A. Rozanov,[81] Y. Rozen,[150] X. Ruan,[32a,dd] I. Rubinskiy,[41] B. Ruckert,[96] N. Ruckstuhl,[103] V. I. Rud,[95] C. Rudolph,[43] G. Rudolph,[60] F. Rühr,[6] F. Ruggieri,[132a,132b] A. Ruiz-Martinez,[62] V. Rumiantsev,[89,*] L. Rumyantsev,[63] K. Runge,[47] Z. Rurikova,[47] N. A. Rusakovich,[63] J. P. Rutherfoord,[6] C. Ruwiedel,[14] P. Ruzicka,[123] Y. F. Ryabov,[119] V. Ryadovikov,[126] P. Ryan,[86] M. Rybar,[124] G. Rybkin,[113] N. C. Ryder,[116] S. Rzaeva,[10] A. F. Saavedra,[148] I. Sadeh,[151] H. F-W. Sadrozinski,[135] R. Sadykov,[63] F. Safai Tehrani,[130a] H. Sakamoto,[153] G. Salamanna,[73] A. Salamon,[131a] M. Saleem,[109] D. Salek,[29] D. Salihagic,[97] A. Salnikov,[141] J. Salt,[165] B. M. Salvachua Ferrando,[5] D. Salvatore,[36a,36b] F. Salvatore,[147] A. Salvucci,[102] A. Salzburger,[29] D. Sampsonidis,[152] B. H. Samset,[115] A. Sanchez,[100a,100b] V. Sanchez Martinez,[165] H. Sandaker,[13] H. G. Sander,[79] M. P. Sanders,[96] M. Sandhoff,[172] T. Sandoval,[27] C. Sandoval,[160] R. Sandstroem,[97] S. Sandvoss,[172] D. P. C. Sankey,[127] A. Sansoni,[46] C. Santamarina Rios,[83] C. Santoni,[33] R. Santonico,[131a,131b] H. Santos,[122a] J. G. Saraiva,[122a] T. Sarangi,[170] E. Sarkisyan-Grinbaum,[7] F. Sarri,[120a,120b] G. Sartisohn,[172] O. Sasaki,[64] N. Sasao,[66] I. Satsounkevitch,[88] G. Sauvage,[4] E. Sauvan,[4] J. B. Sauvan,[113] P. Savard,[156,d] V. Savinov,[121] D. O. Savu,[29] L. Sawyer,[24,l] D. H. Saxon,[52] J. Saxon,[118] L. P. Says,[33] C. Sbarra,[19a] A. Sbrizzi,[19a,19b] O. Scallon,[91] D. A. Scannicchio,[161] M. Scarcella,[148] J. Schaarschmidt,[113] P. Schacht,[97] D. Schaefer,[118] U. Schäfer,[79] S. Schaepe,[20] S. Schaetzel,[57b] A. C. Schaffer,[113] D. Schaile,[96] R. D. Schamberger,[146] A. G. Schamov,[105] V. Scharf,[57a] V. A. Schegelsky,[119] D. Scheirich,[85] M. Schernau,[161] M. I. Scherzer,[34] C. Schiavi,[49a,49b] J. Schieck,[96] M. Schioppa,[36a,36b] S. Schlenker,[29] J. L. Schlereth,[5] E. Schmidt,[47] K. Schmieden,[20] C. Schmitt,[79] S. Schmitt,[57b] M. Schmitz,[20] A. Schöning,[57b] M. Schott,[29] D. Schouten,[157a] J. Schovancova,[123] M. Schram,[83] C. Schroeder,[79] N. Schroer,[57c] G. Schuler,[29] M. J. Schultens,[20] J. Schultes,[172] H.-C. Schultz-Coulon,[57a] H. Schulz,[15] J. W. Schumacher,[20] M. Schumacher,[47] B. A. Schumm,[135] Ph. Schune,[134]

C. Schwanenberger,[80] A. Schwartzman,[141] Ph. Schwemling,[76] R. Schwienhorst,[86] R. Schwierz,[43] J. Schwindling,[134] T. Schwindt,[20] M. Schwoerer,[4] G. Sciolla,[22] W. G. Scott,[127] J. Searcy,[112] G. Sedov,[41] E. Sedykh,[119] E. Segura,[11] S. C. Seidel,[101] A. Seiden,[135] F. Seifert,[43] J. M. Seixas,[23a] G. Sekhniaidze,[100a] S. J. Sekula,[39] K. E. Selbach,[45] D. M. Seliverstov,[119] B. Sellden,[144a] G. Sellers,[71] M. Seman,[142b] N. Semprini-Cesari,[19a,19b] C. Serfon,[96] L. Serin,[113] L. Serkin,[53] R. Seuster,[97] H. Severini,[109] M. E. Sevior,[84] A. Sfyrla,[29] E. Shabalina,[53] M. Shamim,[112] L. Y. Shan,[32a] J. T. Shank,[21] Q. T. Shao,[84] M. Shapiro,[14] P. B. Shatalov,[93] L. Shaver,[6] K. Shaw,[162a,162c] D. Sherman,[173] P. Sherwood,[75] A. Shibata,[106] H. Shichi,[99] S. Shimizu,[29] M. Shimojima,[98] T. Shin,[55] M. Shiyakova,[63] A. Shmeleva,[92] M. J. Shochet,[30] D. Short,[116] S. Shrestha,[62] E. Shulga,[94] M. A. Shupe,[6] P. Sicho,[123] A. Sidoti,[130a] F. Siegert,[47] Dj. Sijacki,[12a] O. Silbert,[169] J. Silva,[122a] Y. Silver,[151] D. Silverstein,[141] S. B. Silverstein,[144a] V. Simak,[125] O. Simard,[134] Lj. Simic,[12a] S. Simion,[113] B. Simmons,[75] R. Simoniello,[87a,87b] M. Simonyan,[35] P. Sinervo,[156] N. B. Sinev,[112] V. Sipica,[139] G. Siragusa,[171] A. Sircar,[24] A. N. Sisakyan,[63] S. Yu. Sivoklokov,[95] J. Sjölin,[144a,144b] T. B. Sjursen,[13] L. A. Skinnari,[14] H. P. Skottowe,[56] K. Skovpen,[105] P. Skubic,[109] N. Skvorodnev,[22] M. Slater,[17] T. Slavicek,[125] K. Sliwa,[159] J. Sloper,[29] V. Smakhtin,[169] B. H. Smart,[45] S. Yu. Smirnov,[94] Y. Smirnov,[94] L. N. Smirnova,[95] O. Smirnova,[77] B. C. Smith,[56] D. Smith,[141] K. M. Smith,[52] M. Smizanska,[69] K. Smolek,[125] A. A. Snesarev,[92] S. W. Snow,[80] J. Snow,[109] J. Snuverink,[103] S. Snyder,[24] M. Soares,[122a] R. Sobie,[167,j] J. Sodomka,[125] A. Soffer,[151] C. A. Solans,[165] M. Solar,[125] J. Solc,[125] E. Soldatov,[94] U. Soldevila,[165] E. Solfaroli Camillocci,[130a,130b] A. A. Solodkov,[126] O. V. Solovyanov,[126] N. Soni,[2] V. Sopko,[125] B. Sopko,[125] M. Sosebee,[7] R. Soualah,[162a,162c] A. Soukharev,[105] S. Spagnolo,[70a,70b] F. Spanò,[74] R. Spighi,[19a] G. Spigo,[29] F. Spila,[130a,130b] R. Spiwoks,[29] M. Spousta,[124] T. Spreitzer,[156] B. Spurlock,[7] R. D. St. Denis,[52] J. Stahlman,[118] R. Stamen,[57a] E. Stanecka,[38] R. W. Stanek,[5] C. Stanescu,[132a] M. Stanescu-Bellu,[41] S. Stapnes,[115] E. A. Starchenko,[126] J. Stark,[54] P. Staroba,[123] P. Starovoitov,[89] A. Staude,[96] P. Stavina,[142a] G. Steele,[52] P. Steinbach,[43] P. Steinberg,[24] I. Stekl,[125] B. Stelzer,[140] H. J. Stelzer,[86] O. Stelzer-Chilton,[157a] H. Stenzel,[51] S. Stern,[97] K. Stevenson,[73] G. A. Stewart,[29] J. A. Stillings,[20] M. C. Stockton,[83] K. Stoerig,[47] G. Stoicea,[25a] S. Stonjek,[97] P. Strachota,[124] A. R. Stradling,[7] A. Straessner,[43] J. Strandberg,[145] S. Strandberg,[144a,144b] A. Strandlie,[115] M. Strang,[107] E. Strauss,[141] M. Strauss,[109] P. Strizenec,[142b] R. Ströhmer,[171] D. M. Strom,[112] J. A. Strong,[74,*] R. Stroynowski,[39] J. Strube,[127] B. Stugu,[13] I. Stumer,[24,*] J. Stupak,[146] P. Sturm,[172] N. A. Styles,[41] D. A. Soh,[149,u] D. Su,[141] HS. Subramania,[2] A. Succurro,[11] Y. Sugaya,[114] T. Sugimoto,[99] C. Suhr,[104] K. Suita,[65] M. Suk,[124] V. V. Sulin,[92] S. Sultansoy,[3d] T. Sumida,[66] X. Sun,[54] J. E. Sundermann,[47] K. Suruliz,[137] S. Sushkov,[11] G. Susinno,[36a,36b] M. R. Sutton,[147] Y. Suzuki,[64] Y. Suzuki,[65] M. Svatos,[123] Yu. M. Sviridov,[126] S. Swedish,[166] I. Sykora,[142a] T. Sykora,[124] B. Szeless,[29] J. Sánchez,[165] D. Ta,[103] K. Tackmann,[41] A. Taffard,[161] R. Tafirout,[157a] N. Taiblum,[151] Y. Takahashi,[99] H. Takai,[24] R. Takashima,[67] H. Takeda,[65] T. Takeshita,[138] Y. Takubo,[64] M. Talby,[81] A. Talyshev,[105,f] M. C. Tamsett,[24] J. Tanaka,[153] R. Tanaka,[113] S. Tanaka,[129] S. Tanaka,[64] Y. Tanaka,[98] A. J. Tanasijczuk,[140] K. Tani,[65] N. Tannoury,[81] G. P. Tappern,[29] S. Tapprogge,[79] D. Tardif,[156] S. Tarem,[150] F. Tarrade,[28] G. F. Tartarelli,[87a] P. Tas,[124] M. Tasevsky,[123] E. Tassi,[36a,36b] M. Tatarkhanov,[14] Y. Tayalati,[133d] C. Taylor,[75] F. E. Taylor,[90] G. N. Taylor,[84] W. Taylor,[157b] M. Teinturier,[113] M. Teixeira Dias Castanheira,[73] P. Teixeira-Dias,[74] K. K. Temming,[47] H. Ten Kate,[29] P. K. Teng,[149] S. Terada,[64] K. Terashi,[153] J. Terron,[78] M. Testa,[46] R. J. Teuscher,[156,j] J. Thadome,[172] J. Therhaag,[20] T. Theveneaux-Pelzer,[76] M. Thioye,[173] S. Thoma,[47] J. P. Thomas,[17] E. N. Thompson,[34] P. D. Thompson,[17] P. D. Thompson,[156] A. S. Thompson,[52] L. A. Thomsen,[35] E. Thomson,[118] M. Thomson,[27] R. P. Thun,[85] F. Tian,[34] M. J. Tibbetts,[14] T. Tic,[123] V. O. Tikhomirov,[92] Y. A. Tikhonov,[105,f] S. Timoshenko,[94] P. Tipton,[173] F. J. Tique Aires Viegas,[29] S. Tisserant,[81] B. Toczek,[37] T. Todorov,[4] S. Todorova-Nova,[159] B. Toggerson,[161] J. Tojo,[64] S. Tokár,[142a] K. Tokunaga,[65] K. Tokushuku,[64] K. Tollefson,[86] M. Tomoto,[99] L. Tompkins,[30] K. Toms,[101] G. Tong,[32a] A. Tonoyan,[13] C. Topfel,[16] N. D. Topilin,[63] I. Torchiani,[29] E. Torrence,[112] H. Torres,[76] E. Torró Pastor,[165] J. Toth,[81,aa] F. Touchard,[81] D. R. Tovey,[137] T. Trefzger,[171] L. Tremblet,[29] A. Tricoli,[29] I. M. Trigger,[157a] S. Trincaz-Duvoid,[76] T. N. Trinh,[76] M. F. Tripiana,[68] W. Trischuk,[156] A. Trivedi,[24,z] B. Trocmé,[54] C. Troncon,[87a] M. Trottier-McDonald,[140] M. Trzebinski,[38] A. Trzupek,[38] C. Tsarouchas,[29] J. C.-L. Tseng,[116] M. Tsiakiris,[103] P. V. Tsiareshka,[88] D. Tsionou,[4,ee] G. Tsipolitis,[9] V. Tsiskaridze,[47] E. G. Tskhadadze,[50a] I. I. Tsukerman,[93] V. Tsulaia,[14] J.-W. Tsung,[20] S. Tsuno,[64] D. Tsybychev,[146] A. Tua,[137] A. Tudorache,[25a] V. Tudorache,[25a] J. M. Tuggle,[30] M. Turala,[38] D. Turecek,[125] I. Turk Cakir,[3e] E. Turlay,[103] R. Turra,[87a,87b] P. M. Tuts,[34] A. Tykhonov,[72] M. Tylmad,[144a,144b] M. Tyndel,[127] G. Tzanakos,[8] K. Uchida,[20] I. Ueda,[153] R. Ueno,[28] M. Ugland,[13] M. Uhlenbrock,[20] M. Uhrmacher,[53] F. Ukegawa,[158] G. Unal,[29] D. G. Underwood,[5] A. Undrus,[24] G. Unel,[161] Y. Unno,[64] D. Urbaniec,[34] G. Usai,[7] M. Uslenghi,[117a,117b] L. Vacavant,[81] V. Vacek,[125] B. Vachon,[83] S. Vahsen,[14] J. Valenta,[123] P. Valente,[130a] S. Valentinetti,[19a,19b] S. Valkar,[124] E. Valladolid Gallego,[165] S. Vallecorsa,[150] J. A. Valls Ferrer,[165] H. van der Graaf,[103] E. van der Kraaij,[103] R. Van Der Leeuw,[103] E. van der Poel,[103] D. van der Ster,[29] N. van Eldik,[82] P. van Gemmeren,[5] Z. van Kesteren,[103] I. van Vulpen,[103] M. Vanadia,[97] W. Vandelli,[29] G. Vandoni,[29] A. Vaniachine,[5] P. Vankov,[41] F. Vannucci,[76] F. Varela Rodriguez,[29] R. Vari,[130a] E. W. Varnes,[6] T. Varol,[82] D. Varouchas,[14] A. Vartapetian,[7] K. E. Varvell,[148] V. I. Vassilakopoulos,[55] F. Vazeille,[33] T. Vazquez Schroeder,[53] G. Vegni,[87a,87b] J. J. Veillet,[113] C. Vellidis,[8] F. Veloso,[122a] R. Veness,[29] S. Veneziano,[130a] A. Ventura,[70a,70b] D. Ventura,[136] M. Venturi,[47] N. Venturi,[156] V. Vercesi,[117a] M. Verducci,[136] W. Verkerke,[103] J. C. Vermeulen,[103] A. Vest,[43] M. C. Vetterli,[140,d] I. Vichou,[163] T. Vickey,[143b,ff] O. E. Vickey Boeriu,[143b] G. H. A. Viehhauser,[116] S. Viel,[166] M. Villa,[19a,19b] M. Villaplana Perez,[165] E. Vilucchi,[46] M. G. Vincter,[28] E. Vinek,[29] V. B. Vinogradov,[63] M. Virchaux,[134,*] J. Virzi,[14] O. Vitells,[169] M. Viti,[41] I. Vivarelli,[47] F. Vives Vaque,[2] S. Vlachos,[9] D. Vladoiu,[96] M. Vlasak,[125] N. Vlasov,[20] A. Vogel,[20] P. Vokac,[125] G. Volpi,[46] M. Volpi,[84] G. Volpini,[87a] H. von der Schmitt,[97] J. von Loeben,[97] H. von Radziewski,[47] E. von Toerne,[20] V. Vorobel,[124] A. P. Vorobiev,[126] V. Vorwerk,[11] M. Vos,[165] R. Voss,[29] T. T. Voss,[172] J. H. Vossebeld,[71] N. Vranjes,[134] M. Vranjes Milosavljevic,[103] V. Vrba,[123]

M. Vreeswijk,[103] T. Vu Anh,[47] R. Vuillermet,[29] I. Vukotic,[113] W. Wagner,[172] P. Wagner,[118] H. Wahlen,[172] J. Wakabayashi,[99] S. Walch,[85] J. Walder,[69] R. Walker,[96] W. Walkowiak,[139] R. Wall,[173] P. Waller,[71] C. Wang,[44] H. Wang,[170] H. Wang,[32b,gg] J. Wang,[149] J. Wang,[54] J. C. Wang,[136] R. Wang,[101] S. M. Wang,[149] T. Wang,[20] A. Warburton,[83] C. P. Ward,[27] M. Warsinsky,[47] C. Wasicki,[41] P. M. Watkins,[17] A. T. Watson,[17] I. J. Watson,[148] M. F. Watson,[17] G. Watts,[136] S. Watts,[80] A. T. Waugh,[148] B. M. Waugh,[75] M. Weber,[127] M. S. Weber,[16] P. Weber,[53] A. R. Weidberg,[116] P. Weigell,[97] J. Weingarten,[53] C. Weiser,[47] H. Wellenstein,[22] P. S. Wells,[29] T. Wenaus,[24] D. Wendland,[15] S. Wendler,[121] Z. Weng,[149,u] T. Wengler,[29] S. Wenig,[29] N. Wermes,[20] M. Werner,[47] P. Werner,[29] M. Werth,[161] M. Wessels,[57a] J. Wetter,[159] C. Weydert,[54] K. Whalen,[28] S. J. Wheeler-Ellis,[161] S. P. Whitaker,[21] A. White,[7] M. J. White,[84] S. R. Whitehead,[116] D. Whiteson,[161] D. Whittington,[59] F. Wicek,[113] D. Wicke,[172] F. J. Wickens,[127] W. Wiedenmann,[170] M. Wielers,[127] P. Wienemann,[20] C. Wiglesworth,[73] L. A. M. Wiik-Fuchs,[47] P. A. Wijeratne,[75] A. Wildauer,[165] M. A. Wildt,[41,q] I. Wilhelm,[124] H. G. Wilkens,[29] J. Z. Will,[96] E. Williams,[34] H. H. Williams,[118] W. Willis,[34] S. Willocq,[82] J. A. Wilson,[17] M. G. Wilson,[141] A. Wilson,[85] I. Wingerter-Seez,[4] S. Winkelmann,[47] F. Winklmeier,[29] M. Wittgen,[141] M. W. Wolter,[38] H. Wolters,[122a,h] W. C. Wong,[40] G. Wooden,[85] B. K. Wosiek,[38] J. Wotschack,[29] M. J. Woudstra,[82] K. W. Wozniak,[38] K. Wraight,[52] C. Wright,[52] M. Wright,[52] B. Wrona,[71] S. L. Wu,[170] X. Wu,[48] Y. Wu,[32b,hh] E. Wulf,[34] R. Wunstorf,[42] B. M. Wynne,[45] S. Xella,[35] M. Xiao,[134] S. Xie,[47] Y. Xie,[32a] C. Xu,[32b,w] D. Xu,[137] G. Xu,[32a] B. Yabsley,[148] S. Yacoob,[143b] M. Yamada,[64] H. Yamaguchi,[153] A. Yamamoto,[64] K. Yamamoto,[62] S. Yamamoto,[153] T. Yamamura,[153] T. Yamanaka,[153] J. Yamaoka,[44] T. Yamazaki,[153] Y. Yamazaki,[65] Z. Yan,[21] H. Yang,[85] U. K. Yang,[80] Y. Yang,[59] Y. Yang,[32a] Z. Yang,[144a,144b] S. Yanush,[89] Y. Yao,[14] Y. Yasu,[64] G. V. Ybeles Smit,[128] J. Ye,[39] S. Ye,[24] M. Yilmaz,[3c] R. Yoosoofmiya,[121] K. Yorita,[168] R. Yoshida,[5] C. Young,[141] S. Youssef,[21] D. Yu,[24] J. Yu,[7] J. Yu,[110] L. Yuan,[32a,ii] A. Yurkewicz,[104] B. Zabinski,[38] V. G. Zaets,[126] R. Zaidan,[61] A. M. Zaitsev,[126] Z. Zajacova,[29] L. Zanello,[130a,130b] A. Zaytsev,[105] C. Zeitnitz,[172] M. Zeller,[173] M. Zeman,[123] A. Zemla,[38] C. Zendler,[20] O. Zenin,[126] T. Ženiš,[142a] Z. Zinonos,[120a,120b] S. Zenz,[14] D. Zerwas,[113] G. Zevi della Porta,[56] Z. Zhan,[32d] D. Zhang,[32b,gg] H. Zhang,[86] J. Zhang,[5] X. Zhang,[32d] Z. Zhang,[113] L. Zhao,[106] T. Zhao,[136] Z. Zhao,[32b] A. Zhemchugov,[63] S. Zheng,[32a] J. Zhong,[116] B. Zhou,[85] N. Zhou,[161] Y. Zhou,[149] C. G. Zhu,[32d] H. Zhu,[41] J. Zhu,[85] Y. Zhu,[32b] X. Zhuang,[96] V. Zhuravlov,[97] D. Zieminska,[59] R. Zimmermann,[20] S. Zimmermann,[20] S. Zimmermann,[47] M. Ziolkowski,[139] R. Zitoun,[4] L. Živković,[34] V. V. Zmouchko,[126,*] G. Zobernig,[170] A. Zoccoli,[19a,19b] A. Zsenei,[29] M. zur Nedden,[15] V. Zutshi,[104] and L. Zwalinski[29]

(ATLAS Collaboration)

[1]*University at Albany, Albany, New York, USA*
[2]*Department of Physics, University of Alberta, Edmonton, Alberta, Canada*
[3a]*Department of Physics, Ankara University, Ankara, Turkey*
[3b]*Department of Physics, Dumlupinar University, Kutahya, Turkey*
[3c]*Department of Physics, Gazi University, Ankara, Turkey*
[3d]*Division of Physics, TOBB University of Economics and Technology, Ankara, Turkey*
[3e]*Turkish Atomic Energy Authority, Ankara, Turkey*
[4]*LAPP, CNRS/IN2P3 and Université de Savoie, Annecy-le-Vieux, France*
[5]*High Energy Physics Division, Argonne National Laboratory, Argonne, Illinois, USA*
[6]*Department of Physics, University of Arizona, Tucson, Arizona, USA*
[7]*Department of Physics, The University of Texas at Arlington, Arlington, Texas, USA*
[8]*Physics Department, University of Athens, Athens, Greece*
[9]*Physics Department, National Technical University of Athens, Zografou, Greece*
[10]*Institute of Physics, Azerbaijan Academy of Sciences, Baku, Azerbaijan*
[11]*Institut de Física d'Altes Energies and Departament de Física de la Universitat Autònoma de Barcelona and ICREA, Barcelona, Spain*
[12a]*Institute of Physics, University of Belgrade, Belgrade, Serbia*
[12b]*Vinca Institute of Nuclear Sciences, University of Belgrade, Belgrade, Serbia*
[13]*Department for Physics and Technology, University of Bergen, Bergen, Norway*
[14]*Physics Division, Lawrence Berkeley National Laboratory and University of California, Berkeley, California, USA*
[15]*Department of Physics, Humboldt University, Berlin, Germany*
[16]*Albert Einstein Center for Fundamental Physics and Laboratory for High Energy Physics, University of Bern, Bern, Switzerland*
[17]*School of Physics and Astronomy, University of Birmingham, Birmingham, United Kingdom*
[18a]*Department of Physics, Bogazici University, Istanbul, Turkey*
[18b]*Division of Physics, Dogus University, Istanbul, Turkey*
[18c]*Department of Physics Engineering, Gaziantep University, Gaziantep, Turkey*
[18d]*Department of Physics, Istanbul Technical University, Istanbul, Turkey*
[19a]*INFN Sezione di Bologna, Italy*
[19b]*Dipartimento di Fisica, Università di Bologna, Bologna, Italy*
[20]*Physikalisches Institut, University of Bonn, Bonn, Germany*
[21]*Department of Physics, Boston University, Boston, Massachusetts, USA*

[22]*Department of Physics, Brandeis University, Waltham, Massachusetts, USA*
[23a]*Universidade Federal do Rio De Janeiro COPPE/EE/IF, Rio de Janeiro, Brazil*
[23b]*Federal University of Juiz de Fora (UFJF), Juiz de Fora, Brazil*
[23c]*Federal University of Sao Joao del Rei (UFSJ), Sao Joao del Rei, Brazil*
[23d]*Instituto de Fisica, Universidade de Sao Paulo, Sao Paulo, Brazil*
[24]*Physics Department, Brookhaven National Laboratory, Upton, New York, USA*
[25a]*National Institute of Physics and Nuclear Engineering, Bucharest, Romania*
[25b]*University Politehnica Bucharest, Bucharest, Romania*
[25c]*West University in Timisoara, Timisoara, Romania*
[26]*Departamento de Física, Universidad de Buenos Aires, Buenos Aires, Argentina*
[27]*Cavendish Laboratory, University of Cambridge, Cambridge, United Kingdom*
[28]*Department of Physics, Carleton University, Ottawa, Ontario, Canada*
[29]*CERN, Geneva, Switzerland*
[30]*Enrico Fermi Institute, University of Chicago, Chicago, Illinois, USA*
[31a]*Departamento de Fisica, Pontificia Universidad Católica de Chile, Santiago*
[31b]*Departamento de Física, Universidad Técnica Federico Santa María, Valparaíso, Chile*
[32a]*Institute of High Energy Physics, Chinese Academy of Sciences, Beijing, China*
[32b]*Department of Modern Physics, University of Science and Technology of China, Anhui*
[32c]*Department of Physics, Nanjing University, Jiangsu, China*
[32d]*School of Physics, Shandong University, Shandong, China*
[33]*Laboratoire de Physique Corpusculaire, Clermont Université and Université Blaise Pascal and CNRS/IN2P3, Aubiere Cedex, France*
[34]*Nevis Laboratory, Columbia University, Irvington, New York, USA*
[35]*Niels Bohr Institute, University of Copenhagen, Kobenhavn, Denmark*
[36a]*INFN Gruppo Collegato di Cosenza, Italy*
[36b]*Dipartimento di Fisica, Università della Calabria, Arcavata di Rende, Italy*
[37]*AGH University of Science and Technology, Faculty of Physics and Applied Computer Science, Krakow, Poland*
[38]*The Henryk Niewodniczanski Institute of Nuclear Physics, Polish Academy of Sciences, Krakow, Poland*
[39]*Physics Department, Southern Methodist University, Dallas, Texas, USA*
[40]*Physics Department, University of Texas at Dallas, Richardson, Texas, USA*
[41]*DESY, Hamburg and Zeuthen, Germany*
[42]*Institut für Experimentelle Physik IV, Technische Universität Dortmund, Dortmund, Germany*
[43]*Institut für Kern- und Teilchenphysik, Technical University Dresden, Dresden, Germany*
[44]*Department of Physics, Duke University, Durham, North Carolina, USA*
[45]*SUPA-School of Physics and Astronomy, University of Edinburgh, Edinburgh, United Kingdom*
[46]*INFN Laboratori Nazionali di Frascati, Frascati, Italy*
[47]*Fakultät für Mathematik und Physik, Albert-Ludwigs-Universität, Freiburg, Germany*
[48]*Section de Physique, Université de Genève, Geneva, Switzerland*
[49a]*INFN Sezione di Genova, Italy*
[49b]*Dipartimento di Fisica, Università di Genova, Genova, Italy*
[50a]*E. Andronikashvili Institute of Physics, Tbilisi State University, Tbilisi, Georgia*
[50b]*High Energy Physics Institute, Tbilisi State University, Tbilisi, Georgia*
[51]*II Physikalisches Institut, Justus-Liebig-Universität Giessen, Giessen, Germany*
[52]*SUPA-School of Physics and Astronomy, University of Glasgow, Glasgow, United Kingdom*
[53]*II Physikalisches Institut, Georg-August-Universität, Göttingen, Germany*
[54]*Laboratoire de Physique Subatomique et de Cosmologie, Université Joseph Fourier and CNRS/IN2P3 and Institut National Polytechnique de Grenoble, Grenoble, France*
[55]*Department of Physics, Hampton University, Hampton, Virgina, USA*
[56]*Laboratory for Particle Physics and Cosmology, Harvard University, Cambridge, Massachusetts, USA*
[57a]*Kirchhoff-Institut für Physik, Ruprecht-Karls-Universität Heidelberg, Heidelberg, Germany*
[57b]*Physikalisches Institut, Ruprecht-Karls-Universität Heidelberg, Heidelberg, Germany*
[57c]*ZITI Institut für technische Informatik, Ruprecht-Karls-Universität Heidelberg, Mannheim, Germany*
[58]*Faculty of Applied Information Science, Hiroshima Institute of Technology, Hiroshima, Japan*
[59]*Department of Physics, Indiana University, Bloomington, Indiana, USA*
[60]*Institut für Astro- und Teilchenphysik, Leopold-Franzens-Universität, Innsbruck, Austria*
[61]*University of Iowa, Iowa City, Iowa, USA*
[62]*Department of Physics and Astronomy, Iowa State University, Ames, Iowa, USA*
[63]*Joint Institute for Nuclear Research, JINR Dubna, Dubna, Russia*
[64]*KEK, High Energy Accelerator Research Organization, Tsukuba, Japan*

[65]*Graduate School of Science, Kobe University, Kobe, Japan*
[66]*Faculty of Science, Kyoto University, Kyoto, Japan*
[67]*Kyoto University of Education, Kyoto, Japan*
[68]*Instituto de Física La Plata, Universidad Nacional de La Plata and CONICET, La Plata, Argentina*
[69]*Physics Department, Lancaster University, Lancaster, United Kingdom*
[70a]*INFN Sezione di Lecce, Italy*
[70b]*Dipartimento di Fisica, Università del Salento, Lecce, Italy*
[71]*Oliver Lodge Laboratory, University of Liverpool, Liverpool, United Kingdom*
[72]*Department of Physics, Jožef Stefan Institute and University of Ljubljana, Ljubljana, Slovenia*
[73]*School of Physics and Astronomy, Queen Mary University of London, London, United Kingdom*
[74]*Department of Physics, Royal Holloway University of London, Surrey, United Kingdom*
[75]*Department of Physics and Astronomy, University College London, London, United Kingdom*
[76]*Laboratoire de Physique Nucléaire et de Hautes Energies, UPMC and Université Paris-Diderot and CNRS/IN2P3, Paris, France*
[77]*Fysiska institutionen, Lunds universitet, Lund, Sweden*
[78]*Departamento de Fisica Teorica C-15, Universidad Autonoma de Madrid, Madrid, Spain*
[79]*Institut für Physik, Universität Mainz, Mainz, Germany*
[80]*School of Physics and Astronomy, University of Manchester, Manchester, United Kingdom*
[81]*CPPM, Aix-Marseille Université and CNRS/IN2P3, Marseille, France*
[82]*Department of Physics, University of Massachusetts, Amherst, Massacusetts, USA*
[83]*Department of Physics, McGill University, Montreal, Quebec, Canada*
[84]*School of Physics, University of Melbourne, Victoria, Australia*
[85]*Department of Physics, The University of Michigan, Ann Arbor, Michigan, USA*
[86]*Department of Physics and Astronomy, Michigan State University, East Lansing, Michigan, USA*
[87a]*INFN Sezione di Milano, Italy*
[87b]*Dipartimento di Fisica, Università di Milano, Milano, Italy*
[88]*B.I. Stepanov Institute of Physics, National Academy of Sciences of Belarus, Minsk, Republic of Belarus*
[89]*National Scientific and Educational Centre for Particle and High Energy Physics, Minsk, Republic of Belarus*
[90]*Department of Physics, Massachusetts Institute of Technology, Cambridge, Massachusetts, USA*
[91]*Group of Particle Physics, University of Montreal, Montreal, Quebec, Canada*
[92]*P. N. Lebedev Institute of Physics, Academy of Sciences, Moscow, Russia*
[93]*Institute for Theoretical and Experimental Physics (ITEP), Moscow, Russia*
[94]*Moscow Engineering and Physics Institute (MEPhI), Moscow, Russia*
[95]*Skobeltsyn Institute of Nuclear Physics, Lomonosov Moscow State University, Moscow, Russia*
[96]*Fakultät für Physik, Ludwig-Maximilians-Universität München, München, Germany*
[97]*Max-Planck-Institut für Physik (Werner-Heisenberg-Institut), München, Germany*
[98]*Nagasaki Institute of Applied Science, Nagasaki, Japan*
[99]*Graduate School of Science, Nagoya University, Nagoya, Japan*
[100a]*INFN Sezione di Napoli, Italy*
[100b]*Dipartimento di Scienze Fisiche, Università di Napoli, Napoli, Italy*
[101]*Department of Physics and Astronomy, University of New Mexico, Albuquerque, New Mexico, USA*
[102]*Institute for Mathematics, Astrophysics and Particle Physics, Radboud University Nijmegen/Nikhef, Nijmegen, Netherlands*
[103]*Nikhef National Institute for Subatomic Physics and University of Amsterdam, Amsterdam, Netherlands*
[104]*Department of Physics, Northern Illinois University, DeKalb, Illinois, USA*
[105]*Budker Institute of Nuclear Physics, SB RAS, Novosibirsk, Russia*
[106]*Department of Physics, New York University, New York, New York, USA*
[107]*Ohio State University, Columbus, Ohio, USA*
[108]*Faculty of Science, Okayama University, Okayama, Japan*
[109]*Homer L. Dodge Department of Physics and Astronomy, University of Oklahoma, Norman, Oklahoma, USA*
[110]*Department of Physics, Oklahoma State University, Stillwater, Oklahoma, USA*
[111]*Palacký University, RCPTM, Olomouc, Czech Republic*
[112]*Center for High Energy Physics, University of Oregon, Eugene, Oregon, USA*
[113]*LAL, Univ. Paris-Sud and CNRS/IN2P3, Orsay, France*
[114]*Graduate School of Science, Osaka University, Osaka, Japan*
[115]*Department of Physics, University of Oslo, Oslo, Norway*
[116]*Department of Physics, Oxford University, Oxford, United Kingdom*
[117a]*INFN Sezione di Pavia, Italy*
[117b]*Dipartimento di Fisica, Università di Pavia, Pavia, Italy*
[118]*Department of Physics, University of Pennsylvania, Philadelphia, Pennsylvania, USA*

[119]*Petersburg Nuclear Physics Institute, Gatchina, Russia*
[120a]*INFN Sezione di Pisa, Italy*
[120b]*Dipartimento di Fisica E. Fermi, Università di Pisa, Pisa, Italy*
[121]*Department of Physics and Astronomy, University of Pittsburgh, Pittsburgh, Pennsylvania, USA*
[122a]*Laboratorio de Instrumentacao e Fisica Experimental de Particulas-LIP, Lisboa, Portugal*
[122b]*Departamento de Fisica Teorica y del Cosmos and CAFPE, Universidad de Granada, Granada, Spain*
[123]*Institute of Physics, Academy of Sciences of the Czech Republic, Praha, Czech Republic*
[124]*Faculty of Mathematics and Physics, Charles University in Prague, Praha, Czech Republic*
[125]*Czech Technical University in Prague, Praha, Czech Republic*
[126]*State Research Center Institute for High Energy Physics, Protvino, Russia*
[127]*Particle Physics Department, Rutherford Appleton Laboratory, Didcot, United Kingdom*
[128]*Physics Department, University of Regina, Regina SK, Canada*
[129]*Ritsumeikan University, Kusatsu, Shiga, Japan*
[130a]*INFN Sezione di Roma I, Italy*
[130b]*Dipartimento di Fisica, Università La Sapienza, Roma, Italy*
[131a]*INFN Sezione di Roma Tor Vergata, Italy*
[131b]*Dipartimento di Fisica, Università di Roma Tor Vergata, Roma, Italy*
[132a]*INFN Sezione di Roma Tre, Italy*
[132b]*Dipartimento di Fisica, Università Roma Tre, Roma, Italy*
[133a]*Faculté des Sciences Ain Chock, Réseau Universitaire de Physique des Hautes Energies - Université Hassan II, Casablanca, Morocco*
[133b]*Centre National de l'Energie des Sciences Techniques Nucleaires, Rabat, Morocco*
[133c]*Faculté des Sciences Semlalia, Université Cadi Ayyad, LPHEA-Marrakech, Morocco*
[133d]*Faculté des Sciences, Université Mohamed Premier and LPTPM, Oujda, Morocco*
[133e]*Faculté des Sciences, Université Mohammed V-Agdal, Rabat, Morocco*
[134]*DSM/IRFU (Institut de Recherches sur les Lois Fondamentales de l'Univers), CEA Saclay (Commissariat a l'Energie Atomique), Gif-sur-Yvette, France*
[135]*Santa Cruz Institute for Particle Physics, University of California Santa Cruz, Santa Cruz, California, USA*
[136]*Department of Physics, University of Washington, Seattle, Washington, USA*
[137]*Department of Physics and Astronomy, University of Sheffield, Sheffield, United Kingdom*
[138]*Department of Physics, Shinshu University, Nagano, Japan*
[139]*Fachbereich Physik, Universität Siegen, Siegen, Germany*
[140]*Department of Physics, Simon Fraser University, Burnaby, British Columbia, Canada*
[141]*SLAC National Accelerator Laboratory, Stanford, California, USA*
[142a]*Faculty of Mathematics, Physics & Informatics, Comenius University, Bratislava, Slovak Republic*
[142b]*Department of Subnuclear Physics, Institute of Experimental Physics of the Slovak Academy of Sciences, Kosice, Slovak Republic*
[143a]*Department of Physics, University of Johannesburg, Johannesburg, South Africa*
[143b]*School of Physics, University of the Witwatersrand, Johannesburg, South Africa*
[144a]*Department of Physics, Stockholm University, Sweden*
[144b]*The Oskar Klein Centre, Stockholm, Sweden*
[145]*Physics Department, Royal Institute of Technology, Stockholm, Sweden*
[146]*Departments of Physics & Astronomy and Chemistry, Stony Brook University, Stony Brook, New York, USA*
[147]*Department of Physics and Astronomy, University of Sussex, Brighton, United Kingdom*
[148]*School of Physics, University of Sydney, Sydney, Australia*
[149]*Institute of Physics, Academia Sinica, Taipei, Taiwan*
[150]*Department of Physics, Technion: Israel Inst. of Technology, Haifa, Israel*
[151]*Raymond and Beverly Sackler School of Physics and Astronomy, Tel Aviv University, Tel Aviv, Israel*
[152]*Department of Physics, Aristotle University of Thessaloniki, Thessaloniki, Greece*
[153]*International Center for Elementary Particle Physics and Department of Physics, The University of Tokyo, Tokyo, Japan*
[154]*Graduate School of Science and Technology, Tokyo Metropolitan University, Tokyo, Japan*
[155]*Department of Physics, Tokyo Institute of Technology, Tokyo, Japan*
[156]*Department of Physics, University of Toronto, Toronto, Ontario, Canada*
[157a]*TRIUMF, Vancouver, British Columbia, Canada*
[157b]*Department of Physics and Astronomy, York University, Toronto, Ontario, Canada*
[158]*Institute of Pure and Applied Sciences, University of Tsukuba,1-1-1 Tennodai, Tsukuba, Ibaraki 305-8571, Japan*
[159]*Science and Technology Center, Tufts University, Medford, Massachusetts, USA*
[160]*Centro de Investigaciones, Universidad Antonio Narino, Bogota, Colombia*
[161]*Department of Physics and Astronomy, University of California Irvine, Irvine, California, USA*
[162a]*INFN Gruppo Collegato di Udine, Italy*

[162b]*ICTP, Trieste, Italy*
[162c]*Dipartimento di Chimica, Fisica e Ambiente, Università di Udine, Udine, Italy*
[163]*Department of Physics, University of Illinois, Urbana, Illinois, USA*
[164]*Department of Physics and Astronomy, University of Uppsala, Uppsala, Sweden*
[165]*Instituto de Física Corpuscular (IFIC) and Departamento de Física Atómica, Molecular y Nuclear and Departamento de Ingeniería Electrónica and Instituto de Microelectrónica de Barcelona (IMB-CNM), University of Valencia and CSIC, Valencia, Spain*
[166]*Department of Physics, University of British Columbia, Vancouver, British Columbia, Canada*
[167]*Department of Physics and Astronomy, University of Victoria, Victoria, British Columbia, Canada*
[168]*Waseda University, Tokyo, Japan*
[169]*Department of Particle Physics, The Weizmann Institute of Science, Rehovot, Israel*
[170]*Department of Physics, University of Wisconsin, Madison, Wisconsin, USA*
[171]*Fakultät für Physik und Astronomie, Julius-Maximilians-Universität, Würzburg, Germany*
[172]*Fachbereich C Physik, Bergische Universität Wuppertal, Wuppertal, Germany*
[173]*Department of Physics, Yale University, New Haven, Connecticut, USA*
[174]*Yerevan Physics Institute, Yerevan, Armenia*
[175]*Domaine scientifique de la Doua, Centre de Calcul CNRS/IN2P3, Villeurbanne Cedex, France*

[a]Also at Laboratorio de Instrumentacao e Fisica Experimental de Particulas-LIP, Lisboa, Portugal.
[b]Also at Faculdade de Ciencias and CFNUL, Universidade de Lisboa, Lisboa, Portugal.
[c]Also at Particle Physics Department, Rutherford Appleton Laboratory, Didcot, United Kingdom.
[d]Also at TRIUMF, Vancouver, British Columbia, Canada.
[e]Also at Department of Physics, California State University, Fresno, California, USA.
[f]Also at Novosibirsk State University, Novosibirsk, Russia.
[g]Also at Fermilab, Batavia, Illinois, USA.
[h]Also at Department of Physics, University of Coimbra, Coimbra, Portugal.
[i]Also at Università di Napoli Parthenope, Napoli, Italy.
[j]Also at Institute of Particle Physics (IPP), Canada.
[k]Also at Department of Physics, Middle East Technical University, Ankara, Turkey.
[l]Also at Louisiana Tech University, Ruston, Louisisna, USA.
[m]Also at Department of Physics and Astronomy, University College London, London, United Kingdom.
[n]Also at Group of Particle Physics, University of Montreal, Montreal, Quebec, Canada.
[o]Also at Department of Physics, University of Cape Town, Cape Town, South Africa.
[p]Also at Institute of Physics, Azerbaijan Academy of Sciences, Baku, Azerbaijan.
[q]Also at Institut für Experimentalphysik, Universität Hamburg, Hamburg, Germany.
[r]Also at Manhattan College, New York, New York, USA.
[s]Also at School of Physics, Shandong University, Shandong, China.
[t]Also at CPPM, Aix-Marseille Université and CNRS/IN2P3, Marseille, France.
[u]Also at School of Physics and Engineering, Sun Yat-sen University, Guanzhou, China.
[v]Also at Academia Sinica Grid Computing, Institute of Physics, Academia Sinica, Taipei, Taiwan.
[w]Also at DSM/IRFU (Institut de Recherches sur les Lois Fondamentales de l'Univers), CEA Saclay (Commissariat a l'Energie Atomique), Gif-sur-Yvette, France.
[x]Also at Section de Physique, Université de Genève, Geneva, Switzerland.
[y]Also at Departamento de Fisica, Universidade de Minho, Braga, Portugal.
[z]Also at Department of Physics and Astronomy, University of South Carolina, Columbia South Carolina, USA.
[aa]Also at Institute for Particle and Nuclear Physics, Wigner Research Centre for Physics, Budapest, Hungary.
[bb]Also at California Institute of Technology, Pasadena, California, USA.
[cc]Also at Institute of Physics, Jagiellonian University, Krakow, Poland.
[dd]Also at LAL, Univ. Paris-Sud and CNRS/IN2P3, Orsay, France.
[ee]Also at Department of Physics and Astronomy, University of Sheffield, Sheffield, United Kingdom.
[ff]Also at Department of Physics, Oxford University, Oxford, United Kingdom.
[gg]Also at Institute of Physics, Academia Sinica, Taipei, Taiwan.
[hh]Also at Department of Physics, The University of Michigan, Ann Arbor, Michigan, USA.
[ii]Also at Laboratoire de Physique Nucléaire et de Hautes Energies, UPMC and Université Paris-Diderot and CNRS/IN2P3, Paris, France.
*Deceased.